DOKUZ EYLÜL UNIVERSITY
GRADUATE SCHOOL OF NATURAL AND APPLIED SCIENCES

HIGH FREQUENCY VIBRATIONS OF THIN PLATES

by
Abdullah SEÇGİN

September, 2008
İZMİR

HIGH FREQUENCY VIBRATIONS OF THIN PLATES

A Thesis Submitted to the
Graduate School of Natural and Applied Sciences of Dokuz Eylül University
In Partial Fulfillment of the Requirements for the Degree of Doctor of Philosophy in Mechanical Engineering, Machine Theory and Dynamics Program

by
Abdullah SEÇGİN

September, 2008
İZMİR

Ph.D. THESIS EXAMINATION RESULT FORM

We have read the thesis entitled **"HIGH FREQUENCY VIBRATIONS OF THIN PLATES"** completed by **ABDULLAH SEÇGİN** under supervision of **PROF. DR. A. SAİDE SARIGÜL** and we certify that in our opinion it is fully adequate, in scope and in quality, as a thesis for the degree of Doctor of Philosophy.

Prof. Dr. A. Saide SARIGÜL

Supervisor

Assist. Prof. Dr. Zeki KIRAL

Thesis Committee Member

Prof. Dr. Cüneyt GÜZELİŞ

Thesis Committee Member

Prof. Dr. Hira KARAGÜLLE

Examining Committee Member

Prof. Dr. Vahit MERMERTAŞ

Examining Committee Member

Prof. Dr. Cahit HELVACI
Director
Graduate School of Natural and Applied Sciences

ACKNOWLEDGMENTS

Firstly, I would like to thank my supervisor Prof. Dr. A.Saide SARIGÜL not only for her valuable help, perfect guidance, positive criticisms and encouragements throughout the Doctorate period but also for always considering me as one of her academic colleagues rather than just her doctorate student.

I also gratefully thank to Prof. Dr. Mustafa SABUNCU and Prof. Dr. Cüneyt GÜZELİŞ for their valuable advices and discussions to improve the quality of the thesis.

I am also thankful to my parents Yeter, Cahit SEÇGİN and my sister Hamide and brother Alpaslan SEÇGİN for their moral supports and for their trust in me. I also thank to graduate student Mr. Sinan ERTUNÇ for his contributions to my studies.

I specially thank to my wife Zeynep, my daughter Alara Begüm, my nephew Ahmet Efe and niece İrem Naz for their rendering every moment of my life worthwhile and meaningful.

This study is dedicated to the memory of my grandfather Abdullah SEÇGİN.

Abdullah SEÇGİN

HIGH FREQUENCY VIBRATIONS OF THIN PLATES

ABSTRACT

In the analysis of high frequency dynamics of vibrating systems, an averaged prediction of energy is generally of interest to describe the response level. However, energetic response parameters do not include modal information and thus exhibit smooth characteristics. Therefore, it is obvious for systems subjected to high frequency excitations that an efficient tool is required. This doctorate study mainly deals with the development of such an approach.

In this regard, a novel scheme for the discrete high frequency response analysis is introduced in the presented thesis. The scheme is based on Discrete Singular Convolution (DSC) and Mode Superposition (MS) methods. The accuracy of the DSC-MS is validated for thin beams and plates by comparing with available analytical solutions. The performance of the DSC-MS is evaluated by predicting spatial distribution and discrete frequency spectra of the vibration response of thin plates with two different boundary conditions.

As a secondary study, this thesis introduces two different application procedures for the classical DSC method. The first one is an algorithm for free vibration analysis of symmetrically laminated composite plates. The second one is an implementation for free vibrations of thick beams and plates. Comprehensive comparisons with open literature state that both procedures presented for the DSC are rather effective and accurate.

Keywords: High frequency, Thin plate, Discrete response, DSC, DSC-MS, Free vibration, Forced vibration, Laminated composite, Timoshenko beam, Mindlin plate.

İNCE PLAKALARIN YÜKSEK FREKANS TİTREŞİMLERİ

ÖZ

Titreşen sistemlerin yüksek frekans dinamiğinin analizinde, cevap düzeyini tanımlayabilmek için genellikle ortalama enerji kestirimi göz önüne alınır. Ancak, cevabın enerji parametreleri ile ifadesi modal bilgi içermediğinden dolayı düzgün bir karakteristik sergiler. Bu yüzden, yüksek frekans zorlamalarına maruz kalan sistemler için etkili bir araca ihtiyaç duyulduğu açıktır. Bu doktora çalışması temelde böyle bir yaklaşım geliştirmekle ilgilenir.

Bu bağlamda, sunulan tezde ayrık yüksek frekans cevap analizi için yeni bir yaklaşım tanıtılmıştır. Yaklaşım ayrık tekil konvolüsyon (DSC) ve mod süperpozisyonu metodlarına (MS) dayanmaktadır. İnce çubuk ve plakalar için DSC-MS' nin doğruluğu varolan analitik çözümlerle karşılaştırılarak kanıtlanmıştır. DSC-MS' nin performansı iki farklı sınır koşuluna sahip ince plakaların titreşim cevabının uzamsal dağılım ve ayrık frekans spektrum kestirimleri yapılarak değerlendirilmiştir.

İkincil bir çalışma olarak, bu tez klasik DSC yöntemi için iki farklı uygulama yordamı ortaya koymuştur. Birincisi simetrik olarak tabakalı kompozit plakaların serbest titreşim analizleri için bir algoritma, diğeri kalın çubuk ve plakaların serbest titreşimleri için bir uygulamadır. Açık literatür ile yapılan kapsamlı karşılaştırmalar DSC için ortaya konulan her iki yordamın da oldukça etkili ve başarılı olduğunu göstermektedir.

Anahtar Sözcükler: Yüksek frekans, İnce plaka, Ayrık cevap, DSC, DSC-MS, Serbest titreşim, Zorlanmış titreşim, Tabakalı kompozit, Timoshenko çubuğu, Mindlin plakası.

CONTENTS

Page

CHAPTER ONE
INTRODUCTION AND LITERATURE REVIEW

1.1 Literature Survey for Vibro-acoustic Methods

In this section, some of the conventional methods for the prediction of vibro-acoustic response are reviewed regarding excitation frequency range classification. As an overall consideration, some of the specifications and capabilities of these methods are tabulated in Table 1.1. Besides, as an alternative to the conventional approaches, some of the semi-analytical, meshless and grid-based approaches for plate vibrations are also reviewed.

1.1.1 Introduction

Vibration analysis is one of the most important issues in the engineering design, since the phenomenon of the resonance may lead to the failure of structures such as bridges, buildings, or airplane wings. Vibration of structures also induces noise. The physical nature of the sound is generally determined by vibration characteristics. Therefore, in order to establish a less noisy environment, vibration analysis should be primarily performed. In modern vibration analysis, numerical simulations and algorithms are being efficiently used as an alternative to analytical and experimental methods.

In the science of vibro-acoustics, vibration and acoustic problems are classified according to their frequency range as, low, medium and high frequency problems. Since dynamic behaviour of systems changes with regard to the excitation frequency, adaptive approaches are required for reliable solutions. In practice, it is not mentioned about definite boundaries separating frequency ranges from each other due to the fact that they may change from system to system. However, Rabbiolo, Bernhard & Milner (2004) have put forward an indicator for approximately defining high-frequency thresholds based on “modal overlap count (modal overlap factor)” of simple structures such as beams, plates and acoustical spaces.

It is known that modelling high frequency dynamic systems using deterministic techniques such as Finite Element Method (FEM) and Boundary Element Method (BEM) is numerically expensive. Besides, since the vibro-acoustic response is very sensitive to the changes in system parameters at higher frequencies, some uncertainties are encountered. Therefore, deterministic techniques are feasible only for low frequency analysis. In the low frequency range, the response of physical subsystems such as beams, plates, and acoustic enclosures are usually dominated by resonant modes that exhibit large responses. For the analysis of high frequency behaviour of structural-acoustic systems, averaged predictions of energy are often used as the variable of interest to describe the response level. The Statistical Energy Analysis (SEA) developed by Lyon and Maidanik in 1962 has proved its validity for high frequency analysis (Lyon & DeJong, 1995). However, SEA is based on some pre-assumptions restricting its efficiency and capacity. Therefore, several alternative energy-based techniques have been developed. Among them, Energy Flow Analysis (EFA) and its finite and boundary element implementations, Energy Finite Element Method (EFEM), Energy Boundary Element Method (EBEM) are common approaches in service. However, since all these methods consider average prediction of energy as system variable to describe the response level, they disregard modal information and thus, loose discrete frequency response behaviour of the structure.

1.1.2 Methods of Low Frequency Analysis

1.1.2.1 Modal Analysis

Modal analysis is the most classical and well-established method for vibration analyses. The principle of modal superposition is that the response of a continuous system is the summation of the individual responses of the system. Each natural mode contributes a different amount to the response. This principle was first noted in 1747 by Bernoulli and proven in 1753 by Euler. At low frequencies, modal analysis is usually very efficient for deriving solutions to vibration problems. As the excitation frequency increases, more modes should be included to obtain a good approximation, hence the computational effort increases. Analytical modal solutions

are available for a limited number of cases where the structure is simple and the boundary conditions are idealized. For practical problems, measurements are often conducted to determine lower-order modes of a structure. This is called experimental modal analysis, and can be used to validate modal predictions. However, for high frequency modal analysis, many more measurements are needed and the reliability of the measurements is often limited by the accuracy of the test instrument and the methodology of the experiment. Therefore experimental modal analysis is generally limited to low frequencies due to computational and experimental limitations.

1.1.2.2 Finite Element Method (FEM) and Boundary Element Method (BEM)

Finite Element Method (FEM) is one of the most popular approaches to model and solve complex engineering problems in a wide range of fields. FEM is extensively used for predictions of both structural and acoustic low frequency responses. In this method, the continuum domain is discretized into small elements. Since field variables within each element are described in terms of shape functions, a substantial amount of elements must be used in order to keep the approximation error within acceptable levels. The wavelength of the displacement decreases with increasing frequency, so in order to keep this dependence the size of elements must be decreased. In addition, the FEM is derived as a discretization of some approximate continuum mechanical theory such as the thin plate theory. In this case it is known that a characteristic wavelength of considered motions should be well above 5-10 element widths for sufficient agreement between numerical and analytical solutions (Wachulec, Kirkegaard & Nielsen, 2000). All these restrictions impede the FEM to be used accurately in higher frequencies. Finite element method is used to predict the structural-acoustic behaviour for coupled structures such as liquid storage tanks, thin walled cavities (car like cavities, box structures etc.) excited by low frequencies (Everstine, 1997; Cho, Lee & Kim, 2002; Kim, Lee & Sung, 1999; Song, Hwang, Lee, & Hedrick, 2003; Lim, 2000; Cummings, 2001). The Boundary Element Method has been utilized to predict acoustic radiation from vibrating structures. The main advantage of BEM is that only the boundary of the domain is discretized, allowing the solution of problems with fewer elements

compared to FEM. For high frequency analysis, like the FEM, BEM is inappropriate due to the huge number of degrees of freedom needed, which results in prohibitive computational cost, and uncertainty of structural acoustic systems at these frequencies.

1.1.2.3 Coupled FEM\BEM

For the numerical simulation of the radiation and scattering of sound, the BEM is superior to the FEM in many cases which needs considerably smaller effort to model the infinite domain. For finite element analysis the entire volume is discretized whereas in boundary element method only the surface of the volume is discretized. However, the FEM has superiority compared to the BEM in respect of the computation time and system matrix holding less memory. In fluid-structure interaction problems, especially, in low frequencies, FEM and BEM may be implemented simultaneously to the structure-fluid system by using the superiorities of both methods. A detailed review and methodologies on the implementation of the coupled FEM\BEM to structural-fluid-interaction problems have been presented in literature (Mariem & Hamdi, 1987; Kopuz, 1995; Vlahopoulos, Raveandra, Vallance, & Messer, 1999; Chen, Hofstetter & Mang, 1998; Coyette,1999; Gaul & Wenzel, 2002; Fritze, Marburg & Hardtke, 2005).

1.1.3 Methods of Mid-Frequency Analysis

In recent years, a vast amount of research has been performed for an adequate solution of mid-frequency vibro-acoustic problems. In the mid-frequency range, deterministic techniques and energy based approaches can not predict valid response behaviour due to their capabilities. Therefore, in general, hybrid methods have been developed and used for this range. The detailed discussion for the mid-frequency analysis and the review of hybrid methods predicting mid-frequency structural-acoustic response may be found in literature, e.g., (Wachulec et al., 2000; Desmet, 2002).

1.1.4 Methods of High Frequency Analysis

1.1.4.1 Statistical Energy Analysis (SEA)

In the SEA, a complex structure is modelled as a composition of many coupled substructures. The Statistical Energy Analysis (SEA) is a statistical technique considering energy flow between the substructures. The theory of SEA modelling is mainly based on the following two issues: Statistical modelling of the modal behaviour of each subsystem and setting a dynamic energy flow balance between these coupled subsystems. A basic requirement for the analysis of vibro-acoustic problems by means of the SEA is the knowledge of modal densities of considered subsystems. The successful application of the SEA depends strongly upon high Modal Density (MD) and high Modal Overlap (MO) count (factor) of a structure. There are several assumptions used for SEA which is reported by Wang (2000) in literature survey of his PhD thesis. Some of these are:

"Coupling between subsystems is 'weak' so that the modal behaviour of each subsystem does not change much because of the other subsystems" (Wang, 2000). This assumption strictly restricts the use of SEA in modeling the strongly coupled structural-acoustic systems accurately, for instance, in modeling small cavities enclosed by thin walled structures.

"The internal damping in each subsystem is 'light'" (Wang, 2000).

"The damping is proportional to mass density so that the equation of motion of each subsystem can be uncoupled" (Wang, 2000). The assumption restricts the modelling of local damping treatments.

"The power and energy variables are averaged across a small frequency band" (Wang, 2000).

“The frequency band contains many resonant modes” (Wang, 2000). This assumption limits the use of the SEA accurately only at higher frequencies leading to high MD and MO.

In this regard, it is important to determine how these assumptions affect the modeling of a real coupled system by SEA. SEA modelling is not sufficient in a system for which the local variables (e.g., the acoustic pressure or displacement distributions on an acoustic or structural element in a single subsystem) are important regarding design purposes.

1.1.4.2 Energy Flow Analysis (EFA), Energy Finite Element Method (EFEM), Energy Boundary Element Method (EBEM)

Energy Flow Analysis (EFA) is a more recent tool for the prediction of the vibrational behaviour of structures in the high frequency range. Energy Flow Analysis, like SEA, predicts mechanical energy based on energy equilibrium equations. But EFA also predicts the spatial variation of the mechanical energy in the structure. Energy flow analysis is able to model local effects such as localized power inputs and local damping treatments. The energy distribution and the energy flow of different waves are predicted in some basic components like beams, plates, acoustic cavities etc. An important advantage is that the energy equations in these basic components are conceptually similar to the equations of static heat flow.

The energy distribution and energy flow within the basic components can thus easily be computed with existing finite element codes for thermal computations. This is called the Energy Finite Element Method (EFEM). Like SEA, EFEM predicts mechanical energy based on energy equilibrium equations for which SEA uses macro subsystems whereas EFEM uses infinitesimal subsystems. Since the database required for EFEM is similar to that of FEM, a low frequency FEM analysis can be easily extended to high frequency band analysis by EFEM. The boundary element implementation of the energy flow analysis (EBEM) is also used recently for high frequency structural-acoustic problems together with EFEM. Considerable studies

have been performed on developing and improving EFA, EFEM and EBEM (Cho, 1993; Bitsie, 1996; Han, 1999; Han, Bernhard & Mongeau, 1997, 1999; Wang, 2000; Dong, 2004; Langley, 1992, 1995; Smith, 1997; Carcaterra & Sestieri, 1997; Sestieri & Carcaterra, 2001; LeBot, 1998; Chae & Ih, 2001). Moens, Vandepitte & Sas (2002) presented a fundamental study of the validity of the Energy Finite Element Method for differently shaped plates with uniform hysteresis damping. The wavelength criterion deduced by Fahy in 1992 and Gur in 1999 for SEA and EFEM analysis was validated by Moens et al. (2002). In this criterion, a non-dimensional parameter is defined as the ratio of the characteristic length of the plate to the wavelength of the flexural waves at a certain frequency. These ratios have been stated as 2.47 by Fahy and 2.43 by Gur and they are close to each other. If a non-dimensional parameter of a system is larger than these levels, EFEM can be used to analyze plate structure.

1.1.4.3 Ray Tracing Method (RTM)

RTM is a recursive technique used generally in the prediction of transient sound field in room acoustics (Schroeder, 1969). However, Vorlaender (1989) used this technique in steady state response of sound fields and Chae et al. (2001) firstly used the Ray Tracing Method (RTM) in the prediction of high frequency time-averaged vibrational energy distribution in thin plates. In this method, the vibration field in a waveguide is decomposed to direct field and reverberant field. Direct field is discretized by a number of ray tubes and its reflections from specular boundaries are also represented by ray tubes for the total vibrational response. Chae et al. (2001) stated that, the time-averaged spatial energy distribution predicted by RTM yields more accurate results compared with those of SEA and EFEM.

Table 1.1 Specifications and capabilities of conventional vibro-acoustic methods

Criterion	**FEM, BEM**	**SEA**	**EFA (EFEM)**	**RTM**
Principle	-Energy minimisation principle	-Energy (Power) flow balance principle -Statistical modeling principle	-Vibration conduction principle -Energy flow balance principle	-Directional energy flow balance principle
Element modelling	-Using finite and boundary elements	-Using modal or geometrical macro elements	-Using finite and boundary elements	-Circular ray tubes
Requirements	-Sufficient number of small elements -Sufficient HD and CPU	-High modal density -High modal overlap count -Accurate determination of CLF and DLF	-High modal density -High modal overlap count -Sufficient HD and CPU	-High modal density -High modal overlap count -Specular boundaries
Excitation frequency range	-Low frequency	-High frequency	-High frequency	-High frequency
Frequency bandwidth	-Discrete or narrow bandwidth	-Wide bandwidth	-Wide bandwidth	-Wide bandwidth
Response characteristics	-Discrete (time, space, frequency)	-Average (time, space, frequency)	-Discrete (space) -Average (time, frequency)	-Discrete (directional, space) -Average (time, frequency)
Loss of local information	-Low	-High	-Low	-High
Strong fluid-structure interaction	√	-	√	?
Response parameters	-Displacement -Velocity -Acceleration	-Modal energy	-Modal energy	-Modal energy
Prediction of modal behaviour	√	-	-	-
Applications	-Simple -Complex structures	-Simple -Complex structures	- Simple -Complex structures	-Simple structures
Numerical algorithm	-Meshing -Standard equation solver	-Sub-structuring -Standard equation solver	-Thermal FEM algorithm -Standard equation solver	-Efficient ray tracing algorithm
Computation time	-Depending on the number of elements	-Low	-Depending on the number of elements	-High

1.1.4.4 Some Other Energy Based Methods

Langley (1992) presented a method called Wave Intensity technique for the analysis of high frequency vibrations based on energy balance equations. In this method, the vibration of each component of a system is defined in terms of a homogeneous random wave field. The directional dependency of the wave intensity in each component is represented by a finite Fourier series. Langley (1992) pointed out that if a single term of Fourier series is used then the standard form of the SEA is obtained. Therefore, wave intensity technique can be considered as a natural extension of conventional SEA and can predict directionality of the response beyond the SEA.

Carcaterra & Sestieri (1997) and Sestieri & Carcaterra (2001) developed and improved a new model called Complex Envelope Displacement Analysis (CEDA) to predict the high frequency structural acoustic response for one dimensional system. CEDA was introduced in these presented studies through several enhancements and treatments based on the other envelope techniques. The analysis, like the other high frequency techniques, predicts averaged levels rather than the solution itself. In this analysis, the envelope trend of field variables (energy or displacement) is described. The envelope is obtained by an appropriate use of Hilbert transformation procedure. The procedure removes the oscillating part of the solution while keeping its main trend along the structure. LeBot (1998) developed a vibro-acoustic model for high frequency analysis based on energetic quantities and energy balance by conserving the spirit of the SEA. But he stated that this model considers local variables on the contrary of the SEA. However, in this model, a smooth frequency response is predicted which can be interpreted as the frequency average response.

1.1.5 Alternative Approaches for Vibration Analysis

As an alternative to the works based on local methods such as the FEM and BEM, many free vibration studies performed by semi-analytical, meshless and grid based global approaches exist in the literature. Analysis principle of these methods is based

on the numerical solution of differential equation of a structural vibration. These methods show very good accuracy compared to local methods. However, handling complex structures and complex boundary conditions by global methods are restricted.

Together with the increase in the use of composite materials, recent studies are generally based on free vibration analysis of composite structural elements. Semi-analytical approaches such as Ritz, *p*-Ritz and Rayleigh-Ritz approaches are successfully employed in the vibration analysis of laminated plates (Hearmon, 1959; Leissa & Narita, 1989; Liew & Lim, 1995; Liew, 1996; Liew, Lam & Chow, 1989; Chow, Liew & Lam, 1992; Hung, Liew, Lim, & Leong, 1993; Dawe & Roufaeil, 1980; Venini & Mariani, 1997). Differential quadrature technique introduced by Bellman, Kashef & Casti (1972) has been also commonly applied in vibration analysis for both isotropic and composite plates (Bert & Malik, 1996; Zeng & Bert, 2001; Zhang, Ng & Liew, 2003; Liew, Huang & Reddy, 2003; Lanhe, Hua & Daobin, 2005; Liew, Wang, Ng, & Tan, 2004). Besides, some meshless methods, pseudospectral and radial basis function methods have been increasingly used for free vibration analysis of isotropic and composite structures (Wang, Liew, Tan, & Rajendran, 2002; Dai, Liu, Lim, & Chen, 2004; Lee & Schultz, 2004; Ferreira & Fasshauer, 2006; Liu, Chua & Ghista, 2007).

In the last decade, a novel approach called Discrete Singular Convolution (DSC) has been introduced by Wei (1999, 2000a, 2000b, 2000c). This is a powerful method for the numerical solution of differential equations. The solution technique of the DSC is based on the theory of distribution and wavelets. The DSC has local methods' flexibility and global methods' accuracy. This approach has been successfully used in various free vibration analyses of isotropic thin simple structures with several boundary conditions (Wei, 2001a, 2001b, 2001c; Wei, Zhao & Xiang, 2001, 2002a; Xiang, Zhao & Wei, 2002; Zhao, Wei & Xiang, 2002a, 2005). Hou, Wei & Xiang (2005) have used DSC-Ritz method for free vibration analysis of thick plates. Civalek (2007a, 2007b, 2007c, 2007d) has applied the DSC to the free vibration and buckling analyses of different laminated shells and plates. Seçgin, Atas

& Sarıgül (2007) have used the DSC for free vibration of fiber-metal laminated composite plates. Seçgin & Sarıgül (2008) have presented open algorithm of the DSC and have shown the superiority of the DSC over several numerical techniques for free vibration analysis of symmetrically laminated composite plates.

Moreover, for high frequency free vibration analysis, Wei, Zhao & Xiang (2002b) and Zhao, Wei & Xiang (2002b) have obtained ten thousands of vibration modes for thin beams and plates. Lim, Li & Wei (2005) have used DSC-Ritz approach for high frequency modal analysis of thick shells. Ng, Zhao & Wei (2004) have pointed out that the DSC yields more accurate prediction compared to differential quadrature method for the plates vibrating at high frequencies.

1.2 Objective of the Thesis

> …. the prediction of medium to high frequency vibration levels is a particularly difficult task. …. there is no single technique which can be applied with confidence to all types of aerospace structures. Furthermore, there are certain problems of pressing practical concern for which it is not possible at present to make a reliable design prediction of high frequency vibration levels. …. (Wei et al., 2002b).

As Wei et al. (2002b) stated by quoting from Professors Langley and Bardell, there is not any method which can discretely predict spatial and frequency responses of a structure subjected to high frequency excitation without missing detailed local and modal information. Furthermore, there is not any unique method valid for all frequency ranges to perform response analysis.

The main objective of this thesis is to develop an efficient approach for high frequency response analysis of thin plates. The success of the DSC in high frequency free vibration analysis inspires that this method would be reliably used for discrete high frequency response analysis without handling averaged energetic parameters unlike available high frequency approaches. For this purpose, it is considered that

obtaining sufficient number of vibration modes by the DSC and accounting the contribution of these discrete modes to the response are key points in the development of an accurate method.

1.3 Thesis Organization

This thesis comprises nine chapters including introduction and conclusions, and appendices.

Chapter 1 mainly discusses the importance of vibro-acoustic analysis and presents a comprehensive literature review for conventional and state of art vibro-acoustic techniques. Besides, it presents an overall tabulation for conventional high frequency methods and deterministic techniques.

Chapter 2 gives a briefing on theoretical foundations of classical plate equations.

Chapter 3 presents the theory, discretization and boundary condition implementation procedures of Discrete Singular Convolution (DSC) method in detail.

Chapter 4 introduces a novel scheme named as Discrete Singular Convolution-Mode Superposition (DSC-MS) approach for high frequency response analysis of thin beams and plates.

Chapter 5 presents several verification and convergence tests of the DSC and DSC-MS.

Chapter 6 gives free and forced vibration analyses of thin plates. Besides, it demonstrates the capabilities of the DSC-MS in the discrete high frequency response prediction by performing self-explanatory numerical applications.

Chapter 7 presents implementation procedure of the DSC for composite plates. The accuracy of the approach is verified by comparing the DSC free vibration results with exact ones and those of some distinguished studies in the open literature. Furthermore, some specific free vibration applications of thin composite plates are given in detail.

Chapter 8 introduces a DSC representation for thick structures. The accuracy of the given approach is displayed by several comparison studies.

Chapter 9 gives a short review and underlines the outcomes of the Doctorate thesis with further suggestions.

Appendix A presents a brief information on the wavelet and wavelet analysis, Appendix B displays matrix representation of DSC algorithm, Appendix C shows a comparison between the DSC and FEM for higher vibration modes and Appendix D presents DSC codes for free vibration analysis of isotropic beams and plates.

CHAPTER TWO
CLASSICAL PLATE THEORY (CPT)

2.1 Introduction

In engineering, structural elements such as string, rod, beam, membrane and plate are main elements to build a complex structure. These elements have particular mechanical characteristics to guide a wave motion. The mathematics of the motion of these structural elements is arranged by strength-of-material theories. Table 2.1 represents the types of waves supported by some of the structural elements.

Thin structure theories are based on some assumptions on the kinematics of deformation. The term “thin” implies that the thickness of a structure is quite small compared to a characteristic length of that structure. In a thin structure, shear deformation and rotary inertia effects are neglected. This provides that a straight line perpendicular to the neutral axis of the beam or plate is inextensible, remains straight and only rotates about the undeformed axis (Figure 2.1).

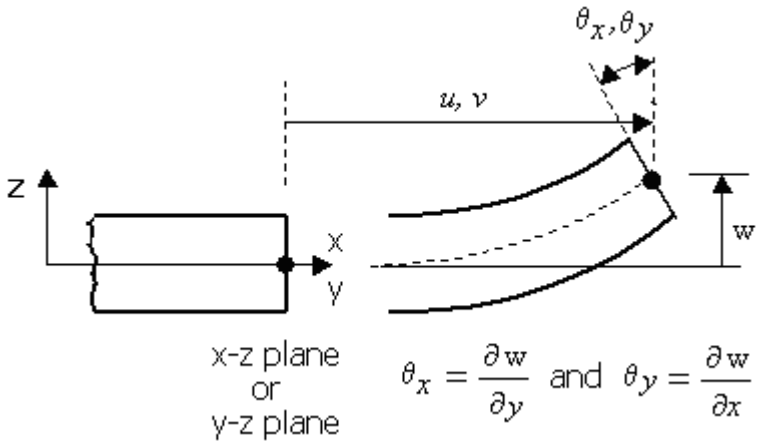

Figure 2.1 Mid-plane displacements of a bending thin plate.

Table 2.1 Wave guides and types of waves they support

Wave Guide	**Supporting Wave Types**
String	Transverse
Thin rod	Longitudinal
Membrane	Transverse
Thin beam (Bernouilli- Euler Beam Theory)	Longitudinal, Bending, Torsional
Thin plate (Classical Plate Theory)	Flexural, Torsional

2.2 Classical Plate Equations in Rectangular Coordinates

Figures 2.2.a and 2.2.b show separately force and moment resultants. It is assumed that mid-surface of the plate is subjected to distributed loads q_x, q_y and q_z as shown in Figure 2.2.c.

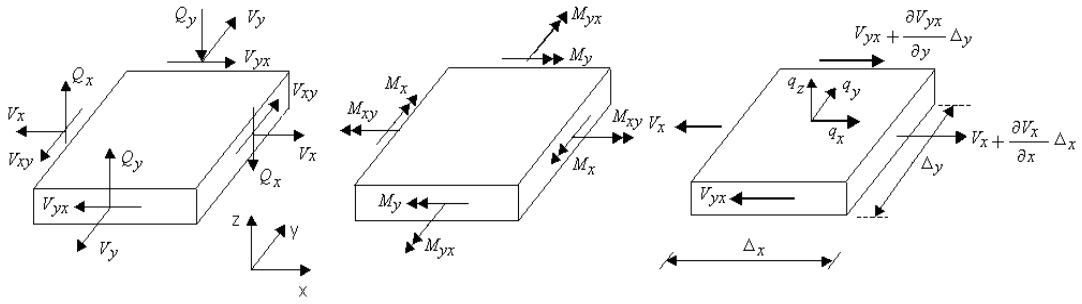

a) b) c)

Figure 2.2 Representation of a) Force resultants b) Moment resultants c) Force balance in x direction, on a plate.

The equilibrium equations, for example, in *x* direction can be written as

$$\sum F_x = \left(V_x + \frac{\partial V_x}{\partial x}\Delta x\right)\Delta y - V_x\Delta y + \left(V_{yx} + \frac{\partial V_{yx}}{\partial y}\Delta y\right)\Delta x - V_{yx}\Delta x + q_x\Delta x\Delta y = 0\,. \quad (2.1)$$

The same force equilibrium in Equation (2.1) can be written for the other two directions (*y* and *z*). Hence five equilibrium equations in terms of force and moment resultants are obtained as follows:

$$\frac{\partial V_x}{\partial x}+\frac{\partial V_{yx}}{\partial y}+q_x=0\ , \qquad \text{(a)}$$

$$\frac{\partial V_{xy}}{\partial x}+\frac{\partial V_y}{\partial y}+q_y=0\ , \qquad \text{(b)}$$

$$\frac{\partial Q_x}{\partial x}+\frac{\partial Q_y}{\partial y}-q_z=0 \qquad \text{(c)} \quad (2.2)$$

$$\frac{\partial M_x}{\partial x}-\frac{\partial M_{yx}}{\partial y}-Q_x=0\ , \qquad \text{(d)}$$

$$\frac{\partial M_{xy}}{\partial x}-\frac{\partial M_y}{\partial y}-Q_y=0\ . \qquad \text{(e)}$$

By using strength of material principles providing stress-strain and stress-displacement relations, bending and twisting moments are related to the displacements;

$$M_x=-D_0\left(\frac{\partial^2 w}{\partial x^2}+\nu\frac{\partial^2 w}{\partial y^2}\right), \qquad \text{(a)}$$

$$M_y=-D_0\left(\frac{\partial^2 w}{\partial y^2}+\nu\frac{\partial^2 w}{\partial y^2}\right), \qquad \text{(b)} \quad (2.3)$$

$$M_{xy}=-D_0(1-\nu)\frac{\partial^2 w}{\partial x\partial y}\ . \qquad \text{(c)}$$

where the flexural rigidity D_0 can be defined in terms of the elasticity modulus, E and the Poisson's ratio, ν, as follows

$$D_0=\frac{Eh^3}{12(1-\nu^2)}\ . \qquad (2.4)$$

Transverse shear forces are given by

$$Q_x = -D_0 \frac{\partial}{\partial x}\left(\nabla^2 w\right), \tag{2.5.a}$$

$$Q_y = -D_0 \frac{\partial}{\partial y}\left(\nabla^2 w\right) \tag{2.5.b}$$

and in-plane shear forces are

$$V_x = Q_x + \frac{\partial M_{xy}}{\partial y}, \tag{2.6.a}$$

$$V_y = Q_y + \frac{\partial M_{xy}}{\partial x} . \tag{2.6.b}$$

By employing in-plane equilibrium equations given in Equation (2.2) with the definitions of Equations (2.3) and (2.6), the differential equation of motion for the transverse displacement of a plate is obtained as (Leissa, 1969):

$$D_0 \nabla^4 w(x,y,t) + \rho h \frac{\partial^2 w(x,y,t)}{\partial t^2} = 0 . \tag{2.7}$$

The operator ∇^4 denotes

$$\nabla^4(\bullet) = \nabla^2 \cdot (\nabla^2)(\bullet) = \left(\frac{\partial^4}{\partial x^4} + 2\frac{\partial^4}{\partial x^2 \partial y^2} + \frac{\partial^4}{\partial y^4} \right)(\bullet) . \tag{2.8}$$

Time-harmonic free vibration displacement may be assumed in the form

$$w(x,y,t) = W(x,y)\, e^{j\omega t} \tag{2.9}$$

where $W(x,y)$ is the displacement depend on position coordinates. Substituting Equation (2.9) into Equation (2.7) yields

$$\left(\nabla^4 - \Omega^4\right) W = 0 . \tag{2.10}$$

Frequency parameter Ω is defined as

$$\Omega^2 = \sqrt{\frac{\rho_0 h}{D_0}}\,\omega^2 \quad . \tag{2.11}$$

For thin plates, some classical boundary conditions at the boundaries ($x(0, a)$, $y(0, b)$) are given as:

Fully simply-supported (SSSS):

$$w(0, y) = \frac{d^2 w(0, y)}{dx^2} = 0, \quad w(a, y) = \frac{d^2 w(a, y)}{dx^2} = 0\,, \tag{2.12.a}$$

$$w(x,0) = \frac{d^2 w(x,0)}{dy^2} = 0, \quad w(x, b) = \frac{d^2 w(x, b)}{dy^2} = 0\,. \tag{2.12.b}$$

Fully clamped (CCCC):

$$w(0, y) = \frac{dw(0, y)}{dx} = 0, \quad w(a, y) = \frac{dw(a, y)}{dx} = 0\,, \tag{2.13.a}$$

$$w(x,0) = \frac{dw(x,0)}{dy} = 0, \quad w(x, b) = \frac{dw(x, b)}{dy} = 0\,. \tag{2.13.b}$$

CHAPTER THREE
DISCRETE SINGULAR CONVOLUTION (DSC) APPROACH

3.1 Introduction

Discrete Singular Convolution (DSC) approach was originally introduced by Wei (1999, 2000a, 2000b, 2000c). The mathematical basis of the DSC is the distribution theory and wavelets. Although, the method numerically solves differential equations in a spatial domain as the other global methods, the DSC can be regarded as a unique method having both; local methods' flexibility and global methods' accuracy. The method requires a grid representation to define a structure with several grid points and utilizes certain auxiliary points so that a symmetric computational domain is being created. The DSC uses wavelet scaling functions as a convolution kernel to accommodate an interpolation function between structure and auxiliary points.

This approach has been successfully used for numerical solutions of several differential equations and various free vibration analyses of simple structures as stated in Chapter 1. Especially for high frequency free vibration analysis, thousands of modes are accurately obtained by the DSC. Therefore, in the present doctorate study, the DSC is mainly considered as a numerical tool to solve high frequency free and forced vibration analyses. In this chapter, the theory, discretization and boundary condition implementation procedures of the DSC are presented in detail.

3.2 The Discrete Singular Convolution (DSC)

3.2.1 Theory of the DSC

Singular convolution is defined by the theory of distributions. Let T be a distribution and $\eta(t)$ be an element of the space of test functions. Then, a singular convolution can be given by (Wei, 1999)

$$F(t) = \left(T * \eta\right)(t) = \int_{-\infty}^{\infty} T(t-x)\ \eta(x)\, dx \ . \tag{3.1}$$

Here, the sign * is the convolution operator, $F(t)$ is the convolution of η and T, $T(t-x)$ is the singular kernel of the convolution integral. Delta kernel is an interpolation function essential for the numerical solution of partial differential equations;

$$T(x) = \delta^n(x) \qquad n = 0,1,2,\cdots \quad . \tag{3.2}$$

Delta kernels given in Equation (3.2) are proper for use in vibration analysis. However, these kernels are singular; thus, they can not be digitized directly in computer. In order to avoid this problem, sequences of approximations T_α of the distributions T can be constructed such that T_α converge to T:

$$\lim_{\alpha \to \alpha_0} T_\alpha(x) \to T(x) \tag{3.3}$$

where α_0 is a generalized limit. With a good approximation, a Discrete Singular Convolution (DSC) can be determined as

$$F_\alpha(x) = \sum_k T_\alpha(x - x_k)\, f(x_k) \quad . \tag{3.4}$$

Here, $F_\alpha(x)$ is an approximation to $F(x)$ and $\{x_k\}$ is an approximate set of discrete points on which the DSC in Equation (3.4) is well defined. $f(x)$ is used here as the test function replacing the original test function $\eta(x)$. A sequence of approximation can be improved by a regularizer in order to increase the regularity of convolution kernels. Gaussian regularizer is a typical delta regularizer and it is in the form of

$$R_\sigma(x) = e^{-x^2/2\sigma^2} \tag{3.5}$$

Delta kernel with sampling parameter α approximately in the form,

$$T_\alpha = \frac{\sin \alpha x}{\pi x} \tag{3.6}$$

is known as Shannon father wavelet (scaling function). Wavelets and wavelet analysis are briefly introduced in Appendix A. In vibration analysis, a discretized form of Equation (3.6), which is sampled by Nyquist frequency ($\alpha = \pi/\Delta$) and improved by Gaussian regularizer, can be chosen as the kernel function of the DSC (Wei, 1999):

$$\delta_{\pi/\Delta,\sigma}(x - x_k) = \frac{\sin\left[\pi/\Delta\left(x - x_k\right)\right]}{\pi/\Delta\left(x - x_k\right)} \exp\left(-(x - x_k)^2/2\sigma^2\right) . \tag{3.7}$$

Here, Δ is determined by considering required precision of the analysis. The DSC expression in Equation (3.4) can be rewritten by using Regularized Shannon Delta Kernel (RSDK) given in Equation (3.7):

$$f(x) \approx \sum_{k=-\infty}^{\infty} \frac{\sin\left[\pi/\Delta\left(x - x_k\right)\right]}{\pi/\Delta\left(x - x_k\right)} \exp\left(-(x - x_k)^2/2\sigma^2\right) f\left(x_k\right) . \tag{3.8}$$

As seen in Equation (3.8), since DSC approach is defined in an infinite region, the kernels must be bounded in a sufficient computational domain for numerical determination. This can be practically achieved by a spatial truncation of the convolution kernel. A translationally invariant symmetric truncation algorithm can be used in an efficient bandwidth $\left(2M+1\right)$ as follows;

$$f^{(n)}(x_m) \approx \sum_{k=-M}^{M} \delta^{(n)}_{\pi/\Delta,\sigma}\left(x_m - x_k\right) f\left(x_k\right) . \tag{3.9}$$

Here, x_m is the specific central point considered and $\delta^{(n)}_{\pi/\Delta,\sigma}\left(x\right)$ is the n_{th} derivative of $\delta\left(x\right)$ given in Equation (3.7) with respect to *x*. First, second, third and fourth order derivatives of the RSDK can be analytically given respectively by

$$\delta^{(1)}_{\pi/\Delta,\sigma}(x_m - x_k) = \left(\frac{\cos[\pi/\Delta(x_m - x_k)]}{(x_m - x_k)} - \frac{\sin[\pi/\Delta(x_m - x_k)]}{\pi/\Delta(x_m - x_k)^2} - \frac{\sin[\pi/\Delta(x_m - x_k)]}{\pi/\Delta\sigma^2} \right) \times \exp\left(-(x_m - x_k)^2/2\sigma^2\right), \tag{3.10}$$

$$\delta^{(2)}_{\pi/\Delta,\sigma}(x_m - x_k) = \left\{ -\left(\frac{(\pi/\Delta)\sin[\pi/\Delta(x_m - x_k)]}{(x_m - x_k)} + 2\frac{\cos[\pi/\Delta(x_m - x_k)]}{(x_m - x_k)^2} \right) - \left(2\frac{\cos[\pi/\Delta(x_m - x_k)]}{\sigma^2} - 2\frac{\sin[\pi/\Delta(x_m - x_k)]}{\pi/\Delta(x_m - x_k)^3} \right) + \left(\frac{\sin[\pi/\Delta(x_m - x_k)]}{\pi/\Delta(x_m - x_k)\sigma^2} + \frac{\sin[\pi/\Delta(x_m - x_k)]}{\pi/\Delta\sigma^4}(x_m - x_k) \right) \right\} \times \exp\left(-(x_m - x_k)^2/2\sigma^2\right), \tag{3.11}$$

$$\delta^{(3)}_{\pi/\Delta,\sigma}(x_m - x_k) = \left\{ -\left(\frac{(\pi^2/\Delta^2)\cos[\pi/\Delta(x_m - x_k)]}{(x_m - x_k)} + 3\frac{(\pi/\Delta)\sin[\pi/\Delta(x_m - x_k)]}{(x_m - x_k)^2} \right) + \left(3\frac{(\pi/\Delta)\sin[\pi/\Delta(x_m - x_k)]}{\sigma^2} + 6\frac{\cos[\pi/\Delta(x_m - x_k)]}{(x_m - x_k)^3} + 3\frac{\cos[\pi/\Delta(x_m - x_k)]}{(x_m - x_k)\sigma^2} \right) + \left(3\frac{(x_m - x_k)\cos[\pi/\Delta(x_m - x_k)]}{\sigma^4} - 6\frac{\sin[\pi/\Delta(x_m - x_k)]}{\pi/\Delta(x_m - x_k)^4} - 3\frac{\sin[\pi/\Delta(x_m - x_k)]}{\pi/\Delta(x_m - x_k)^2\sigma^2} \right) - \left(\frac{(x_m - x_k)^2\sin[\pi/\Delta(x_m - x_k)]}{\pi/\Delta\sigma^6} \right) \right\} \times \exp\left(-(x_m - x_k)^2/2\sigma^2\right) \tag{3.12}$$

and

$$\delta^{(4)}_{\pi/\Delta,\sigma}(x_m - x_k) = \left\{ \left(4\frac{(\pi^2/\Delta^2)\cos[\pi/\Delta(x_m - x_k)]}{(x_m - x_k)^2} + \frac{(\pi^3/\Delta^3)\sin[\pi/\Delta(x_m - x_k)]}{(x_m - x_k)} \right) + \left(4\frac{(\pi^2/\Delta^2)\cos[\pi/\Delta(x_m - x_k)]}{\sigma^2} - 12\frac{(\pi/\Delta)\sin[\pi/\Delta(x_m - x_k)]}{(x_m - x_k)^3} \right)$$

$$
-\left(6\frac{(\pi/\Delta)\sin\left[\pi/\Delta\left(x_m-x_k\right)\right]}{\left(x_m-x_k\right)\sigma^2}+6\frac{(\pi/\Delta)\left(x_m-x_k\right)\sin\left[\pi/\Delta\left(x_m-x_k\right)\right]}{\sigma^4}\right)
$$

$$
-\left(24\frac{\cos\left[\pi/\Delta\left(x_m-x_k\right)\right]}{\left(x_m-x_k\right)^4}+12\frac{\cos\left[\pi/\Delta\left(x_m-x_k\right)\right]}{\left(x_m-x_k\right)^2\sigma^2}\right)
$$

$$
-\left(4\frac{\left(x_m-x_k\right)^2\cos\left[\pi/\Delta\left(x_m-x_k\right)\right]}{\sigma^6}-24\frac{\sin\left[\pi/\Delta\left(x_m-x_k\right)\right]}{\pi/\Delta\left(x_m-x_k\right)^5}\right)
$$

$$
+\left(12\frac{\sin\left[\pi/\Delta\left(x_m-x_k\right)\right]}{\pi/\Delta\left(x_m-x_k\right)^3\sigma^2}+3\frac{\sin\left[\pi/\Delta\left(x_m-x_k\right)\right]}{\pi/\Delta\left(x_m-x_k\right)\sigma^4}\right)
$$

$$
-\left(2\frac{\left(x_m-x_k\right)\sin\left[\pi/\Delta\left(x_m-x_k\right)\right]}{\pi/\Delta\sigma^6}-\frac{\left(x_m-x_k\right)^3\sin\left[\pi/\Delta\left(x_m-x_k\right)\right]}{\pi/\Delta\sigma^8}\right)\Bigg\}
$$

$$
\times\exp\left(-\left(x_m-x_k\right)^2/2\sigma^2\right). \qquad (3.13)
$$

The values of these differentiated kernels at $x_m = x_k$ are obtained as follows:

$$
\lim_{x_k\to x_m}\delta^{(1)}_{\pi/\Delta,\sigma}(x_m-x_k)\to\delta^{(1)}_{\pi/\Delta,\sigma}(0)=0\ , \qquad (3.14)
$$

$$
\lim_{x_k\to x_m}\delta^{(2)}_{\pi/\Delta,\sigma}(x_m-x_k)\to\delta^{(2)}_{\pi/\Delta,\sigma}(0)=-\frac{1}{\sigma^2}-\frac{\pi^2}{3\Delta^2}\quad , \qquad (3.15)
$$

$$
\lim_{x_k\to x_m}\delta^{(3)}_{\pi/\Delta,\sigma}(x_m-x_k)\to\delta^{(3)}_{\pi/\Delta,\sigma}(0)=0 \qquad (3.16)
$$

and

$$
\lim_{x_k\to x_m}\delta^{(4)}_{\pi/\Delta,\sigma}(x_m-x_k)\to\delta^{(4)}_{\pi/\Delta,\sigma}(0)=\frac{3+2\left(\pi^2/\Delta^2\right)\sigma^2+\left(\pi^4/5\Delta^4\right)\sigma^4}{\Delta^4}\quad . \qquad (3.17)
$$

3.2.2 DSC Discretization of Operator

In the DSC implementation to any differential equation, a linear DSC operator **L** having a differential part **D** and a function part **F** is written as,

$$\mathbf{L} = \mathbf{D} + \mathbf{F} . \tag{3.18}$$

It is essential to define a grid representation so that the function part of the operator is diagonal. Hence, the grid discretization is simply given by a direct interpolation:

$$\mathbf{F}(x) \to \mathrm{F}(x_k)\,\delta^{(0)}_{\pi/\Delta,\sigma}(x_m - x_k) \tag{3.19}$$

where $\delta^{(0)}_{\pi/\Delta,\sigma}(x_m - x_k)$ is the RSDK given in Equation (3.7). The differential part of the operator on the coordinate grid is then represented by functional derivatives;

$$\mathbf{D} = \sum_n d_n(x)\frac{d^n}{dx_n} \to \sum_n d_n(x_m)\,\delta^{(n)}_{\pi/\Delta,\sigma}\left(x_m - x_k\right) \tag{3.20}$$

where d_n is a coefficient. Finally, linear DSC operator **L** can be rewritten by summing Equations (19) and (20):

$$\mathbf{L}(x_m - x_k) = \sum_n d_n(x_m)\,\delta^{(n)}_{\pi/\Delta,\sigma}\left(x_m - x_k\right) + \mathrm{F}(x_k)\,\delta^{(0)}_{\pi/\Delta,\sigma}(x_m - x_k),\ n \neq 0 . \tag{3.21}$$

3.2.3 Grid Discretization in DSC Algorithm

A thin beam having length a is illustrated in Figure 3.1 as an example to DSC grid discretization. Structure points $(x_0, x_1, \cdots, x_{N-1})$ are defined with uniform interval $\Delta = a/(N-1)$. The function derivatives on these points are approximated by a linear summation of function values on the $2M+1$ points centred at those points. Since the summation requires function values at the points outside the structural domain, M

auxiliary points can be fictitiously positioned both on the left and right side of the structural domain. For an effective algorithm, three indices; $i = 0,1,2,\cdots,N-1$, $k = -M,\cdots,0,\cdots,M$ and $j = -M,\cdots,0,\cdots,N-1+M$ may be determined with the condition that $N \geq M+1$. Regarding these determinations, DSC given in Equation (3.9) can be rewritten as

$$F^{(n)}(x_i) \approx \sum_{k=-M}^{M} \delta^{(n)}_{\pi/\Delta,\sigma}(x_i - x_k)\, F\left(x_{i+k}\right) . \tag{3.22}$$

By using translationally invariant algorithm, a set of $(2M+1)$ coefficients for $\forall i \in \{0,1,\ldots,N-1\}$ points is obtained ($k\Delta = (x_0 - x_k) = (x_1 - x_k) = \ldots = (x_{N-1} - x_k)$):

$$\left\{ C^{(n)}_{-M},\cdots,C^{(n)}_{0},\cdots,C^{(n)}_{M} \right\} = \left\{ \delta^{(n)}_{\pi/\Delta,\sigma}(-M\Delta),\cdots,\delta^{(n)}_{\pi/\Delta,\sigma}(0),\cdots,\delta^{(n)}_{\pi/\Delta,\sigma}(M\Delta) \right\} . \tag{3.23}$$

Thus, the DSC reduces to

$$F^{(n)}(x_i) \approx \sum_{k=-M}^{M} C^{(n)}_{k}\, F\left(x_{i+k}\right) . \tag{3.24}$$

Similar representations and notations can be properly defined for other structures such as plates and acoustic enclosures.

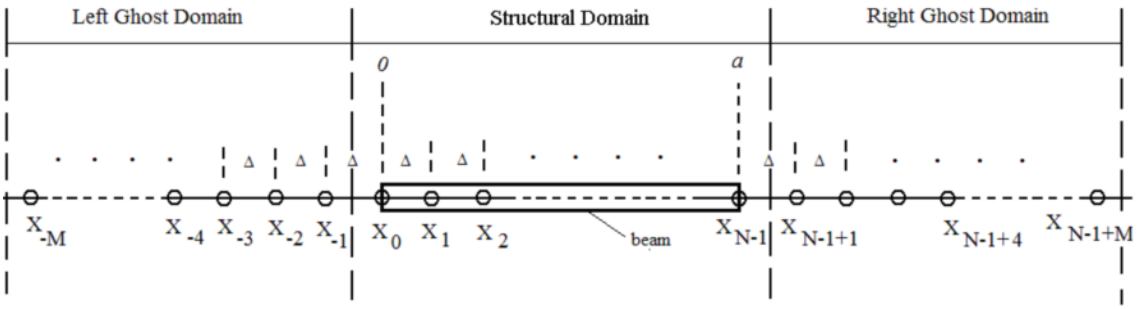

Figure 3.1 Computational domain representation for a beam structure in DSC algorithm.

3.2.4 Boundary Condition Implementation in DSC Algorithm

The numerical scheme of the DSC is completed by implementing appropriate boundary conditions to a system of equation. As an example, for a beam structure, the boundary implementation procedure is given by making an assumption on the relation between the auxiliary points and structure points shown in Figure 3.1. The relation between the left-right ghost domains and the computational domain may be expressed as (Wei, 2001a, 2001b, 2001c) in terms of a displacement function W:

For left boundary, $$W(x_{-p}) - W(x_0) = A_p \left[\left(W(x_p) - W(x_0)\right)\right] . \quad (3.25)$$

For right boundary, $$W(x_{N-1+p}) - W(x_{N-1}) = B_p \left[\left(W(x_{N-1-p}) - W(x_{N-1})\right)\right] . \quad (3.26)$$

Here p is an arbitrary index (p = 1,…, M). A_p and B_p are determined by using boundary conditions. After rearrangement, Equations (3.25) and (3.26) become

$$W(x_{-p}) = A_p W(x_p) + \left(1 - A_p\right) W(x_0) \quad (3.27)$$

and

$$W(x_{N-1+p}) = B_p W(x_{N-1-p}) + (1 - B_p) W(x_{N-1}), \quad (3.28)$$

respectively. According to DSC definition given in Equation (3.24), the first and second derivative of a displacement function W at the left boundary (x_0) can be approximated by using Equation (3.27) as:

$$\frac{dW}{dx}(x_0) \approx \sum_{k=-M}^{M} C_k^{(1)} W\left(x_k\right) = \sum_{k=1}^{M} C_k^{(1)} W\left(x_k\right) + C_0{}^{(1)} W(x_0) + \sum_{k=1}^{M} C_{-k}^{(1)} W\left(x_{-k}\right)$$

$$= \sum_{k=1}^{M} C_k^{(1)}\, W(x_k) + C_0{}^{(1)} W(x_0) - \sum_{k=1}^{M} C_k^{(1)} \left\{ A_p\, W(x_k) + (1 - A_p) W(x_0) \right\}$$

$$= \left[C_0{}^{(1)} - \sum_{k=1}^{M} C_k^{(1)} (1 - A_p) \right] W(x_0) + \sum_{k=1}^{M} C_k^{(1)}\, (1 - A_p) W(x_k) \qquad (3.29)$$

and

$$\frac{d^2 W}{dx^2}(x_0) \approx \sum_{k=-M}^{M} C_k^{(2)}\, W(x_k) = \sum_{k=1}^{M} C_k^{(2)}\, W(x_k) + C_0{}^{(2)} W(x_0) + \sum_{k=1}^{M} C_{-k}^{(2)}\, W(x_{-k})$$

$$= \sum_{k=1}^{M} C_k^{(2)}\, W(x_k) + C_0{}^{(2)} W(x_0) + \sum_{k=1}^{M} C_k^{(2)} \left\{ A_p\, W(x_k) + (1 - A_p) W(x_0) \right\}$$

$$= \left[C_0{}^{(2)} + \sum_{k=1}^{M} C_k^{(2)} (1 - A_p) \right] W(x_0) + \sum_{k=1}^{M} C_k^{(2)}\, (1 + A_p) W(x_k) \ . \qquad (3.30)$$

By performing the same operations for the right boundary yields

$$\frac{dW}{dx}(x_{N-1}) \approx \sum_{k=-M}^{M} C_k^{(1)}\, W(x_{N-1+k})$$

$$= \sum_{k=1}^{M} C_k^{(1)}\, W(x_{N-1+k}) + C_0{}^{(1)} W(x_{N-1}) + \sum_{k=1}^{M} C_{-k}^{(1)}\, W(x_{N-1-k})$$

$$= \sum_{k=1}^{M} C_k^{(1)}\, \left\{ B_p\, W(x_{N-1-k}) + (1 - B_p) W(x_{N-1}) \right\} + C_0{}^{(1)} W(x_{N-1}) - \sum_{k=1}^{M} C_k^{(1)}\, W(x_{N-1-k})$$

$$= \left[C_0{}^{(1)} + \sum_{k=1}^{M} C_k^{(1)} (1 - B_p) \right] W(x_{N-1}) - \sum_{k=1}^{M} C_k^{(1)} (1 - B_p)\, W(x_{N-1-k}) \qquad (3.31)$$

and

$$\frac{d^2 W}{dx^2}(x_{N-1}) \approx \sum_{k=-M}^{M} C_k^{(2)}\, W(x_{N-1+k})$$

$$= \sum_{k=1}^{M} C_k^{(2)}\, W\left(x_{N-1+k}\right) + C_0^{(2)} W(x_{N-1}) + \sum_{k=1}^{M} C_{-k}^{(2)}\, W\left(x_{N-1-k}\right)$$

$$= \sum_{k=1}^{M} C_k^{(2)} \left\{B_p\, W(x_{N-1-k}) + (1-B_p) W(x_{N-1})\right\} + C_0^{(2)} W(x_{N-1}) + \sum_{k=1}^{M} C_k^{(2)}\, W\left(x_{N-1-k}\right)$$

$$= \left[C_0^{(2)} + \sum_{k=1}^{M} C_k^{(2)}\, (1-B_p) \right] W(x_{N-1}) + \sum_{k=1}^{M} C_k^{(2)} (1+B_p)\, W(x_{N-1-k}) . \qquad (3.32)$$

Equations (3.29)-(3.32) are constructed by the fact that $C_{-k}^{(1)} = -C_k^{(1)}$ and $C_{-k}^{(2)} = C_k^{(2)}$. For classical boundary conditions, since $W(x_0) = W(x_{N-1}) = 0$, selecting $A_p = B_p = A = -1$ and $A_p = B_p = A = +1$, for all p, satisfies simply supported and clamped boundary conditions, respectively. Displacements of auxiliary points in the whole ghost domain can be written in terms of displacements of structural points in the computational domain for any differentiation degree (n). Then Equation (3.24) may be decomposed for each of structure points by using the relations given in Equations (3.27) and (3.28):

For $i = 0$;

$$\frac{d^{(n)}W}{dx^{(n)}}(x_0) = \sum_{k=-M}^{M} C_k^{(n)}\, W\left(x_k\right) = C_{-M}^{(n)} W\left(x_{-M}\right) + C_{-M+1}^{(n)} W\left(x_{-M+1}\right) + \cdots + C_{-1}^{(n)} W\left(x_{-1}\right)$$
$$+ C_0^{(n)} W\left(x_0\right) + C_1^{(n)} W\left(x_1\right) + \cdots + C_M^{(n)} W\left(x_M\right) \qquad (3.33.a)$$

and Equation (3.33.a) leads to

$$\frac{d^{(n)}W}{dx^{(n)}}(x_0) = C_{-M}^{(n)} \left\{A\, W(x_M) + (1-A) W(x_0)\right\} + C_{-M+1}^{(n)} \left\{A\, W(x_{M+1}) + (1-A)\, W(x_0)\right\}$$
$$+ \cdots + C_{-1}^{(n)} \left\{A\, W(x_1) + (1-A) W(x_0)\right\} + C_0^{(n)} W\left(x_0\right)$$
$$+ C_1^{(n)} W\left(x_1\right) + \cdots + C_M^{(n)} W\left(x_M\right) . \qquad (3.33.b)$$

Finally, Equation (3.33.b) becomes

$$\frac{d^{(n)}W}{dx^{(n)}}(x_0)=\left(C_0^{(n)}+\sum_{k=-M}^{-1}(1-A)C_k^{(n)}\right)W(x_0)+\left(C_1^{(n)}+C_{-1}^{(n)}A\right)W(x_1)$$
$$+\cdots+\left(C_M^{(n)}+C_{-M}^{(n)}A\right)W(x_M)\ . \qquad (3.33.c)$$

Similarly, for i = 1;

$$\frac{d^{(n)}W}{dx^{(n)}}(x_1)=\left(C_{-1}^{(n)}+\sum_{k=-M}^{-2}(1-A)C_k^{(n)}\right)W(x_0)+\left(C_0^{(n)}+C_{-2}^{(n)}A\right)W(x_1)$$
$$+\left(C_1^{(n)}+C_{-3}^{(n)}A\right)W(x_2)+\cdots+C_{M-1}^{(n)}\,W(x_M)+C_M^{(n)}\,W(x_{M+1})\ . \qquad (3.34)$$

.
.
.

For i = N-2;

$$\frac{d^{(n)}W}{dx^{(n)}}(x_{N-2})=\left(C_1^{(n)}+\sum_{k=2}^{M}(1-A)C_k^{(n)}\right)W(x_{N-1})+\left(C_0^{(n)}+C_2^{(n)}A\right)W(x_{N-2})$$
$$+\left(C_{-1}^{(n)}+C_3^{(n)}A\right)W(x_{N-3})+\cdots+\left(C_{-M+2}^{(n)}+C_M^{(n)}A\right)W(x_{N-M})\ . \qquad (3.35)$$

For i = N-1;

$$\frac{d^{(n)}W}{dx^{(n)}}(x_{N-1})=\left(C_0^{(n)}+\sum_{k=1}^{M}(1-A)C_k^{(n)}\right)W(x_{N-1})+\left(C_{-1}^{(n)}+C_1^{(n)}A\right)W(x_{N-2})$$
$$+\left(C_{-2}^{(n)}+C_2^{(n)}A\right)W(x_{N-3})+\cdots+\left(C_{-M}^{(n)}+C_M^{(n)}A\right)W(x_{N-1-M})\ . \qquad (3.36)$$

General DSC matrix representations formed by Equations (3.33)-(3.36) for an eigenvalue problem are illustrated in Appendix B.

CHAPTER FOUR
DISCRETE SINGULAR CONVOLUTION-MODE SUPERPOSITION (DSC-MS) APPROACH

4.1 Introduction

It is known that the DSC is able to accurately predict very higher number of natural modes for a structural system. As proper for the objective of the thesis, it was purposed to reliably use this high amount of modes for the discrete prediction of high frequency vibration response by utilizing mode superposition (MS) technique. The MS is a common approach assuming a solution that all system modes discretely contribute to local displacement response. In this chapter, a novel scheme based on the DSC and MS is introduced in detail.

4.2 Discrete Singular Convolution-Mode Superposition (DSC-MS) Scheme

4.2.1 Mode Superposition (MS) Technique for Thin Plates

The mathematical foundation of the MS is based on the separation of variables. Bending displacement response of a plate $w(x,y,t)$ can be expressed by infinite summation of the product of two variables; $\phi_p(x,y)$, and $w_p(t)$ (Timoshenko, Young & Weaver, 1971):

$$w(x,y,t) = \sum_{p=1}^{\infty} w_p(t)\phi_p(x,y) \quad . \tag{4.1}$$

Equation (4.1) can be approximately written in terms of sufficient number of modes P contributing the response:

$$w(x,y,t) \approx \sum_{p=1}^{P} w_p(t)\phi_p(x,y) \quad . \tag{4.2}$$

The equation of bending motion of a thin plate, given in Equation (2.7), with internal loss factor $\zeta < 1$ and harmonic forced term $f(x,y,t)$ can be rewritten as follows:

$$D^2(1+j\zeta)\nabla^4 w(x,y,t) + \ddot{w}(x,y,t) = \frac{1}{\rho_0 h} f(x,y,t) \tag{4.3}$$

where $D^2 = D_0/\rho_0 h$. By applying Equation (4.2) to the homogenous part of Equation (4.3) yields,

$$D^2(1+\zeta^2)\sum_{p=1}^{P}\nabla^4\phi_p(x,y)\,w_p(t) + (1-j\zeta)\sum_{p=1}^{P}\phi_p(x,y)\,\ddot{w}_p(t) = 0 \ . \tag{4.4}$$

Equation (4.4) leads to following equations:

$$D^2(1+\zeta^2)\sum_{p=1}^{P}\nabla^4\phi_p(x,y)\frac{1}{\phi_p(x,y)} = -(1-j\zeta)\sum_{p=1}^{P}\ddot{w}_p(t)\frac{1}{w_p(t)} = \sum_{p=1}^{P}k_p \ , \tag{4.5}$$

$$D^2(1+\zeta^2)\sum_{p=1}^{P}\nabla^4\phi_p(x,y) - \sum_{p=1}^{P}k_p\phi_p(x,y) = 0 \ , \tag{4.6}$$

$$(1-j\zeta)\sum_{p=1}^{P}\ddot{w}_p(t) + \sum_{p=1}^{P}k_p w_p(t) = 0 \ . \tag{4.7}$$

Here k_p is always a positive number which represents the square of the natural frequency of the *p*th mode, ω_p.

For multi excitations, point force $f(x,y,t) = \sum_{i=1}^{N}\sum_{j=1}^{N} f_{i,j}(t)\delta(x-x_i)\delta(y-y_j)$ (δ is the Dirac-delta function) can be identified as

$$f(x,y,t)=\sum_{p=1}^{P}\left(\sum_{i=1}^{N}\sum_{j=1}^{N}f_{i,j}(t)\phi_p(x_i,y_j)\right) \quad . \tag{4.8}$$

4.2.2 DSC-MS Implementation

Defining a full mode shape function $\Phi_f=\sum_{p=1}^{P}\phi_p$ and applying DSC expression in Equation (3.22) or (3.24) to Equation (4.6) by introducing the non-dimensional parameters; $X=x/a$, $Y=y/b$, $\Phi=\Phi_f/a$, $\lambda=a/b$, $\Omega=\omega a^2/D\sqrt{1+\zeta^2}$ yields:

$$\begin{aligned}&\sum_{k=-M}^{M}\delta^{(4)}_{\pi/\Delta_x,\sigma}(k\Delta_x)\ \Phi(X_{i_x+k},Y)\\&\quad+2\lambda^2\sum_{k=-M}^{M}\delta^{(2)}_{\pi/\Delta_x,\sigma}(k\Delta_x)\ \Phi(X_{i_x+k},Y)\cdot\sum_{k=-M}^{M}\delta^{(2)}_{\pi/\Delta_y,\sigma}(k\Delta_y)\ \Phi(X,Y_{i_y+k})\\&\quad+\lambda^4\sum_{k=-M}^{M}\delta^{(4)}_{\pi/\Delta_y,\sigma}(k\Delta_y)\ \Phi(X,Y_{i_y+k})=\boldsymbol{\Omega}^2\boldsymbol{\Phi}(X,Y)\ .\end{aligned} \tag{4.9}$$

Here, the subscripts *x* and *y* of indices *i, j* denote direction of discretization points. $\boldsymbol{\Omega}$ is the diagonal natural frequency parameter matrix. The mode shape vector of the plate is formed as:

$$\boldsymbol{\Phi}=\left\{\Phi_{0,0},\ldots,\Phi_{0,N_y-1},\Phi_{1,0},\ldots,\Phi_{1,N_y-1},\ldots,\ldots,\Phi_{N_x-1,0},\ldots,\Phi_{N_x-1,N_y-1}\right\}^T \tag{4.10}$$

This discretization is illustrated in Figure 4.1.

DSC kernels in Equation (4.9) can be written in a DSC matrix form as (*r* = *x* or *y*);

$$\boldsymbol{\Psi}_r{}^{(n)}{}_{i_r,j_r}=\begin{cases}\delta^{(n)}_{\pi/\Delta_r,\sigma}((j_r-i_r)\Delta_r), & if\ -M\le j_r-i_r\le M\\ 0\ , & otherwise\end{cases}\ . \tag{4.11}$$

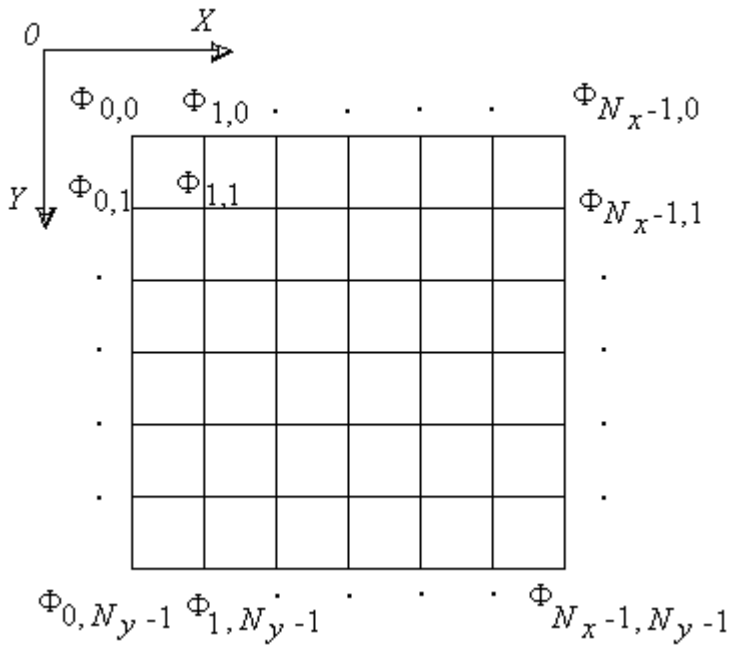

Figure 4.1 DSC grid representations for plates.

The numerical scheme of the DSC-MS is completed by implementing the boundary conditions to Equation (4.9). Any auxiliary point can be written in terms of structure points by using one of the proper relations in Equations (3.25) and (3.26). Then by using the DSC expression given in Equation (3.24) one can obtain the coefficients as $A=-1$ for SSSS and $A=1$ for CCCC plates. For these plates, after implementation of the displacement boundary condition $\mathbf{\Phi}(r_0)=\mathbf{\Phi}(r_{N-1})=0$, Equation (4.9) can be reconstructed by DSC matrices as an eigenvalue equation:

$$(\mathbf{T}-\mathbf{\Omega}^2)\,\mathbf{\Phi}=0 \quad . \tag{4.12}$$

Here $\mathbf{T}$ matrix can be expressed as,

$$\mathbf{T}=\left\{(\mathbf{\Gamma}_x{}^{(4)}\otimes\mathbf{I}_y)+2\lambda^2\,(\mathbf{\Gamma}_x{}^{(2)}\otimes\mathbf{\Gamma}_y{}^{(2)})+\lambda^4(\mathbf{I}_x\otimes\mathbf{\Gamma}_y{}^{(4)})\right\} \tag{4.13}$$

where $\mathbf{\Gamma}_r^{(n)}$ is the DSC characteristic matrix, $\mathbf{I}_r$ is the identity matrix. For square plates $\lambda=1$; $\mathbf{I}_x$ = $\mathbf{I}_y$. A characteristic matrix is obtained by applying specific boundary conditions to the DSC matrix $\mathbf{\Psi}_r{}^{(n)}{}_{N\times(2M+N)}$ defined in Equation (4.11).

From Equation (4.12), one can obtain natural frequencies $(\omega_1, \omega_2, \cdots, \omega_P)$ and the corresponding mode shapes $(\phi_1, \phi_2, \cdots, \phi_P)$ by using a standard solver.

Equation (4.7) can be reconstructed by the force term:

$$(1 - j\zeta)\sum_{p=1}^{P}\left(\ddot{w}_p(t) + \omega_p^2 w_p(t)\right) = \frac{1}{\rho h}\sum_{p=1}^{P}\left(\sum_{i=1}^{N}\sum_{j=1}^{N} f_{i,j}(t)\phi_p(x_i, y_j)\right) . \tag{4.14}$$

Assuming a harmonic response in the form of $w_p(t) = W_p e^{i\omega t}$, the steady-state frequency response can be obtained as follows;

$$W_p(\omega) = \frac{1}{\rho h}\sum_{p=1}^{P}\left(\frac{1}{\omega_p^2 - (1 - j\zeta)\omega^2}\sum_{i=1}^{N}\sum_{j=1}^{N} F_{i,j}(\omega)\phi_p(x_i, y_j)\right) \tag{4.15}$$

where $F_{i,j}(\omega)$ is the Fourier transform of $f_{i,j}(t)$. Substituting Equation (4.15) into Fourier transform of Equation (4.2), one can obtain a space-frequency dependent response equation for thin plates as follows;

$$W(x, y, \omega) = \frac{1}{\rho h}\sum_{p=1}^{P}\left(\frac{\phi_p(x, y)}{\omega_p{}^2 - (1 - j\zeta)\omega^2}\sum_{i=1}^{N}\sum_{j=1}^{N} F_{i,j}(\omega)\phi_p(x_i, y_j)\right) . \tag{4.16}$$

4.3 High Frequency Concept

In vibro-acoustics, modal overlap count is an indicator of the threshold of high frequency region. This count is defined as (Rabbiolo, Bernhard & Milner, 2004):

$$MO = \frac{\Delta f_n}{\delta f} = \frac{\zeta f_n}{\delta f} . \tag{4.17}$$

A schematic representation for these parameters is given in Figure 4.2. Rabbiolo et al. (2004) have defined three different high frequency thresholds based upon the approximate modal overlap counts; $\overline{MO} = 1$ for beams, $\overline{MO} = 2.5$ for plates and $\overline{MO} = 3$ for acoustic enclosures. Modal overlap count is also defined as follows (Fredö, 1997);

$$MO = \zeta \; f_c \, n(f) \; . \tag{4.18}$$

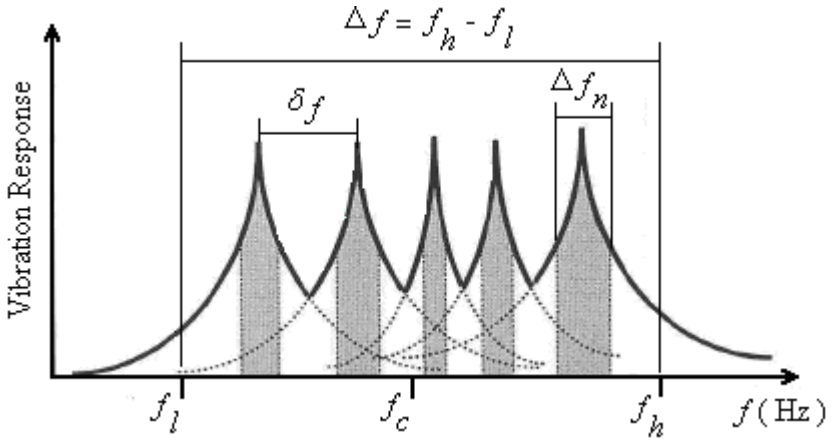

Figure 4.2 Representation of modal parameters in a bandwidth.

Modal density is the number of modes in a considered frequency bandwidth i.e., $n(f) = P/\Delta f$. For simple structures, modal density can be analytically determined. For instance, modal density for plates is given as (Harris & Piersoll, 2002a)

$$n(\omega) = \frac{A_s}{4\pi\sqrt{D_0 / \rho_0 h}} \quad . \tag{4.19}$$

It is noted that $n(f) = 2\pi n(\omega)$. Generally, if MO given in Equation (4.18) is higher than unity, the energy based approaches such as Statistical Energy Analysis (SEA) and Energy Finite Element Method (EFEM) can be reliably used in this region (Fahy & Mohammed, 1992). Equations (4.17) and (4.18) indicate that the modal overlap count is determined only for damped systems with a sufficiently wide frequency band. Therefore, for an undamped system solution, the modal overlap count can not be used as an indicator of high frequency range.

CHAPTER FIVE
VERIFICATION AND CONVERGENCE STUDIES OF THE DSC AND DSC-MS

5.1 Introduction

In this chapter, in order to expose the accuracy of DSC and DSC-MS methods, several verification and convergence tests are presented.

5.2 Verification and Convergence Study for the DSC

5.2.1 Verification of Natural Frequency Parameters and Mode Shapes

Table 5.1 compares natural frequency parameters predicted by the DSC with those of the analytical solutions for simply-supported thin beams and plates. Natural frequency parameters of the plates were defined as Ω^2/π^2 for numerical facility. Table 5.1 shows that as the number of grid points (N) increases the discrepancy between the DSC prediction and analytical results decreases. For beams, even with low grid numbers such as $N=11$, the first few natural frequency parameters are accurately predicted by the DSC. For $N=31$ grid points, analytical results are obtained up to the computed one ten-thousandth digits for the considered number of modes. Table 5.1 also shows an excellent prediction of frequency parameters for plates especially with $N=21\times21$ grid points. This perfect agreement clearly verifies the accuracy of the DSC.

Figure 5.1 displays well-known first four mode shapes of simply supported beam obtained by the DSC using $N=31$ grid points. In addition, a simple comparison demonstrating the accuracy of the DSC and finite element method (FEM) for high frequency analysis of beams is given in Appendix C.

Table 5.1 Verification and convergence study of DSC method for thin beams and plates

Beam (SS)					Square Plate (SSSS)			
Beam Length: $a = \pi$ meters. Natural frequency parameter: $\Omega = \omega\sqrt{\frac{\rho_0 A}{EI}}$					$\lambda = 1, D_\gamma = D_\phi = 1,$ $D_\alpha = D_\beta = 0$. Natural frequency parameter: $\Omega/\pi^2 = \omega\frac{a^2}{\pi^2}\sqrt{\frac{\rho_0 h}{D}}$			
Mode Number	DSC			Analytical (Timoshenko, Young & Weaver, 1971)	Mode Number (p, q)	DSC		Analytical (Whitney, 1987)
	N=11	N=21	N=31			N=11×11	N=21×21	
1	1.0050	1.0000	1.0000	1	(1,1)	2.0051	2.0000	2
2	3.9994	4.0000	4.0000	4	(1,2)	5.0006	5.0000	5
3	9.0095	9.0000	9.0000	9	(2,1)	5.0006	5.0000	5
4	16.0764	16.0000	16.0000	16	(2,2)	7.9993	8.0000	8
5	25.4813	25.0000	25.0000	25	(1,3)	10.0092	10.0000	10
6	38.0834	36.0000	36.0000	36	(3,1)	10.0092	10.0000	10
7	55.0104	49.0000	49.0000	49	(2,3)	13.0066	13.0000	13
8	75.1793	64.0000	64.0000	64	(3,2)	13.0066	13.0000	13
9	92.8390	81.0002	81.0000	81	(1,4)	17.0728	17.0000	17
10	-	100.0022	100.0000	100	(4,1)	17.0728	17.0000	17
11	-	121.0168	121.0000	121	(3,3)	18.0102	18.0000	18
12	-	144.1010	144.0000	144	(2,4)	20.0628	20.0000	20
13	-	169.4850	169.0000	169	(4,2)	20.0628	20.0000	20
14	-	197.8500	196.0000	196	(3,4)	25.0560	25.0000	25
15	-	230.5612	225.0000	225	(4,3)	25.0560	25.0000	25
16	-	269.0423	256.0000	256	(1,5)	26.4671	26.0000	26
17	-	312.5090	289.0000	289	(5,1)	26.4671	26.0000	26
18	-	355.4072	324.0000	324	(2,5)	29.4290	29.0000	29
19	-	387.8306	361.0000	361	(5,2)	29.4290	29.0000	29
20	-	-	400.0000	400	(4,4)	32.0854	32.0000	32

5.2.2 Convergence of Natural Frequency Parameters

In order to demonstrate the convergence of natural frequency parameters obtained by the DSC, three different number of discretization points *N* associated with three different discretization parameters *r* are considered. The relative error is defined as $100 \times (\Omega_A - \Omega_D)/\Omega_A$, where Ω_A and Ω_D are non-dimensional frequency parameters obtained analytically and by the DSC, respectively.

The discretization parameter for regularization r is defined as a ratio depending on the regularization parameter σ and the discretization interval Δ, i.e., $r = \sigma/\Delta$. In addition to the selection of high number of discretization points, the reliable modal prediction also directly depends on the appropriate selection of discretization parameter. However, adapting very low and very high r values may cause some numerical instability. The proper selection of r value can be made by trial and error method. Actually, Qian & Wei (2000) have presented a mathematical estimation for the relative selection of r, σ and M in a reliable wide range. According to this estimation, $r(\pi - B\Delta) > \sqrt{4.61\eta}$ and $\frac{M}{r} > \sqrt{4.61\eta}$ should be satisfied for reliable DSC analysis. Here, B is the frequency bound for a function of interest. η is the order of approximation error leading to the error value of $10^{-\eta}, (\eta > 0)$ for the considered function. Some brief statements for this estimation can also be found in (Wei, 2001c; Wei et al., 2002a; Zhao et al., 2002a).

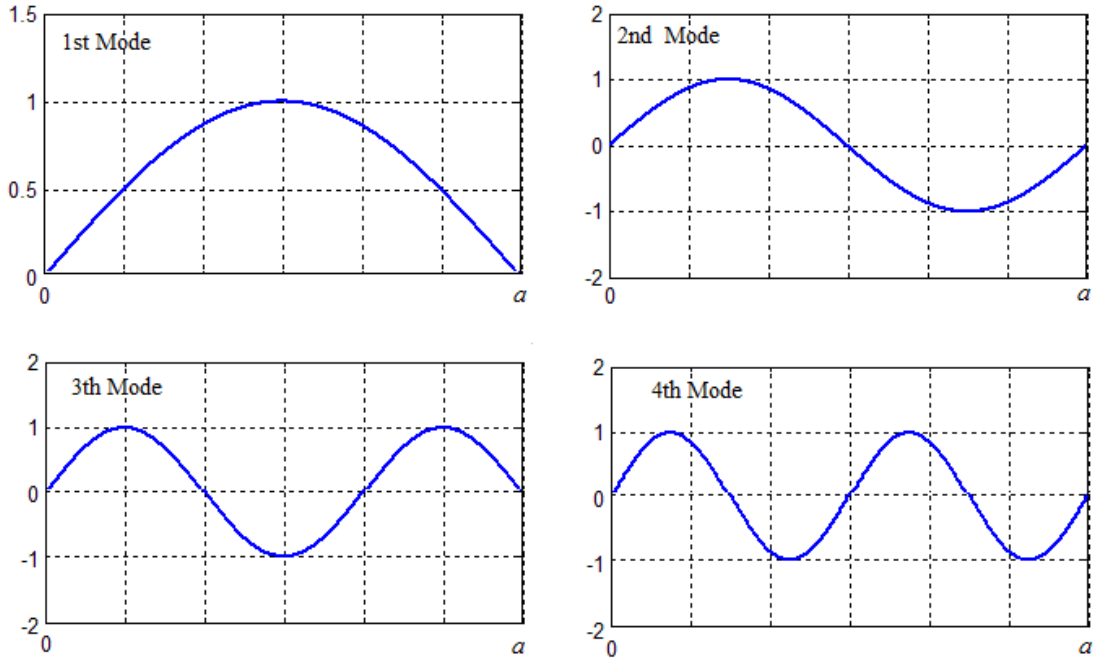

Figure 5.1 The first four mode shapes of simply supported thin beam predicted by the DSC ($N = 31$).

Figures 5.2.a, b and Figures 5.3.a-c show relative error for frequency parameters of simply supported beams whereas Figures 5.4.a-i present errors for simply supported plates. In Figure 5.2, r values are selected as 2.1 for $N = 11$ and 3.1 for

$N = 101$, respectively. Since the influence of the discretization parameter is more important for higher number of modes compared to lower numbers, three different *r* values were considered for higher numbers as shown in Figure 5.3 and 5.4. These values were selected as from 4.1 to 8.1, 6.1 to 10.1 and 8.1 to 12.1 corresponding to $N = 1001$, $N = 2001$ and $N = 3001$ respectively, for beams and corresponding to $N = 51 \times 51$, $N = 61 \times 61$ and $N = 71 \times 71$ respectively, for plates. As Figures 5.3.a-c are examined, it is clearly seen that increasing *r* decreases the relative errors for each of *N* values; and also increasing *N* decreases the error values of considered modes. For *N*=3001 with *r*=12.1, the first 2999 natural modes of beams can be obtained by maximum error of 0.018%. However, *N*=1001 grid points corresponding to the first 999 natural modes state the error under 0.07%. Actually, this score is also reliable for high frequency analysis. The same effect of *r* is also realized for plates as Figures 5.4.a-i are examined. The first 4761 modes are accurately obtained for $N = 71 \times 71$ with *r*=12.1; and approximately 1% error is observed for the first 4750. Selecting $N = 51 \times 51$ for each *r*, predicts at least the first 1000 modes with zero error. This amount of modes also indicates high frequency region.

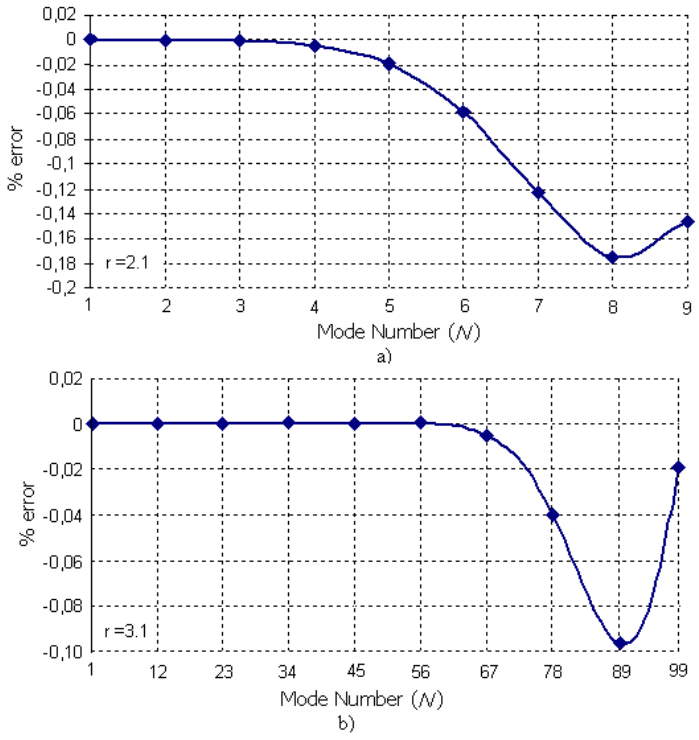

Figure 5.2 Convergence test for the DSC modal predictions of simply supported beams a) $N = 11$, b) $N = 101$.

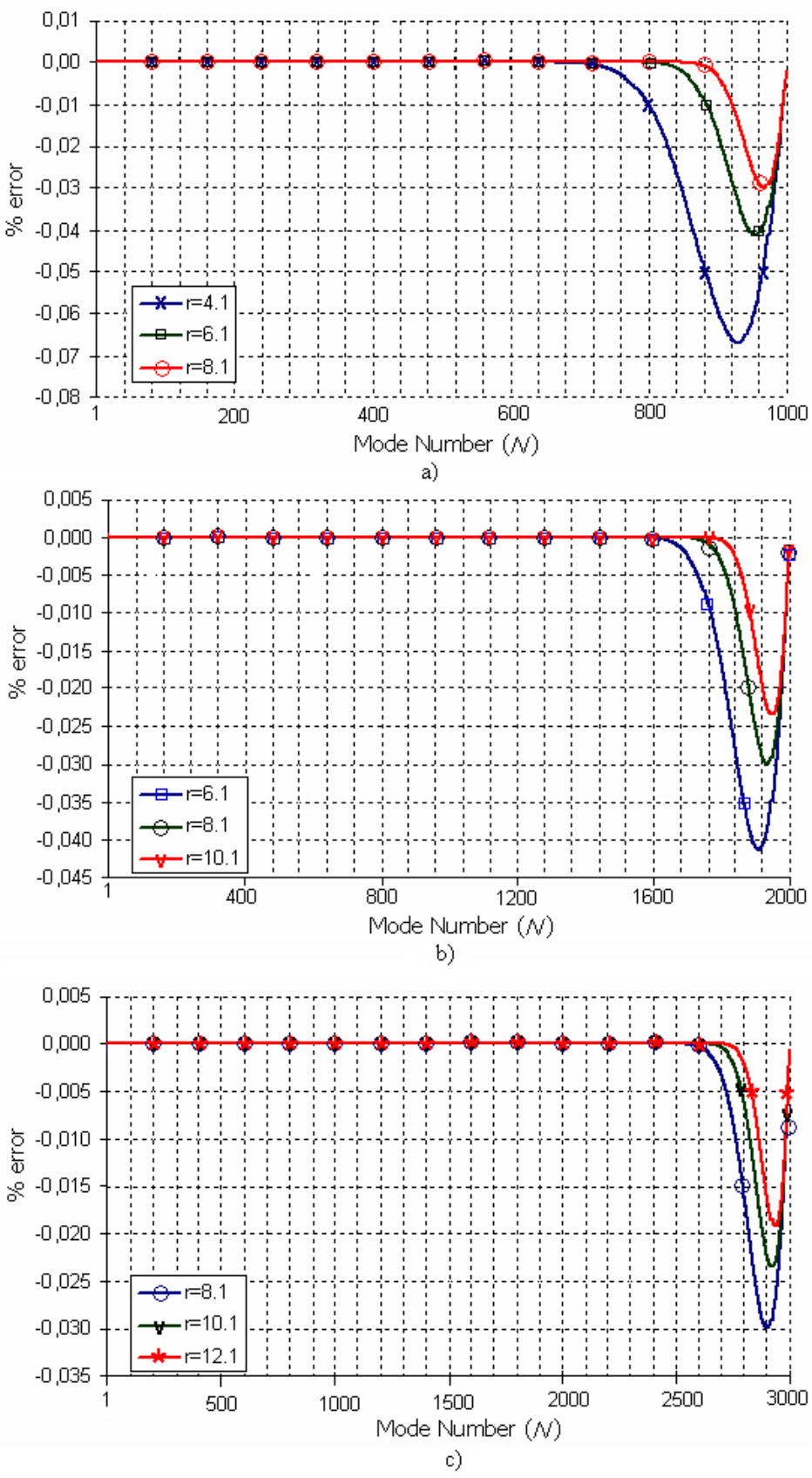

Figure 5.3 Convergence test for the DSC modal predictions of simply supported beams a) $N = 1001$, b) $N = 2001$, c) $N = 3001$.

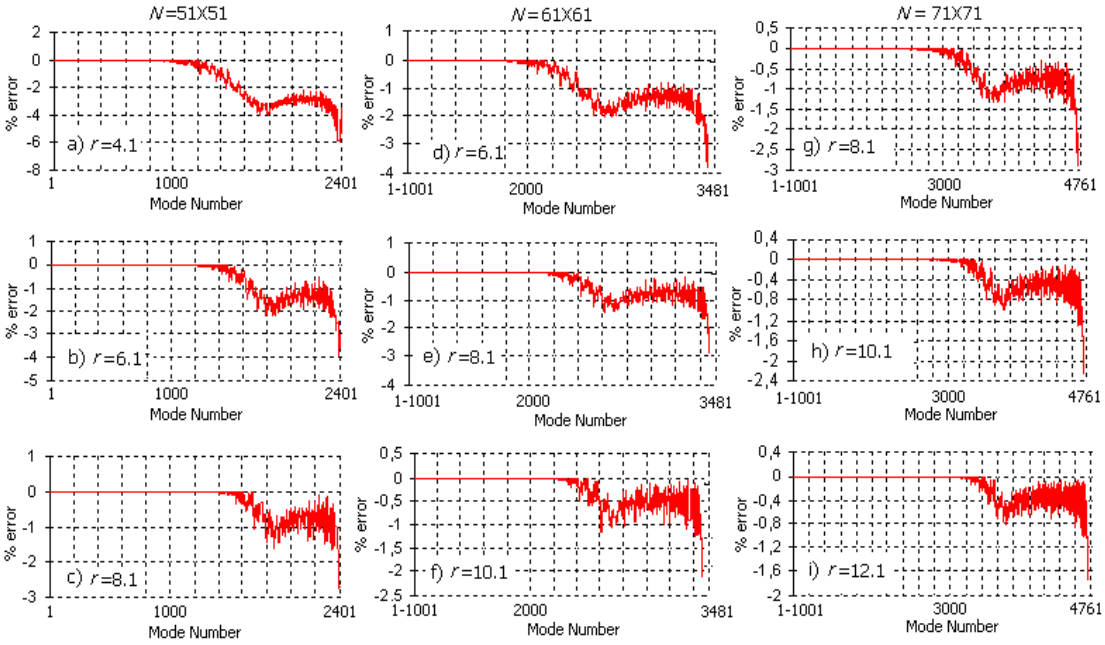

Figure 5.4 Convergence test for the DSC modal predictions of simply supported plates.

5.3 Verification Study for the DSC-MS

5.3.1 Vibration Displacement Response for a Thin Beam

Analytical solution for the displacement response of a simply-supported undamped beam subjected to a point force F applied at the centre is (Harris & Piersoll, 2002b),

$$w(x,t) = \frac{2F}{\rho_0 Aa}\sum_{n=1}^{\infty}\frac{\sin(n\pi/2)}{\omega_n{}^2\left(1-(\omega/\omega_n)^2\right)}\frac{\sin(n\pi x)}{a}\sin(\omega t) \tag{5.1}$$

where

$$\omega_n{}^2 = \frac{n^4\pi^4 EI}{\rho_0 Aa^4}, \qquad n = 1,2,3,\cdots \ . \tag{5.2}$$

In the analysis, the beam was discretized by N=3001 grid points with r = 12.1 providing P = 2999 natural modes; and a harmonic point force in the form of $F = 100\sin(200\pi t)$ N was applied. The physical properties of the beam are followings; $a = 1\,\text{m}$, $\rho_0 = 2700\,\text{kg/m}^3$, A=1×10^{-4} m^2, $E = 7.1\times10^{10}$ N/m^2, $I = 8.33\times10^{-10}$ m^4 and the natural frequency parameters are given as

$$\Omega_n = \omega_n\sqrt{\frac{\rho A}{EI}} = \left(\frac{n\pi}{a}\right)^2, \quad n = 1,2,3,\cdots \quad . \tag{5.3}$$

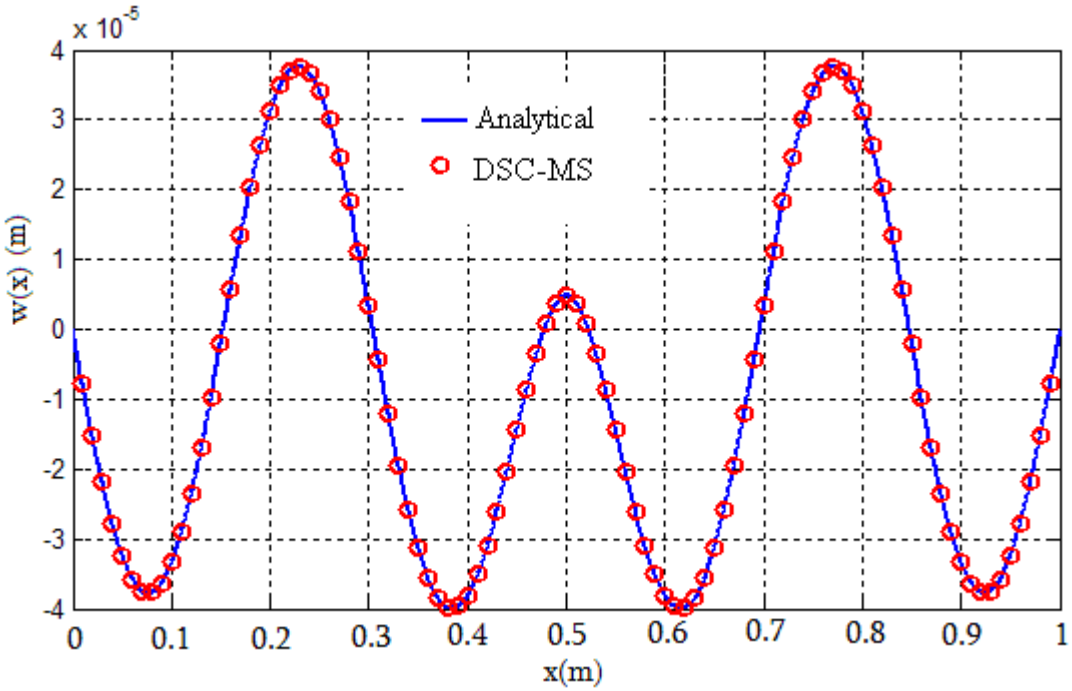

Figure 5.5 Comparison of the spatially distributed displacement response predicted by the DSC-MS with analytical results for simply supported beam with $\zeta = 0$.

Figure 5.5 shows the perfect match between the vibration displacement response predictions of DSC-MS approach and analytical expression given in Equation (5.1) for the frequency $f = 100$ Hz.

5.3.2 Vibration Displacement Response for a Thin Plate

Analytical expression of the non-dimensional natural frequency parameter of a simply supported thin plate is given as (Leissa, 1969);

$$\Omega_{m,n} = \pi^2 (m^2 + n^2), \quad m,n = 1,2,3,\cdots . \tag{5.4}$$

In the present analysis, the plate was discretized by $N = 71 \times 71$ grid points and discretization parameter r was chosen as 12.1. The plate with side lengths of 1m × 1m has the following parameters: $\rho_0 = 7900\,\text{kg/m}^3$, h=0.001 m, $E = 2.1 \times 10^{11}$ N/m^2. Figure 5.6 displays the relative error of the first 4761 ($P = 4761$) modes of the simply supported plate predicted by the DSC, corresponding up to almost 21200 Hz. The region including the first 4750 modes can be thought as acceptable frequency range, since the maximum absolute error is approximately 1% here. However, when comparing the predicted results with the analytical frequencies, it was noticed that after 3253th mode (=10355 Hz), having 0.127% error, some predicted natural modes shift to the position of subsequent analytical modes. This phenomenon arising due to high modal density causes the loss of some modal information. It is observed from this comparison that the situation is actually caused due to numerical illnesses. Accommodating better computational configurations, this limit can be extended to higher frequencies. For definitely reliable solutions, only up to the first 3254 modes were considered in all the present plate analyses. However considered number of modes can be regarded as rather sufficient for an acceptable high frequency analysis.

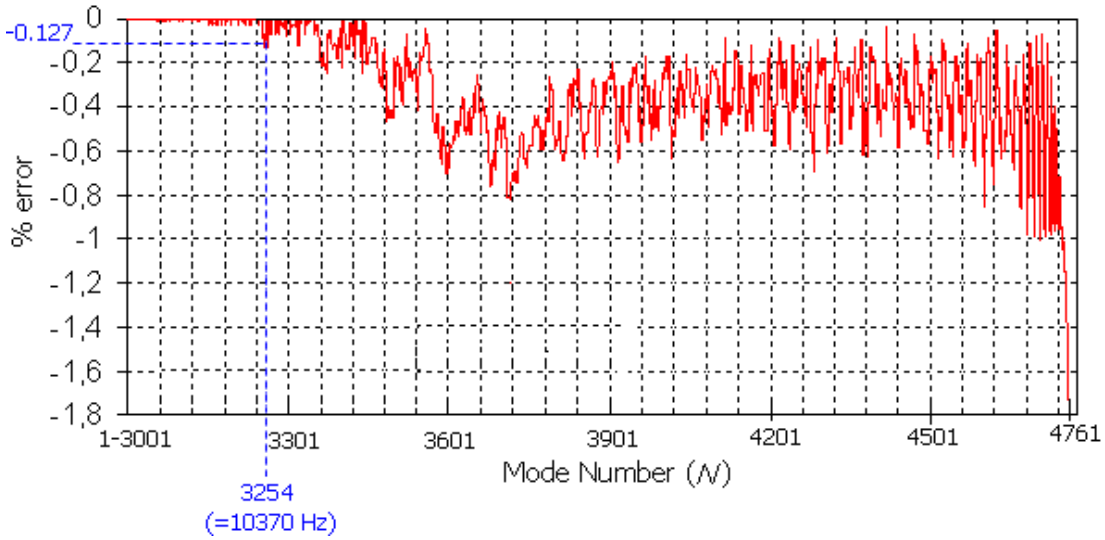

Figure 5.6 Relative error of DSC solutions compared to the analytical results for simply-supported plate.

Since there is no analytical solution for the vibration response of finite plates, the comparison study has been performed by using the approximate analytical solution of infinite plates. The plate with $1\text{m}\times 1\text{m}$ dimensions is sufficiently large to approximately simulate an infinite plate. Displacement field of an infinite, thin, transversely vibrating plate subjected to a harmonic point force $F(t)$ applied at the centre is examined by the wave propagation and the response is given with the far field assumption ($kr >> 1$) as (Cremer, Heckl & Ungar, 1998):

$$w(r) \approx \frac{jF}{8D_0(1+j\zeta)k^2}\sqrt{\frac{2}{\pi kr}}e^{j(\omega t-kr+\pi/4)} \quad . \tag{5.5}$$

Here r is the distance between excitation point (x_f, y_f) and observation point (x, y), i.e., $r = \sqrt{(x-x_f)^2+(y-y_f)^2}$. For $\zeta << 1$,

$$k = k_0 - j\gamma/2 \tag{5.6}$$

The damping coefficient is $\gamma = \omega\zeta/c_g$. The group velocity is defined as $c_g = 2\sqrt{\omega}\sqrt[4]{D_0/\rho_0 h}$. It is seen that in Equation (5.5), the response leads to an asymptotic behaviour near the excitation point and it yields an infinite value at the excitation point. However, a finite maximum value of $w(r)$ can be obtained by determining an initial radius satisfying the condition of $|w(r_0)| = |w(0)|$ as follows,

$$r_0^{-1} \approx \frac{\pi|k|}{2} + \gamma \quad . \tag{5.7}$$

At that point, the response approximately leads to:

$$|w(r_0)| \approx \left|\frac{jF}{8D_0(1+j\zeta)k^2}\right| \quad . \tag{5.8}$$

In the verification study, the central excitation had an amplitude of F=100 N and its frequency was varied between 10^2 Hz and 10^4 Hz. The DSC-MS response at the centre of the plate is presented in Figures 5.6.a-c for three internal damping factors $\zeta = 0$, $\zeta = 0.01$ and $\zeta = 0.1$, respectively together with analytical solutions.

It is observed in Figure 5.7 that DSC-MS results accurately follow the general tendency of the infinite plate response. Since Equation (5.5) does not include natural frequency information, the response of infinite plate exhibits a decreasing smooth line with increasing excitation frequency. However, the DSC-MS predicts the response peaks corresponding to natural modes of undamped system discretely as shown in Figure 5.7.a. When damping is included, response peaks rapidly disappear (Figure 5.7.b) and DSC-MS results become perfectly matching with the analytical solutions for higher internal damping factors (Figure 5.7.c).

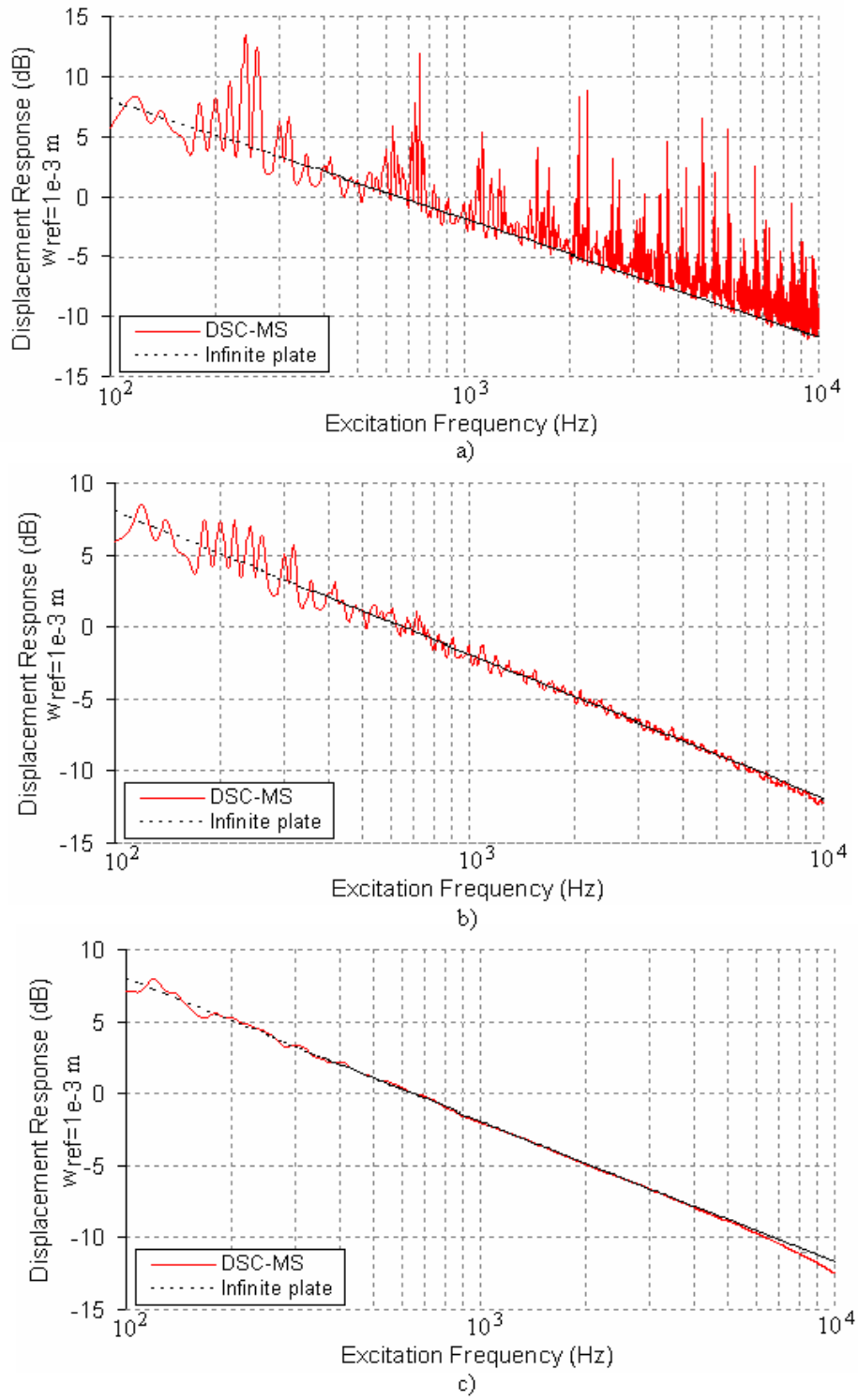

Figure 5.7 Comparison of the frequency response spectra predicted by the DSC-MS and approximate analytical solution for infinite plates a) $\zeta = 0$, b) $\zeta = 0.01$, c) $\zeta = 0.1$.

CHAPTER SIX
NUMERICAL STUDIES 1:
HIGH FREQUENCY FREE AND FORCED VIBRATION ANALYSES OF THIN PLATES BY THE DSC-MS

6.1 Introduction

In this chapter, comprehensive numerical studies for high frequency free and forced vibrations of thin plates with two different boundary conditions by using the DSC and DSC-MS are presented. In the previous chapter, since convergence tests were given in terms of error values of frequency parameters, free vibration analysis is generally considered here from the point of view of mode shapes. This chapter of the study shows the capabilities of the DSC-MS method in the discrete high frequency response analysis. In all numerical applications, the same plate parameters given in the verification study in Chapter 5 were used.

6.2 Free Vibration Analysis

A simply-supported thin plate was represented by $N_x = N_y = 71 \times 71 = 5041$ DSC grid points. Figure 6.1 presents computed first few mode shapes of the plate. Figure 6.2 shows higher mode shapes with high resolution. These figures clearly show the validity of the DSC also in the computation of mode shapes.

6.3 Forced Vibration Analysis

For the spatial and frequency response analyses, fully simply supported and fully clamped boundary conditions were considered, respectively.

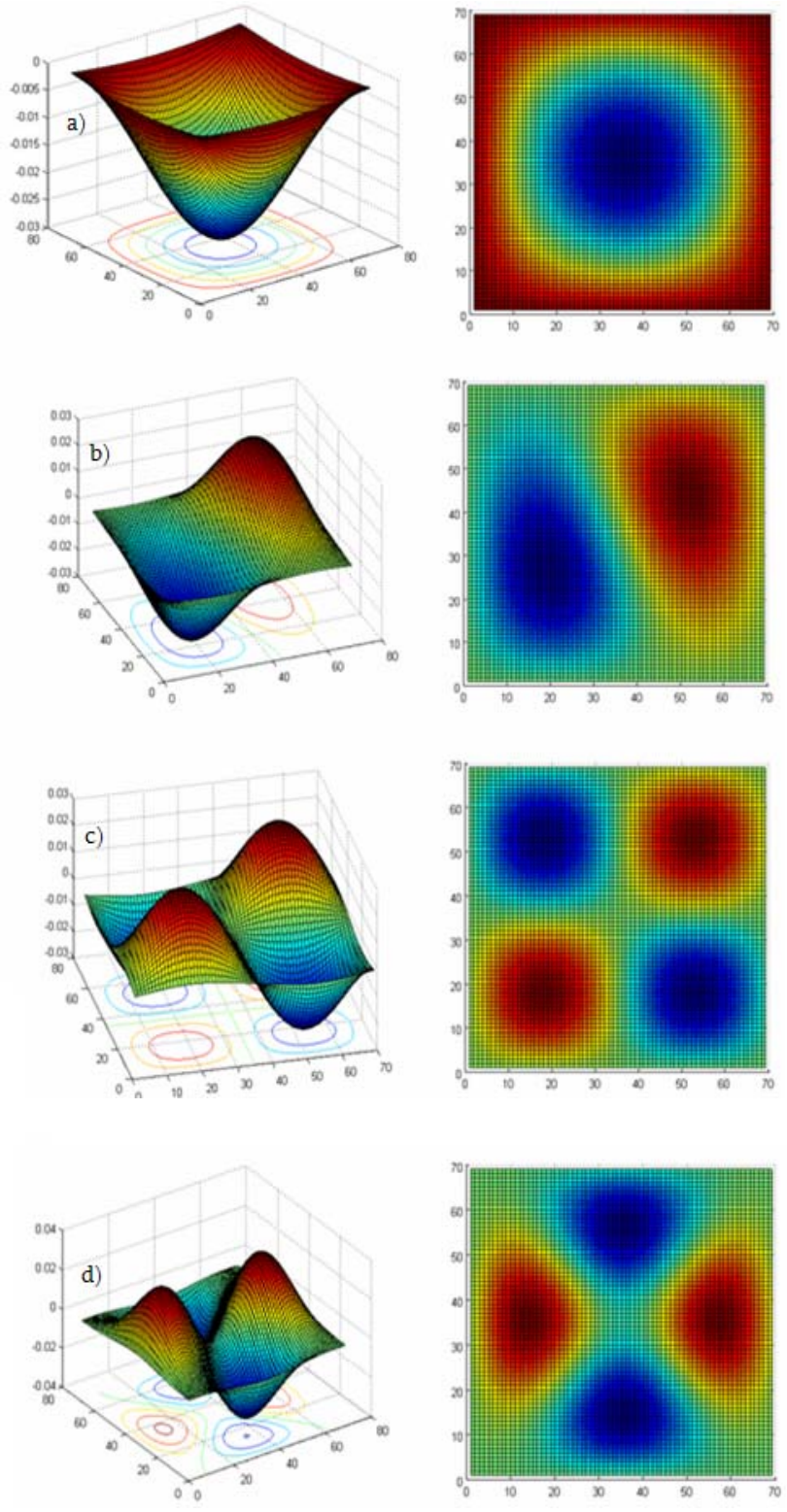

Figure 6.1 The first few mode shapes of the simply supported plate a) Mode 1, b) Mode 2-3, c) Mode 4, d) Mode 5-6.

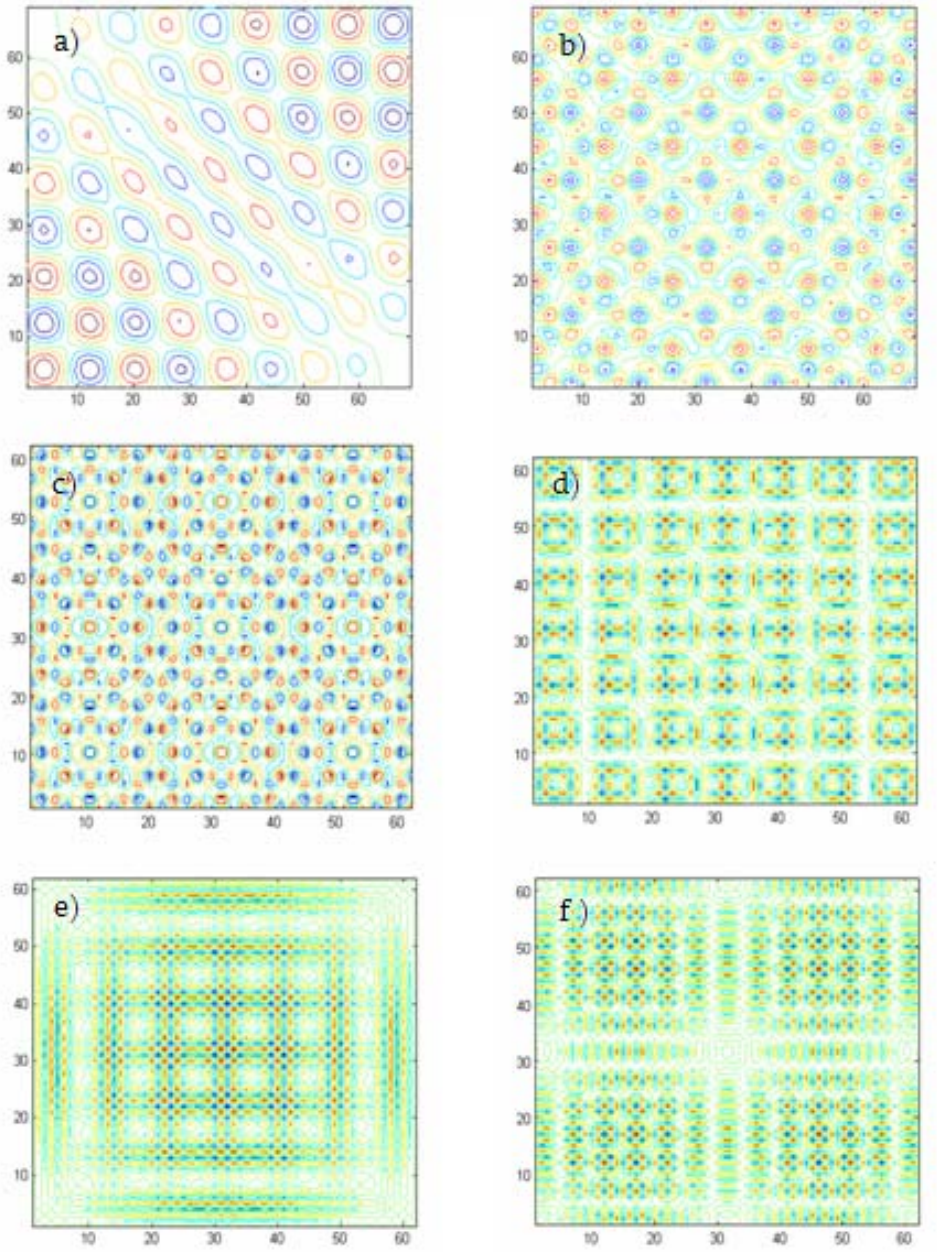

Figure 6.2 Several higher mode shapes of the simply-supported plate a) Mode 100, b) Mode 500, c) Mode 1000, d) Mode 2000, e) Mode 2500, f) Mode 3000.

6.3.1 Spatial Response Analysis

DSC-MS approach was used for spatially distributed displacement response of fully simply-supported undamped thin plate subjected to time-harmonic point forces with different frequency content and having an amplitude of F=100 N.

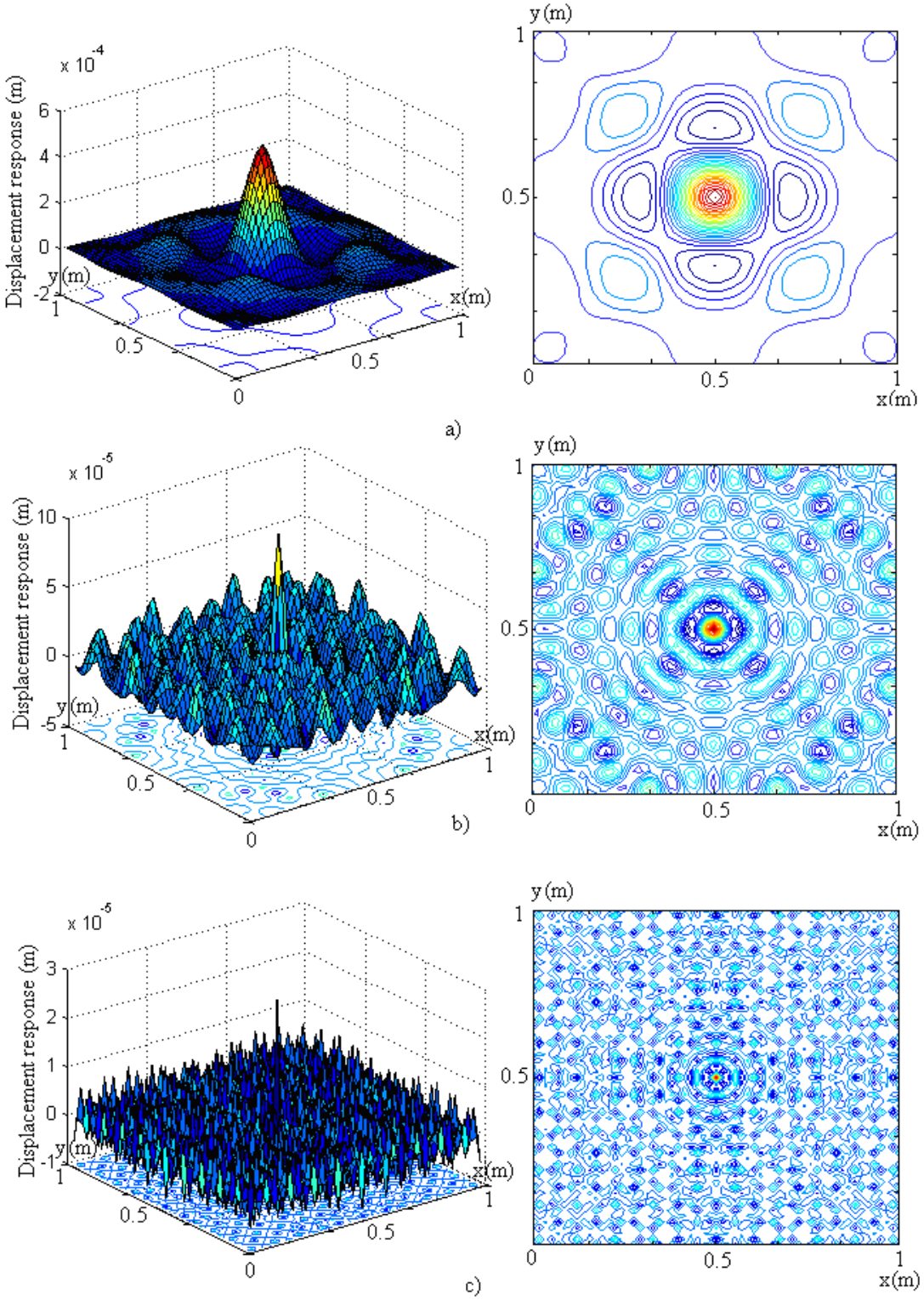

Figure 6.3 Spatially-distributed vibration response of simply supported plate subjected to single central excitation a) $f = 100$ Hz, b) $f = 1000$ Hz, c) $f = 5000$ Hz (f: excitation frequency).

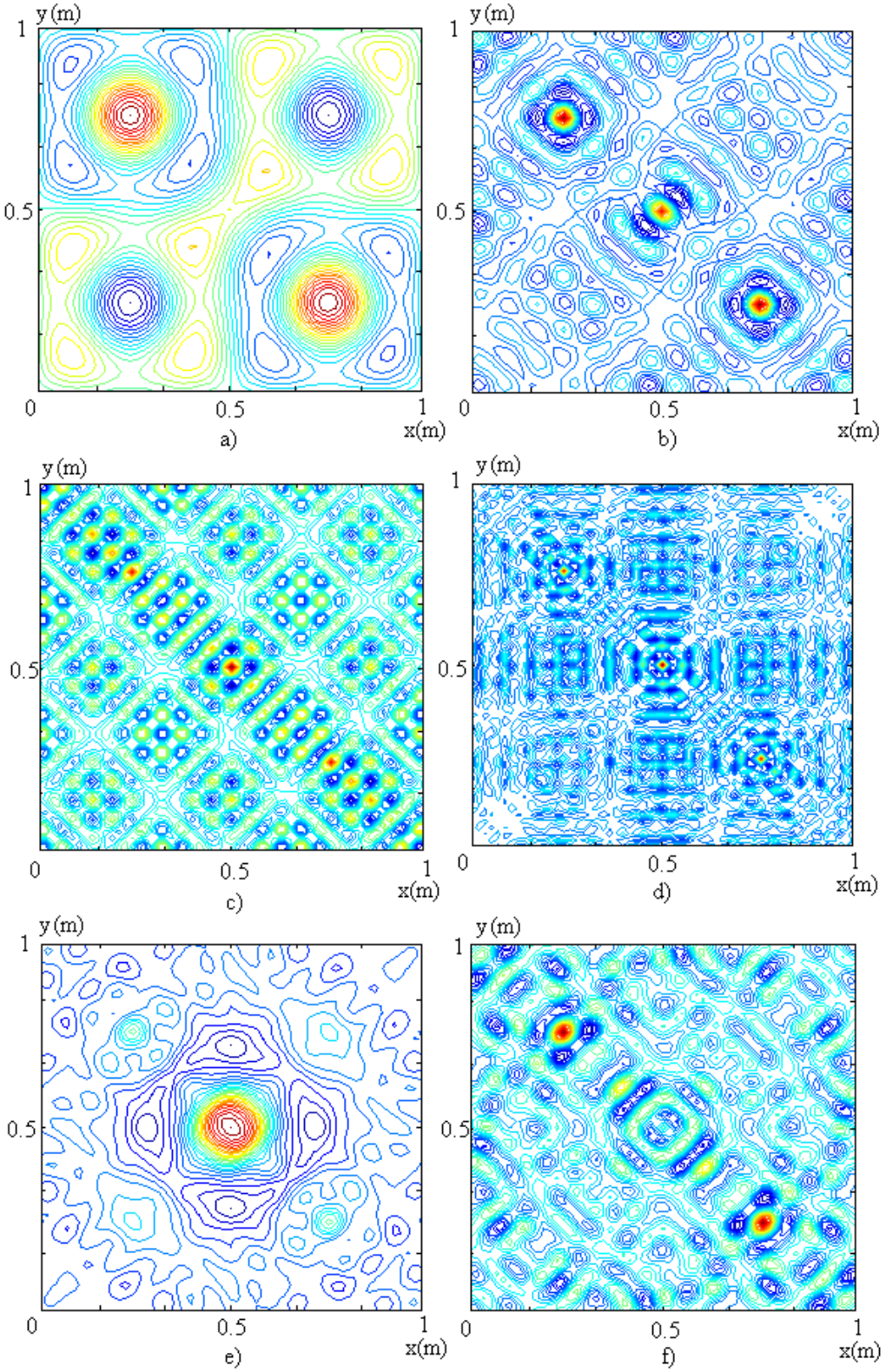

Figure 6.4 Six different spatially-distributed vibration responses of simply supported plate subjected to three different excitations.

Figures 6.3.a-c show the spatially distributed response of the plate to the single harmonic central excitations at 100 Hz, 1000 Hz and 5000 Hz frequencies, respectively. Figure 6.4 presents response contours of the plate subjected to three point forces with several frequencies and frequency combinations.

In Figure 6.4, excitation locations e_1, e_2, e_3 are defined as, $e_1 = (0.25, 0.75)$ m, $e_2 = (0.5, 0.5)$ m, $e_3 = (0.75, 0.25)$ m and excitation frequencies are as follows:
a) $f_1 = f_2 = f_3 = 100$ Hz, b) $f_1 = f_2 = f_3 = 1000$ Hz, c) $f_1 = f_2 = f_3 = 2000$ Hz, d) $f_1 = f_2 = f_3 = 5000$ Hz, e) $f_1 = f_3 = 1000$ Hz, $f_2 = 100$ Hz, f) $f_1 = f_3 = 1000$ Hz, $f_2 = 2000$ Hz. These embroidered contours show the versatility of the DSC-MS on predicting spatially distributed response field.

6.3.2 Frequency Response Analysis

The frequency response analysis of a fully clamped thin plate was performed by DSC-MS approach for the time-harmonic excitation forces for which frequency spectra are given in Figure 6.5. The analysis included low, mid and high frequency regions. The excitation forces were applied to the centre of the plate.

Firstly, an excitation in the form of ideal white noise throughout 0-100 Hz as shown in Figure 6.5.a was applied. In this analysis, *P* = 25 modes (= 8.9357 Hz to113.79 Hz) were sufficiently contributed to the response.

Secondly, an excitation again in the form of ideal white noise but in a much wider range, throughout 0-10000 Hz, was considered (Figure 6.5.b).

Finally, for high frequency band analysis, a 1/3 octave band of the previous excitation at the 1000 Hz centre frequency was applied (Figure 6.5.c). In the last two cases, *P*=3254 modes (= 8.9357 Hz to10561 Hz) were taken into account.

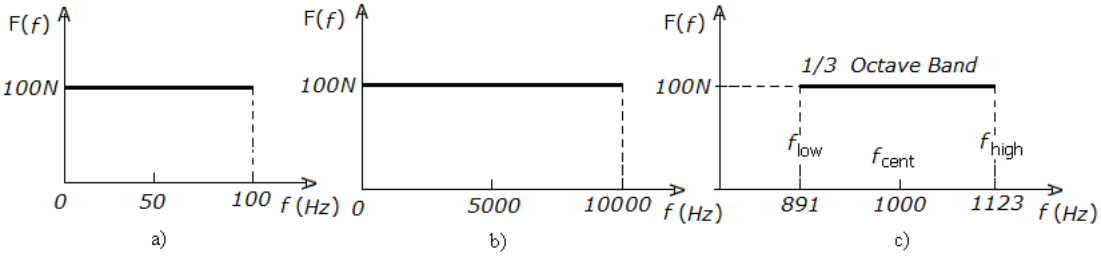

Figure 6.5 Time-harmonic excitation force spectra a) Ideal white noise (0-100 Hz), b) Ideal white noise (0-7500 Hz), c) 1/3 octave band-limited white noise ($f_{low} = 891\,\text{Hz}$, $f_{cent} = 1000$ Hz, $f_{high} = 1123$ Hz).

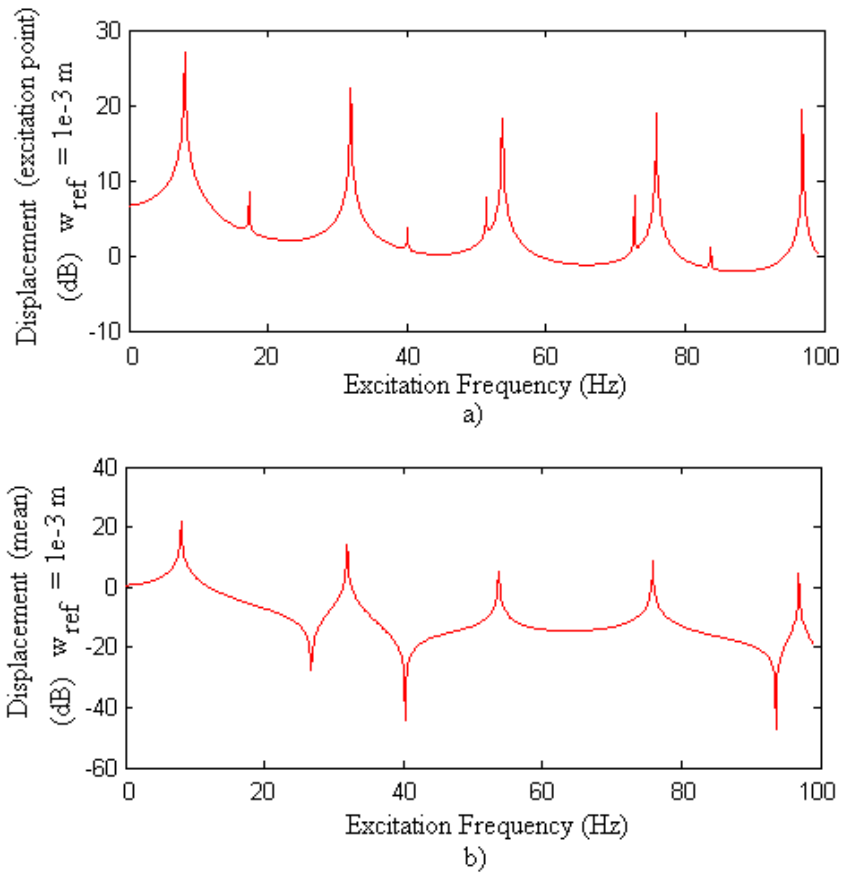

Figure 6.6 Frequency response spectra of the clamped plate subjected to central harmonic point force acting at 0-100 Hz. a) Displacement of the excitation point, b) Mean (spatially averaged) displacement.

Figure 6.6 shows the frequency response of the undamped plate to the first excitation. The resonant modes are clearly observed as disturbances for the excitation point response in Figure 6.6.a. Since spatial averaging causes some weak modal

information to be lost, the mean value spectrum in Figure 6.6.b includes only stronger modes.

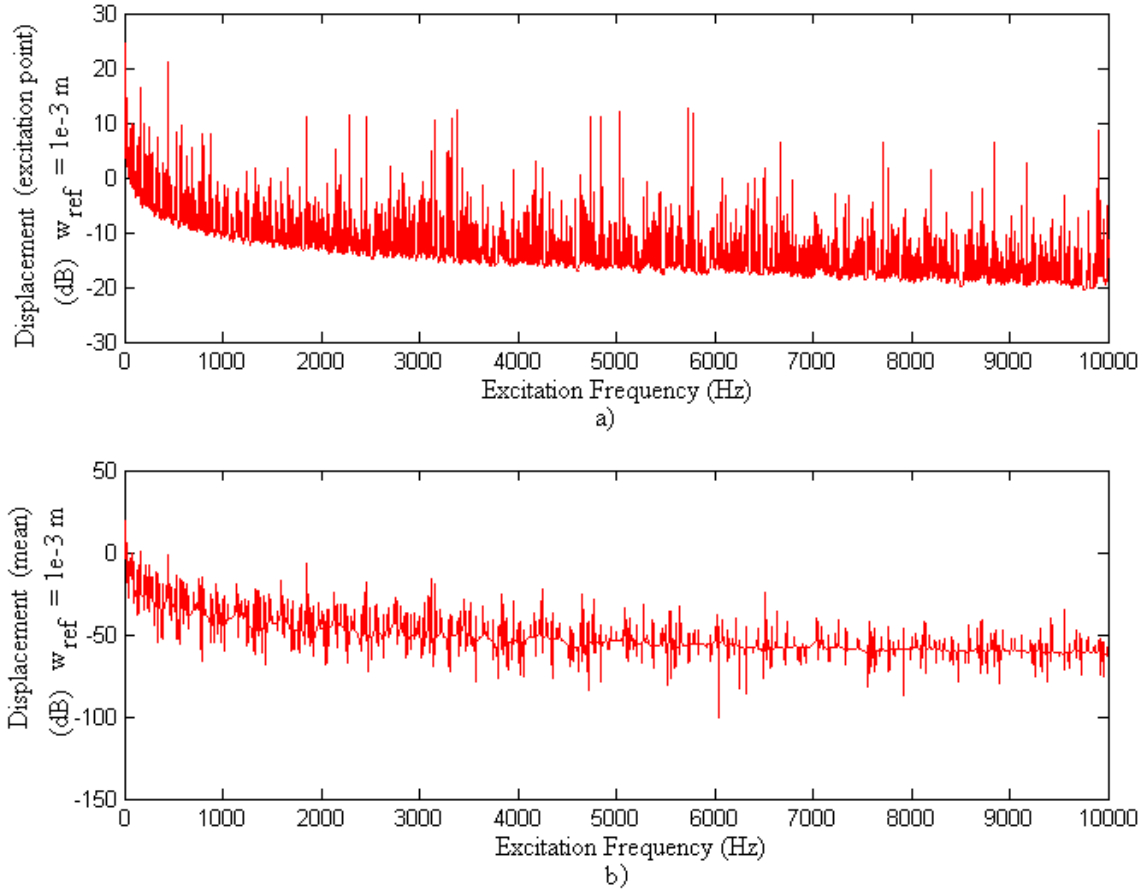

Figure 6.7 Frequency response spectra of the clamped plate subjected to a central harmonic point force acting at 0-10000 Hz. a) Displacement of the excitation point, b) Mean (spatially averaged) displacement.

The response spectra of the undamped plate to the second excitation are given in Figure 6.7. It is clearly seen that the DSC-MS is capable of predicting vibration response for the entire frequency range (0-10000 Hz). In contrast to the smooth response predicted by the conventional high-frequency methods, the present scheme yields discrete high frequency response. The spectra at high frequencies can be better visualized by focusing into 7500 Hz-10000 Hz and 9900 Hz-10000 Hz frequency ranges as displayed in Figures 6.8 and 6.9, respectively.

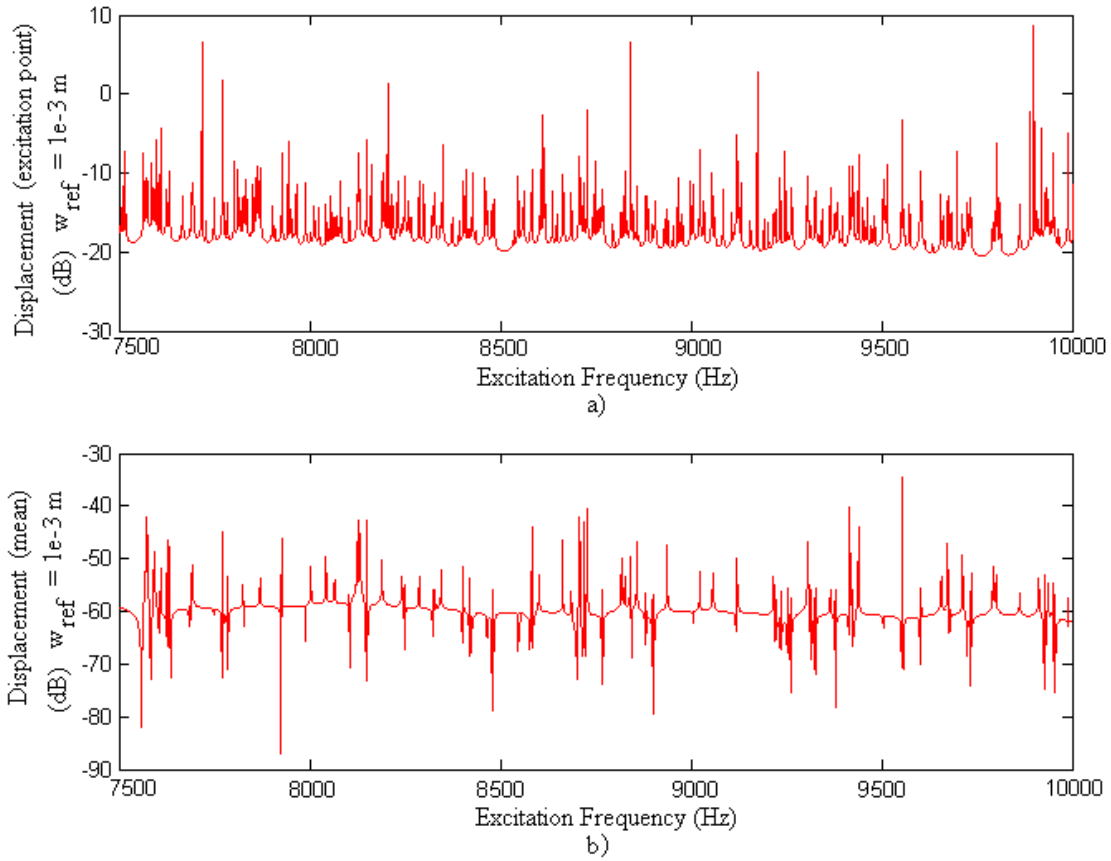

Figure 6.8 The focused part of Figure 6.7 in the range of 7500-10000 Hz. a) Displacement of the excitation point, b) Mean (spatially averaged) displacement.

The analysis in a limited frequency band shown in Figure 6.5.c for the last application is generally performed by energy-based methods. These methods use the modal energy within a bandwidth to predict an average response along the band. However, in order for these methods to be valid in a frequency region, the considered band must include sufficient number of modes, i.e. the band must have high modal density. The DSC-MS results obtained for undamped ($\zeta = 0$) and slightly-damped ($\zeta = 0.01$) plates are presented in Figure 6.10.

The modal overlap count for plates can be derived by using Equations (4.18) and (4.19):

$$MO = \frac{A_s}{2D} \zeta \, f_c \tag{6.1}$$

For $\zeta = 0.01$ and $f_c = 1000$ Hz, *MO* is calculated as 3.2047; that is greater than Rabbiolo's plate criterion i.e., $\overline{MO}$ = 2.5. Therefore, the frequency band with the 1000 Hz centre frequency may be regarded as high frequency band for the plate at hand.

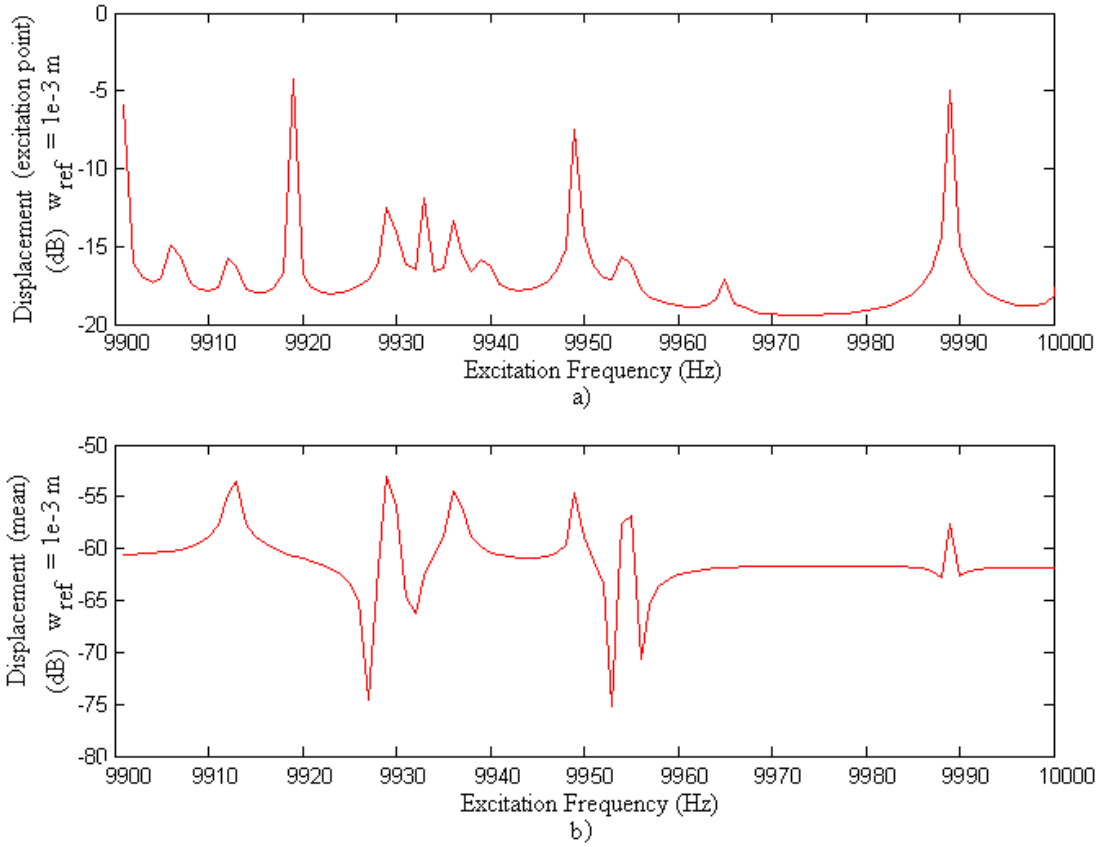

Figure 6.9 The focused part of Figure 6.7 in the range of 9900-10000 Hz. a) Displacement of the excitation point, b) Mean (spatially averaged) displacement.

In Figure 6.10, it is clearly seen that undamped high frequency behaviour predicted by the DSC-MS yields the discrete response peaks as much as accurately obtained in the low frequency analysis. However, the damping decreases resonance peaks and therefore the response spectra provide weak modal information.

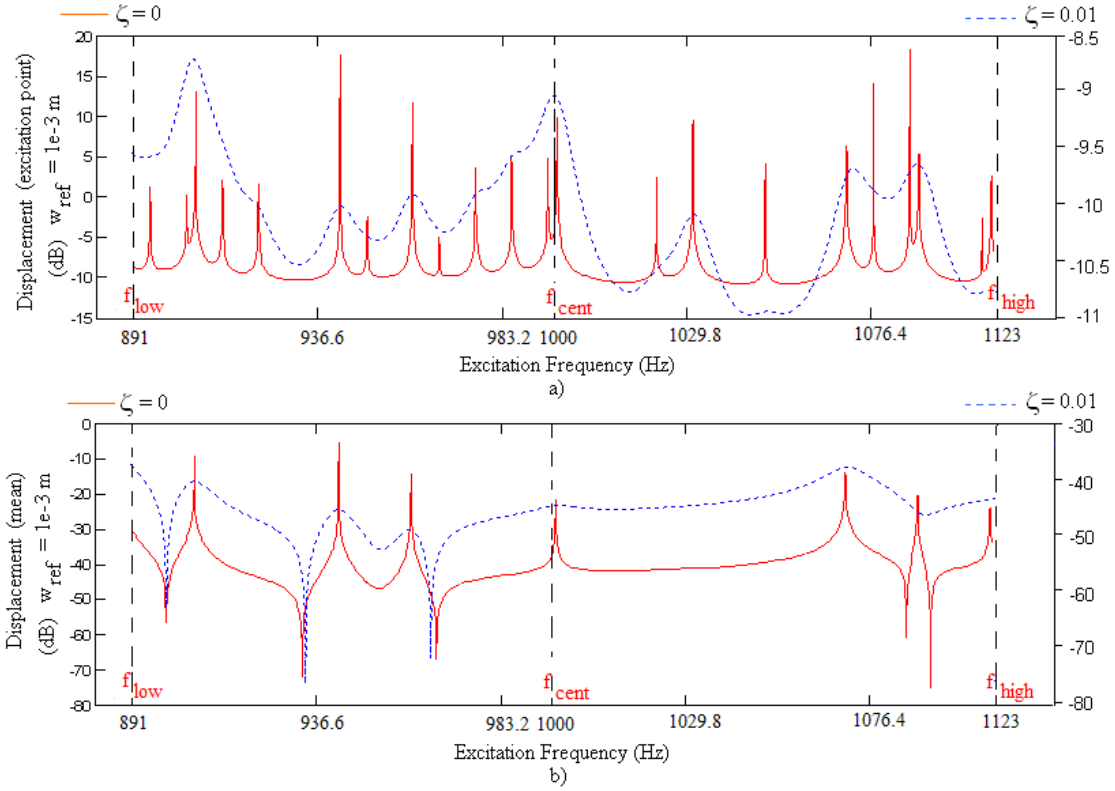

Figure 6.10 Frequency response spectra of the clamped plate subjected to central harmonic point force acting at 1000 Hz with 1/3 octave band a) Displacement of the excitation point, b) Mean (spatially averaged) displacement.

In practice, all systems have damping and for a realistic design, damping behaviour must be adapted to the vibro-acoustic model. The modal content of any real high frequency system can be discretely obtained by the DSC-MS. The other advantage of the present scheme is that it does not require any pre-condition for the modal density and damping.

CHAPTER SEVEN
NUMERICAL STUDIES 2:
FREE VIBRATION ANALYSIS OF SYMMETRICALLY LAMINATED THIN COMPOSITE PLATES BY THE DSC

7.1 Introduction

Laminated composites are increasingly used in various mechanical structures and industrial applications such as aircrafts, automobiles, marines, buildings and several house-hold appliances due to their, in particular, higher stiffness and higher strength to weight ratio compared to isotropic or wooden materials. Composite plates generally are made of alternating layers of fiber-reinforced polymer prepregs or different combinations of polymer prepregs and metals. The material type and orientation angle of the layers drastically change the modal characteristics of the composites beside the mechanical properties such as strength, roughness, durability, fatigue and fracture behaviour. Since the application of composite materials to real life structures have been accelerated, the researches on vibrational characteristics of composite structures, including thin plates became important. In this regard, free vibration analysis of symmetrically laminated thin composite plates was performed by using the DSC algorithm.

In this chapter, an implementation procedure of the DSC for the composite plates is introduced. The accuracy of the code is verified by comparing the DSC free vibration results with the exact ones for specially orthotropic plates, and some symmetrically laminated thin composite plates orientated as become specially orthotropic. In addition, free vibrations of several laminated thin composite plates which have no analytical solution are examined by the DSC for different boundary conditions and ply numbers. The results are compared with the published solutions of different methods.

Furthermore, some specific free vibration applications of thin composite plates based on Discrete Singular Convolution (DSC) approach are presented. As the first

application, a parametric analysis is performed on the bases of number of lamination, boundary condition and orientation angle of symmetrically laminated composite plates. Secondly, the effects of material type, boundary condition and stacking sequence on the modal characteristics of laminated plates made of E-glass/epoxy, Kevlar/epoxy and Carbon/epoxy are investigated. Thirdly, linear modal characteristics of fiber metal laminates (FML) are specifically analysed due to their common use in aircraft design. Hybrid composites offer superior mechanical properties over conventional composite laminates and high-strength metal alloys. Specifically, fiber metal laminates (FML) combine the good fatigue and fracture behaviour of polymer composites with the excellent durability, toughness and impact resistance of metals in addition to the weight and cost reductions. Due to these excellent properties, FMLs are being used in commercial aircrafts and advanced aerospace structures.

Design parameters are material type, orientation angle of stacks, stacking sequence, number of lamination and boundary condition. Three case studies are independently considered for practical purposes. Firstly, symmetrically laminated three-ply, four-ply and five-ply composite plates with six different boundary conditions are considered in order to examine the effects of number of lamination, boundary condition and orientation angle of stacks on natural frequency parameters. Secondly, the effects of material type and stacking sequences on the modal characteristics of laminated plates made of E-glass/epoxy, Kevlar/epoxy and Carbon/epoxy with two different boundary conditions are investigated. Finally, due to their practical importance, fiber metal laminates (FML) are specifically considered on a linear base in order to compare the effects of material type of fiber, boundary condition and orientation angle of stacks on natural frequency parameters. The results are evaluated together with those of monolithic aluminium alloys.

7.2 DSC Implementation for Symmetrically Laminated Plates

Time-independent differential equation of harmonic bending vibration for a symmetrically laminated thin composite plate is given as follows (Whitney, 1987);

$$D_{11}\frac{\partial^4 w(x,y)}{\partial x^4}+4D_{16}\frac{\partial^4 w(x,y)}{\partial x^3\partial y}+2(D_{12}+2D_{66})\frac{\partial^4 w(x,y)}{\partial x^2\partial y^2}$$

$$+4D_{26}\frac{\partial^4 w(x,y)}{\partial x\partial y^3}+D_{22}\frac{\partial^4 w(x,y)}{\partial y^4}-\rho_0 h\,\omega^2\, w(x,y)=0\ . \qquad (7.1)$$

Here, D_{11}, D_{12}, D_{22}, D_{66} are the bending rigidities in the principle material directions whereas D_{16} and D_{26} are the bend-twist coupling stiffnesses. For fully simply supported (SSSS) and fully clamped (CCCC) edges the following boundary conditions are applicable:

For SSSS;

$$\text{at } x=0,\ a: \quad w=0 \ ; \quad -D_{11}\frac{\partial^2 w}{\partial x^2}-2D_{16}\frac{\partial^2 w}{\partial x\partial y}-D_{12}\frac{\partial^2 w}{\partial y^2}=0, \qquad (7.2.a)$$

$$\text{at } y=0,\ b: \quad w=0 \ ; \quad -D_{12}\frac{\partial^2 w}{\partial x^2}-2D_{26}\frac{\partial^2 w}{\partial x\partial y}-D_{22}\frac{\partial^2 w}{\partial y^2}=0. \qquad (7.2.b)$$

For CCCC;

$$\text{at } x=0,\ a: \quad w=0 \ ; \quad \frac{\partial w}{\partial x}=0, \qquad (7.3.a)$$

$$\text{at } y=0,\ b: \quad w=0 \ ; \quad \frac{\partial w}{\partial y}=0. \qquad (7.3.b)$$

Introducing new non-dimensional parameters; $X=x/a$, $Y=y/b$, $W=w/a$, $\lambda=a/b$, $D_\gamma=(D_{11}/D_{22})$, $D_\phi=(D_{12}+2D_{66})/D_{22}$, $D_\alpha=(D_{16}/D_{22})$, $D_\beta=(D_{26}/D_{22})$, Equation (7.1) can be rewritten in the following form:

$$D_\gamma\frac{\partial^4 W(X,Y)}{\partial X^4}+2\lambda^2 D_\phi\frac{\partial^4 W(X,Y)}{\partial X^2\partial Y^2}+\lambda^4\frac{\partial^4 W(X,Y)}{\partial Y^4}$$

$$+4\left(\lambda D_\alpha\frac{\partial^4 W(X,Y)}{\partial X^3\partial Y}+\lambda^3 D_\beta\frac{\partial^4 W(X,Y)}{\partial X\,\partial Y^3}\right)-\Omega^2 W(X,Y)=0. \qquad (7.4)$$

Here, natural frequency parameter is $\Omega = \omega a^2 \sqrt{\rho h / D_{22}}$. For specially orthotropic plates (SOP) and isotropic plates (IP), Equation (7.4) can be simplified based on the following two features:

- For specially orthotropic plates (SOP): The composite is symmetrically laminated and has only plies in the 0 and 90-degree directions; therefore, $D_\gamma \neq D_\phi$ and $D_\alpha = D_\beta = 0$ (i.e., $D_{16} = D_{26} = 0$).

- For isotropic plates (IP): The rigidities $D_\gamma = D_\phi = 1$ and $D_\alpha = D_\beta = 0$ (i.e., $D_{11} = D_{22} = D = Eh^3 / 12\left(1 - \upsilon^2\right)$ and $D_{16} = D_{26} = 0$).

For fully simply supported SOP; natural frequency parameter $\Omega_{p,q}$ is analytically given by (Whitney, 1987);

$$\Omega_{p,q} = \omega_{p,q}\, a^2 \sqrt{\frac{\rho_0 h}{D_{22}}} = \pi^2 \sqrt{p^4 D_\gamma + 2\, p^2 q^2 \lambda^2 D_\phi + q^4 \lambda^4} \qquad p, q = 1, 2, 3, \cdots . \quad (7.5)$$

By applying linear DSC operator **L** defined in Equation (3.18), that performs the DSC approach in Equation (3.24), to Equation (7.4); one can obtain a discretized governing equation of symmetrically laminated composite plates in a non-dimensional form:

$$\begin{aligned}
&D_\gamma \sum_{k=-M}^{M} \delta^{(4)}_{\pi/\Delta,\sigma}(k\Delta)\, W(X_{i+k}, Y) \\
&+ 2\lambda^2 D_\phi \left(\sum_{k=-M}^{M} \delta^{(2)}_{\pi/\Delta,\sigma}(k\Delta)\, W(X_{i+k}, Y) \sum_{k=-M}^{M} \delta^{(2)}_{\pi/\Delta,\sigma}(k\Delta)\, W(X, Y_{i+k}) \right) \\
&+ \lambda^4 \sum_{k=-M}^{M} \delta^{(4)}_{\pi/\Delta,\sigma}(k\Delta)\, W(X, Y_{i+k})
\end{aligned}$$

$$+4\,\lambda D_{\alpha}\left(\sum_{k=-M}^{M}\delta^{(3)}_{\pi/\Delta,\sigma}(k\Delta)\,W(X_{i+k},Y)\sum_{k=-M}^{M}\delta^{(1)}_{\pi/\Delta,\sigma}(k\Delta)\,W(X,Y_{i+k})\right)$$

$$+4\lambda^{3}D_{\beta}\left(\sum_{k=-M}^{M}\delta^{(1)}_{\pi/\Delta,\sigma}(k\Delta)\,W(X_{i+k},Y)\sum_{k=-M}^{M}\delta^{(3)}_{\pi/\Delta,\sigma}(k\Delta)\,W(X,Y_{i+k})\right)=\Omega^{2}\,W(X,Y). \tag{7.6}$$

After applying boundary conditions as defined in Chapter 3, a vector for a discretized plate is obtained:

$$\mathbf{W}=\left\{W_{0,0},\ldots,W_{0,N-1},W_{1,0},\ldots,W_{1,N-1},\ldots,\ldots,W_{N-1,0},\ldots,W_{N-1,N-1}\right\}^{T}. \tag{7.7}$$

Finally, after implementation of displacement boundary conditions $W(r_0)=W(r_{N-1})=0$, Equation (7.6) can be reconstructed by DSC matrices as an eigenvalue equation for symmetrically laminated composite plates:

$$\left\{D_{\gamma}(\boldsymbol{\Gamma}_x^{(4)}\otimes\mathbf{I}_y)+2\lambda^{2}D_{\phi}(\boldsymbol{\Gamma}_x^{(2)}\otimes\boldsymbol{\Gamma}_y^{(2)})+\lambda^{4}(\mathbf{I}_x\otimes\boldsymbol{\Gamma}_y^{(4)})\right.$$
$$\left.+4\lambda D_{\alpha}(\boldsymbol{\Gamma}_x^{(3)}\otimes\boldsymbol{\Gamma}_y^{(1)})+4\lambda^{3}D_{\beta}(\boldsymbol{\Gamma}_x^{(1)}\otimes\boldsymbol{\Gamma}_y^{(3)})\right\}\mathbf{W}=\boldsymbol{\Omega}^{2}\,\mathbf{W}. \tag{7.8}$$

7.3 Comparison Study for Laminated Composite Plates

7.3.1 Verification of Natural Frequency Parameters

Here, natural frequency parameters of specially orthotropic square thin plates (SOP) are presented for a simple verification of the DSC. These frequency parameters are compared with analytical results for SSSS and approximate results for CCCC given by Whitney (1987) in Table 7.1. The comparison shows perfect agreement. Here, natural frequency parameters of the plates were defined as Ω/π^{2} for numerical facility.

Table 7.1 Natural frequency parameters of specially orthotropic plates (SOP) ($\lambda = 1$, DSC: $N = 21\times 21$, $\Omega/\pi^2 = \left(\omega a^2/\pi^2\right)\sqrt{\rho_0 h/D_{22}}$, $D_\gamma = 10$, $D_\phi = 1$, $D_\alpha = D_\beta = 0$)

	SSSS:		CCCC:	
Mode Number (p, q)	Present: DSC	Analytical (Whitney, 1987)	Present: DSC	Whitney (1987)
(1,1)	3.6056	3.6056	7.7199	7.7221
(1,2)	5.8310	5.8310	10.0990	10.102
(1,3)	10.4403	10.4403	15.0440	15.0475
(2,1)	13.0000	13.0000	20.1740	20.1835
(2,2)	14.4222	14.4222	21.7380	21.7402
(1,4)	17.2627	17.2627	22.4670	22.4673

Secondly, natural frequency parameters of three-ply laminates predicted by DSC approach are compared with those of some selected studies in Table 7.2-7.4: Leissa & Narita (1989) use Ritz method; Chow et al. (1992) utilize Rayleigh-Ritz approach; whereas Dai et al. (2004) introduce a mesh free technique and present results from classical laminated plate theory (CLPT) and also Reddy's third order shear deformation theory (TSDT). (i.e., $D_{0,1} = E_1 h^3/(1-\nu_{12}\nu_{21})$). In this comparison, natural frequency parameter is determined as $\beta_1 = \omega a^2\sqrt{\rho h/D_{0,1}}$ by means of an arbitrary rigidity expression $E_1/E_2 = 2.45$, $G_{12} = 0.48E_2$, $\upsilon_{12} = 0.23$, $\upsilon_{21} = 0.0939$, $\rho = 8000\,kg\cdot m^{-3}$, $h = 0.06m$, $h/a = 0.006$ (i.e., a typical thin plate).

Table 7.2 gives frequency parameters of the plates with fully simply supported (SSSS), Table 7.3 with fully clamped (CCCC) and Table 7.4 with simply supported-clamped (SCSC) boundary conditions. Tabulated frequency parameters computed by the DSC yield good agreement with those of the compared studies.

Table 7.2 Natural frequency parameters $\beta_1 = \omega a^2 \sqrt{\rho h / D_{0,1}}$ of fully simply supported (SSSS) square three-ply laminates with several orientations ($\lambda = 1$, DSC: $N = 21 \times 21$)

Three-ply	Resource	Mode Sequence Number					
Ply angle		1	2	3	4	5	6
SSSS:							
(0^0, 0^0, 0^0)	Analytical (Whitney, 1987) (CLPT: SOP)	15.171	33.248	44.387	60.682	64.457	90.145
	Present: DSC	15.171	33.248	44.387	60.682	64.457	90.145
	Dai et al. (2004) (CLPT)	15.17	33.32	44.51	60.78	64.79	90.42
	Dai et al. (2004) (TSDT)	15.22	33.76	44.79	61.11	66.76	91.69
	Chow et. al (1992) (CLPT)	15.19	33.31	44.52	60.79	64.55	90.31
	Leissa and Narita (1989) (CLPT)	15.19	33.30	44.42	60.78	64.53	90.29
(15^0, -15^0, 15^0)	Present: DSC	15.469	34.153	43.879	60.954	66.635	91.393
	Dai et al. (2004) (CLPT)	15.40	34.12	43.96	60.91	66.92	91.76
	Dai et al. (2004) (TSDT)	15.45	34.54	44.25	61.36	68.68	92.99
	Chow et. al (1992) (CLPT)	15.37	34.03	43.93	60.80	66.56	91.40
	Leissa and Narita (1989) (CLPT)	15.43	34.09	43.80	60.85	66.67	91.40
(30^0, -30^0, 30^0)	Present: DSC	16.058	36.060	42.743	61.757	71.849	85.780
	Dai et al. (2004) (CLPT)	15.87	35.92	42.70	61.53	71.10	86.31
	Dai et al. (2004) (TSDT)	15.92	36.28	43.00	62.05	73.55	87.37
	Chow et. al (1992) (CLPT)	15.86	35.77	42.48	61.27	71.41	85.67
	Leissa and Narita (1989) (CLPT)	15.90	35.86	42.62	61.45	71.71	85.72
(45^0, -45^0, 45^0)	Present: DSC	16.348	37.146	42.033	62.234	77.213	80.130
	Dai et al. (2004) (CLPT)	16.10	37.00	41.89	61.93	77.99	80.11
	Dai et al. (2004) (TSDT)	16.15	37.33	42.20	62.45	78.96	81.55
	Chow et. al (1992) (CLPT)	16.08	36.83	41.67	61.65	76.76	79.74
	Leissa and Narita (1989) (CLPT)	16.14	36.93	41.81	61.85	77.04	80.00

Table 7.3 Natural frequency parameters $\beta_1 = \omega a^2 \sqrt{\rho h / D_{0,1}}$ of fully clamped (CCCC) square three-ply laminates with several orientations ($\lambda = 1$, DSC: $N = 21 \times 21$)

Three-ply	Resource	Mode Sequence Number					
Ply angle		1	2	3	4	5	6
CCCC:							
(0^0, 0^0, 0^0)	Present: DSC	29.087	50.792	67.279	85.629	87.112	118.50
	Dai et al. (2004) (CLPT)	29.27	51.21	67.94	86.25	87.97	119.3
	Dai et al. (2004) (TSDT)	30.02	54.68	70.41	89.36	92.58	123.6
	Chow et. al (1992) (CLPT)	29.13	50.82	67.29	85.67	87.14	118.6
(15^0, -15^0, 15^0)	Present: DSC	28.897	51.405	65.911	84.515	89.712	119.21
	Dai et al. (2004) (CLPT)	29.07	51.83	66.55	85.17	90.56	120.0
	Dai et al. (2004) (TSDT)	29.85	55.25	69.14	88.53	94.92	124.3
	Chow et. al (1992) (CLPT)	28.92	51.43	65.92	84.55	89.76	119.3
(30^0, -30^0, 30^0)	Present: DSC	28.522	53.124	62.683	83.821	95.158	114.13
	Dai et al. (2004) (CLPT)	28.69	53.57	63.26	84.43	96.15	115.5
	Dai et al. (2004) (TSDT)	29.51	56.84	66.17	87.83	100.5	118.9
	Chow et. al (1992) (CLPT)	28.55	53.15	62.71	83.83	95.21	114.1
(45^0, -45^0, 45^0)	Present: DSC	28.337	54.623	60.430	83.658	101.94	105.60
	Dai et al. (2004) (CLPT)	28.50	55.11	60.94	84.25	103.2	106.7
	Dai et al. (2004) (TSDT)	29.34	58.19	64.14	87.67	107.4	110.6
	Chow et. al (1992) (CLPT)	28.38	54.65	60.45	83.65	102.0	105.6

Table 7.4 Natural frequency parameters $\beta_1 = \omega a^2 \sqrt{\rho h / D_{0,1}}$ of simply supported-clamped (SCSC) square three-ply laminates with several orientations ($\lambda = 1$, DSC: $N = 21 \times 21$)

Three-ply	Resource	Mode Sequence Number					
Ply angle		1	2	3	4	5	6
SCSC:							
(0^0, 0^0, 0^0)	Present: DSC	20.402	45.638	46.998	69.434	83.677	95.247
	Dai et al. (2004) (CLPT)	20.48	46.04	47.15	70.12	84.54	95.85
	Dai et al. (2004) (TSDT)	21.08	47.73	49.64	72.05	89.25	96.97
(15^0, -15^0, 15^0)	Present: DSC	20.791	45.514	47.739	70.200	85.623	93.210
	Dai et al. (2004) (CLPT)	20.85	45.56	48.14	70.66	86.47	94.00
	Dai et al. (2004) (TSDT)	21.42	46.78	51.04	72.63	91.01	95.04
(30^0, -30^0, 30^0)	Present: DSC	21.786	44.476	50.622	71.73	87.959	91.845
	Dai et al. (2004) (CLPT)	21.84	44.42	51.03	71.89	88.96	92.82
	Dai et al. (2004) (TSDT)	22.35	45.31	54.09	73.93	90.07	96.85
(45^0, -45^0, 45^0)	Present: DSC	23.059	43.047	54.979	72.655	82.688	101.21
	Dai et al. (2004) (CLPT)	23.15	43.07	55.44	72.78	83.90	102.26
	Dai et al. (2004) (TSDT)	23.63	43.84	58.36	74.82	85.04	106.01

Thirdly, natural frequency parameters of four-ply and five-ply laminates are compared in Table 7.5 and Table 7.6, respectively with those of Leissa & Narita (1989) and Chow et al. (1992). Here, the frequency parameter and plate parameters are the same as given in the second case. These DSC predictions also exhibit very good harmony with the compared results.

Table 7.5 Natural frequency parameters $\beta_1 = \omega a^2 \sqrt{\rho h / D_{0,1}}$ of fully simply supported (SSSS) and clamped (CCCC) square four-ply laminates with several orientations ($\lambda = 1$, DSC: $N = 21 \times 21$)

Four -ply	Resource	Mode Sequence Number					
Ply angle		1	2	3	4	5	6
SSSS:							
(0^0, 0^0, 0^0 , 0^0)	Analytical (Whitney, 1987) (CLPT: SOP)	15.171	33.248	44.387	60.682	64.457	90.145
	Present: DSC	15.171	33.248	44.387	60.682	64.457	90.145
	Chow et. al (1992) (CLPT)	15.19	33.31	44.52	60.78	64.55	90.31
	Leissa and Narita (1989) (CLPT)	15.19	33.30	44.42	60.77	64.53	90.29
(15^0, -15^0, -15^0, 15^0)	Present: DSC	15.490	34.235	43.904	61.333	66.520	91.446
	Chow et. al (1992) (CLPT)	15.40	34.15	43.84	61.23	66.48	91.47
	Leissa and Narita (1989) (CLPT)	15.47	34.21	43.91	61.28	66.57	91.47
(30^0, -30^0, -30^0, 30^0)	Present: DSC	16.117	36.426	42.696	62.764	71.737	85.828
	Chow et. al (1992) (CLPT)	15.94	36.23	42.52	62.46	71.45	85.79
	Leissa and Narita (1989) (CLPT)	16.02	36.30	42.62	62.57	71.68	85.81
(45^0, -45^0, -45^0 , 45^0)	Present: DSC	16.424	37.837	41.766	63.540	77.644	79.646
	Chow et. al (1992) (CLPT)	16.17	37.62	41.52	63.15	77.33	79.40
	Leissa and Narita (1989) (CLPT)	16.29	37.71	41.63	63.29	77.56	79.60
CCCC:							
(0^0, 0^0, 0^0 , 0^0)	Present: DSC	29.087	50.792	67.279	85.629	87.112	118.50
	Chow et. al (1992) (CLPT)	29.13	50.82	67.29	85.67	87.14	118.6
(15^0, -15^0, -15^0, 15^0)	Present: DSC	28.940	51.528	65.959	85.07	89.53	119.88
	Chow et. al (1992) (CLPT)	28.98	51.56	65.97	85.11	89.57	119.9
(30^0, -30^0, -30^0, 30^0)	Present: DSC	28.648	53.597	62.720	85.093	95.088	114.26
	Chow et. al (1992) (CLPT)	28.69	53.62	62.74	85.09	95.15	114.3
(45^0, -45^0, -45^0 , 45^0)	Present: DSC	28.503	55.534	60.197	85.254	102.52	105.18
	Chow et. al (1992) (CLPT)	28.53	55.56	60.22	85.25	102.6	105.2

Table 7.6 Natural frequency parameters $\beta_1 = \omega a^2 \sqrt{\rho h / D_{0,1}}$ of fully simply supported (SSSS) and clamped (CCCC) square five-ply laminates with several orientations ($\lambda = 1$, DSC: $N = 21 \times 21$)

Five-ply Ply angle	Resource	Mode Sequence Number 1	2	3	4	5	6
SSSS:							
(0^0, 0^0, 0^0 , 0^0 ,0^0)	Analytical (Whitney, 1987)	15.171	33.248	44.387	60.682	64.457	90.145
	Present: DSC	15.171	33.248	44.387	60.682	64.457	90.145
	Chow et. al (1992) (CLPT)	15.19	33.31	44.52	60.78	64.55	90.31
	Leissa and Narita (1989) (CLPT)	15.19	33.30	44.42	60.77	64.53	90.29
(15^0, -15^0, 15^0, -15^0, 15^0)	Present: DSC	15.506	34.296	43.922	61.630	66.419	91.485
	Chow et. al (1992) (CLPT)	15.46	34.24	43.88	61.59	66.42	91.52
	Leissa and Narita (1989) (CLPT)	15.50	34.30	43.93	61.62	66.48	91.51
(30^0, -30^0, 30^0, -30^0, 30^0)	Present: DSC	16.161	36.705	42.652	63.561	71.598	85.864
	Chow et. al (1992) (CLPT)	15.98	36.58	42.53	63.37	71.43	85.86
	Leissa and Narita (1989) (CLPT)	16.10	36.64	42.62	63.45	71.60	85.88
(45^0, -45^0, 45^0, -45^0, 45^0)	Present: DSC	16.480	38.436	41.478	64.563	77.958	79.223
	Chow et. al (1992) (CLPT)	16.29	38.30	41.32	64.35	77.77	79.09
	Leissa and Narita (1989) (CLPT)	16.40	38.37	41.40	64.41	77.94	79.23
CCCC:							
(0^0, 0^0, 0^0 , 0^0 ,0^0)	Present: DSC	29.087	50.792	67.279	85.629	87.112	118.50
	Chow et. al (1992) (CLPT)	29.13	50.82	67.29	85.67	87.14	118.6
(15^0, -15^0, 15^0, -15^0, 15^0)	Present: DSC	28.972	51.620	65.995	85.527	89.350	120.40
	Chow et. al (1992) (CLPT)	29.00	51.65	66.01	85.55	89.40	120.5
(30^0, -30^0, 30^0, -30^0, 30^0)	Present: DSC	28.740	53.951	62.741	86.097	94.968	114.35
	Chow et. al (1992) (CLPT)	28.78	53.98	62.76	86.09	95.04	114.4
(45^0, -45^0, 45^0, -45^0, 45^0)	Present: DSC	28.624	56.308	59.917	86.486	102.95	104.81
	Chow et. al (1992) (CLPT)	28.68	56.34	59.94	86.48	103.0	104.9

Finally, another comparison is given for (0^0, 90^0, 0^0) fiber orientation in Table 7.7. Here the reference studies are Liew (1996) using *p*-Ritz approach; Ferreira & Fasshauer (2006) introducing radial basis function-pseudospectral approach; and Lanhe et al. (2005) utilizing moving least squares-differential quadrature method. In this case, natural frequency parameter is determined as $\beta_2 = \omega a^2 / \pi^2 \sqrt{\rho h / D_{0,2}}$ by

means of another arbitrary rigidity expression (i.e., $D_{0,2} = E_2 h^3/(1-\nu_{12}\nu_{21})$). The plate parameters are $E_1/E_2 = 40$, $G_{12} = 0.6E_2$, $\upsilon_{12} = 0.25$, $\upsilon_{21} = 0.00625$, $h = 0.001m$, $h/a = 0.001$. DSC solutions for fully simply supported (SSSS) and fully clamped (CCCC) plates are very close to the compared results.

Table 7.7 Natural frequency parameters $\beta_2 = \omega a^2/\pi^2\sqrt{\rho h/D_{0,2}}$ of fully simply supported (SSSS) and fully clamped (CCCC) square three-ply laminates with (0^0, 90^0, 0^0) orientation ($\lambda = 1$, DSC: $N = 21\times 21$)

Three-ply $(0^0, 90^0, 0^0)$	Mode Sequence Number							
Resource	1	2	3	4	5	6	7	8
SSSS:								
Analytical (Whitney, 1987) (CLPT: SOP)	6.6254	9.4473	16.2056	25.1181	26.5017	26.6585	30.3175	37.7892
Present: DSC	6.6254	9.4473	16.2056	25.1181	26.5017	26.6585	30.3175	37.7892
Liew (1996)	6.6252	9.4470	16.2051	25.1146	26.4982	26.6572	30.3139	37.7854
Ferreira and Fasshauer (2006)	6.6180	9.4368	16.2192	25.1131	26.4938	26.6667	30.2983	37.7850
Lanhe et al. (2005)	6.632	9.464	16.364	25.325	26.886	-	-	-
CCCC:								
Present: DSC	14.6692	17.6191	24.5235	35.5614	39.1818	40.7945	44.8174	50.3613
Liew (1996)	14.6655	17.6138	24.5114	35.5318	39.1572	40.7685	44.7865	50.3226
Ferreira and Fasshauer (2006)	14.8138	17.6181	24.1145	36.0900	39.0170	40.8323	44.9457	49.0715
Lanhe et al. (2005)	14.674	17.668	24.594	35.897	39.625	-	-	-

Moreover, as seen from Tables 7.2, 7.5, 7.6 and 7.7, in the given number of digits, DSC predictions completely match with the analytical results of simply supported laminates orientated as become specially orthotropic. This implies the superiority of the DSC compared to the other techniques. It is known that thin plate theory is not very accurate in the vibration analysis of laminated plates. However, the presented DSC results based on CLPT are sensitive because of sufficiently small thickness to length ratio of the considered plates; as seen the same predictions of exact CLPT and SOP cases.

7.3.2 Verification of Mode Shapes

In Figure 7.1, the first four mode shapes of SOP by the DSC are given together with symbolic nodal line representations given by Whitney (1987).

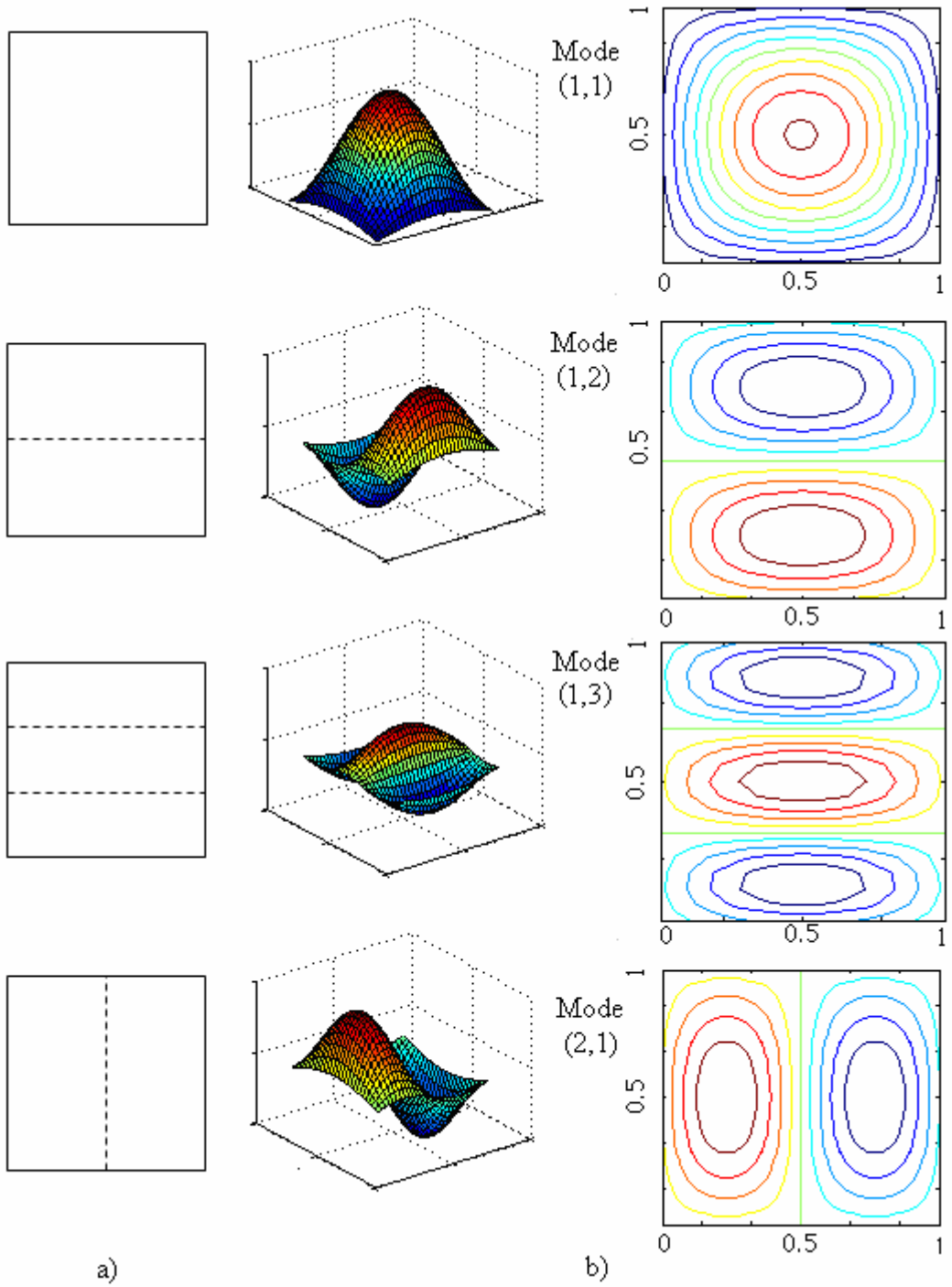

Figure 7.1 The first four mode shapes of simply supported specially orthotropic thin plate: a) Analytical (Whitney, 1987), b) DSC ($N = 21 \times 21$).

For the verification of mode shapes of laminated plates, five-ply fully simply supported composite plates having $\{\theta, -\theta, \theta, -\theta, \theta\}$ sequence with four orientation angles $\theta = 0^0, 15^0, 30^0, 45^0$ are considered. In Figure 7.2, the first eight mode

shapes ($n = 1, 2, \cdots, 8$) corresponding to the first eight natural frequency parameters ($\beta_1 = \omega a^2 \sqrt{\rho h / D_{0,1}}$) tabulated in Table 7.8 are compared with those of Chow et al. (1992). Here the material properties are $E_1 / E_2 = 15.4$, $G_{12} = 0.79 E_2$, $\upsilon_{12} = 0.3$, $\upsilon_{21} = 0.0195$. These consistent mode shapes simply verify the accuracy of the DSC for composite plates.

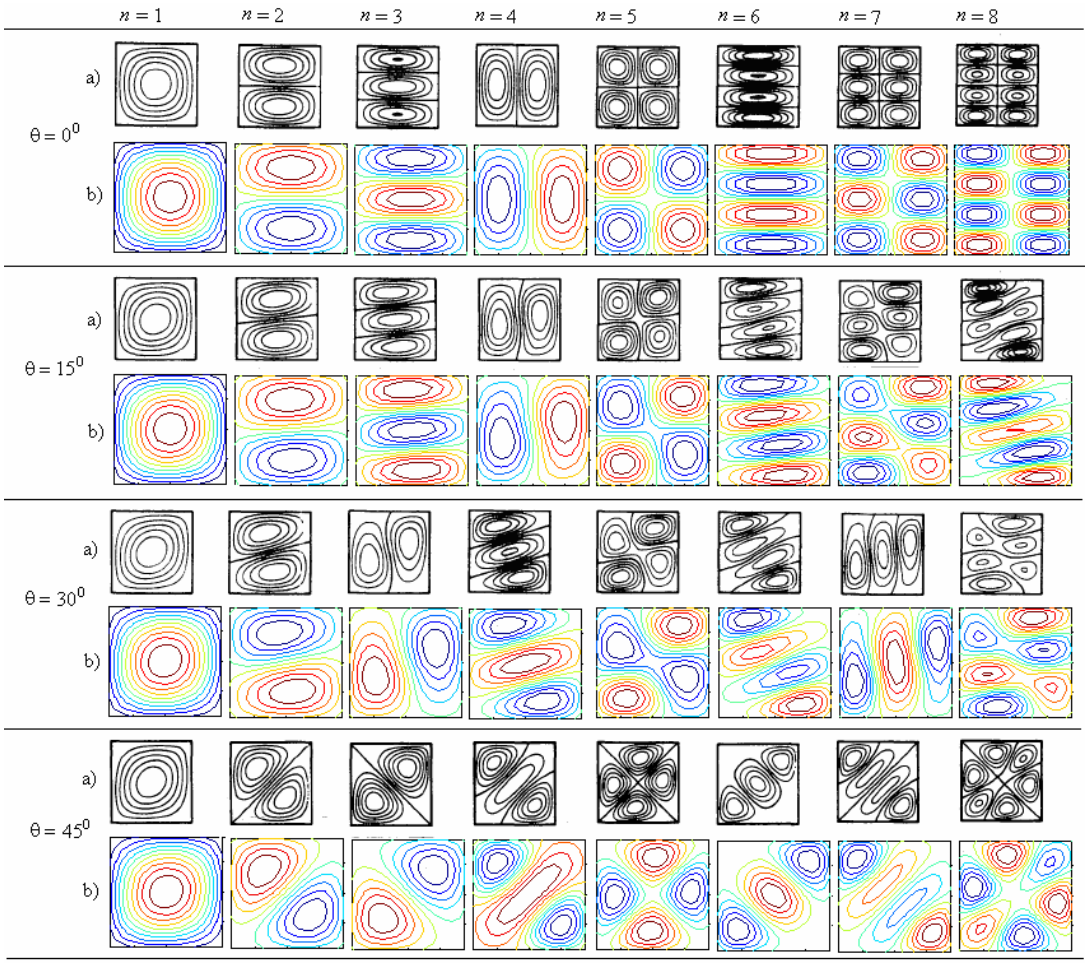

Figure 7.2 The first eight mode shapes of simply supported five-ply composite plates: a) Chow et al. (1992), b) DSC ($N = 21 \times 21$) (*n*: Mode sequence number, θ : Orientation angle).

Table 7.8 Natural frequency parameters $\beta_1 = \omega a^2 \sqrt{\rho h / D_{0,1}}$ corresponding to the first eight mode shapes of fully simply supported (SSSS) square five-ply laminates with several orientations ($\lambda = 1$, DSC: $N = 21 \times 21$)

Five-ply	Resource	Mode Sequence Number							
Ply angle		1	2	3	4	5	6	7	8
(0^0, 0^0, 0^0, 0^0, 0^0)	Present DSC	11.29	17.13	28.68	40.74	45.15	45.78	54.06	68.14
	Chow et al. (1992)	11.30	17.13	28.70	40.77	45.18	46.23	54.98	69.64
(15^0, -15^0, 15^0, -15^0, 15^0)	Present DSC	12.01	20.07	33.38	39.78	47.80	51.75	61.44	74.27
	Chow et al. (1992)	11.82	19.76	32.93	39.53	47.42	52.73	61.11	74.08
(30^0, -30^0, 30^0, -30^0, 30^0)	Present DSC	13.40	25.83	37.41	43.60	53.80	66.50	76.06	77.23
	Chow et al. (1992)	12.98	25.21	36.97	42.65	52.83	66.48	75.76	77.65
(45^0, -45^0, 45^0, -45^0, 45^0)	Present DSC	14.06	29.38	35.36	49.94	60.22	66.19	75.31	89.17
	Chow et al. (1992)	13.61	28.75	34.68	48.90	59.25	65.34	74.28	88.86

7.4 Case Studies for the Effects of Composite Plate Design Parameters

In all applications, linear vibration analyses were performed. The plates were assumed to be thin, square, and discretized by using $N = 21 \times 21$ grid points.

7.4.1 The Effects of Number of Plies, Orientation Angle and Boundary Conditions on Natural Frequency Parameters of Thin Composite Plates

The DSC predictions of the first ten natural frequency parameters of three-, four- and five-ply laminates are tabulated in Tables 7.9-7.11 respectively, for six different boundary conditions and four different stacking sequences. The orientations of the stacks are considered as $(\theta, -\theta, \theta)$ for three-, $(\theta, -\theta, -\theta, \theta)$ for four- and $(\theta, -\theta, \theta, -\theta, \theta)$ for five-ply laminates. Stacking sequences are labelled as P1 for $\theta = 0^0$, P2 for $\theta = 15^0$, P3 for $\theta = 30^0$ and P4 for $\theta = 45^0$. Boundary conditions are labelled as BC1, BC2,…, BC6 as presented in Tables 7.9-7.11. The natural frequency parameter $\beta = \omega a^2 \sqrt{\rho h / D_0}$ is determined by means of the rigidity $D_0 = E_1 h^3 / (1 - \nu_{12} \nu_{21})$. The plate parameters are $E_1 / E_2 = 2.45$, $G_{12} = 0.48 E_2$, $\upsilon_{12} = 0.23$, $\upsilon_{21} = 0.0939$.

Figure 7.3 demonstrates the variation of the first natural mode with respect to number of lamination, boundary condition and stacking sequence. Figure 7.4 shows

the variation of the tenth natural mode with respect to the same parameters. Figure 7.3 is an indicator of lower modes whereas Figure 7.4 reflects the feature of higher modes.

- For P1: Number of lamination and boundary condition do not influence frequencies.
- For P2: Number of lamination becomes to be effective on the frequency parameters regardless the type of boundary condition. Simply, increase in the number of lamination increases the natural frequency parameters.
- For P3: Except BC4, number of lamination is quite effective for the other conditions.
- For P4: In this sequence, number of lamination affects only BC2, BC4 and BC5 plates.

Table 7.9 Natural frequency parameters of three-ply laminates $(\theta, -\theta, \theta)$ with six different boundary conditions ($\beta = \omega a^2 \sqrt{\rho h / D_0}$)

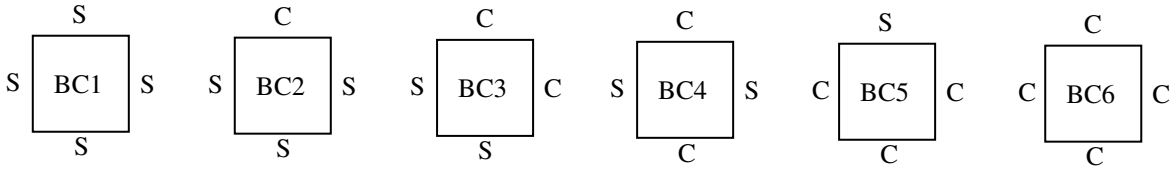

Three-ply Ply angle	Boundary Condition	Mode Sequence Number									
		1	2	3	4	5	6	7	8	9	10
P1: $(0^0, 0^0, 0^0)$	BC1	15.171	33.248	44.387	60.682	64.457	90.145	93.630	108.46	108.97	132.99
	BC2	17.354	38.989	45.511	64.670	73.628	94.356	97.646	111.76	120.97	142.36
	BC3	21.398	41.419	55.176	72.474	75.276	103.68	109.26	122.20	125.22	148.83
	BC4	20.402	45.638	46.998	69.434	83.677	95.247	106.06	115.06	134.34	148.94
	BC5	27.007	44.856	66.216	77.465	81.733	110.94	123.75	125.49	140.12	154.50
	BC6	29.087	50.792	67.279	85.629	87.112	118.50	126.18	136.87	142.84	165.84
P2: $(15^0, -15^0, 15^0)$	BC1	15.469	34.153	43.879	60.954	66.635	91.393	91.659	108.96	111.12	132.52
	BC2	17.707	39.813	45.192	65.290	75.599	92.211	98.975	112.30	123.59	140.57
	BC3	21.471	42.213	54.243	72.187	77.563	104.87	106.45	124.16	125.31	148.40
	BC4	20.791	45.514	47.739	70.200	85.623	93.210	106.82	116.38	137.04	148.24
	BC5	26.731	45.417	64.738	77.841	82.626	111.57	121.97	126.43	138.63	155.18
	BC6	28.897	51.405	65.911	84.515	89.712	119.21	122.74	139.30	141.93	165.24
P3: $(30^0, -30^0, 30^0)$	BC1	16.058	36.060	42.743	61.757	71.849	85.780	94.096	109.23	119.25	133.47
	BC2	18.495	41.053	45.229	66.506	81.026	86.983	100.81	114.13	132.19	140.98
	BC3	21.629	44.109	52.052	72.280	82.937	99.361	106.91	123.28	133.61	148.77
	BC4	21.786	44.476	50.622	71.730	87.959	91.845	107.41	120.40	146.07	148.10
	BC5	26.046	46.935	61.041	78.224	86.059	113.03	113.03	132.74	137.05	156.28
	BC6	28.522	53.124	62.683	83.821	95.158	114.13	120.64	138.58	149.10	164.97
P4: $(45^0, -45^0, 45^0)$	BC1	16.348	37.146	42.033	62.234	77.213	80.130	95.076	109.48	130.82	132.82
	BC2	19.214	40.331	47.506	67.279	80.153	89.555	101.05	116.67	133.04	141.37
	BC3	21.707	45.480	50.521	72.467	89.174	92.119	107.84	122.75	146.60	148.55
	BC4	23.059	43.047	54.979	72.655	82.688	101.21	106.97	125.16	134.84	148.71
	BC5	25.247	48.930	56.869	78.013	92.264	102.55	114.18	130.64	148.89	156.83
	BC6	28.337	54.623	60.430	83.658	101.94	105.60	121.41	137.29	163.18	165.04

Table 7.10 Natural frequency parameters of four-ply laminates $(\theta, -\theta, -\theta, \theta)$ with six different boundary conditions ($\beta = \omega a^2 \sqrt{\rho h / D_0}$)

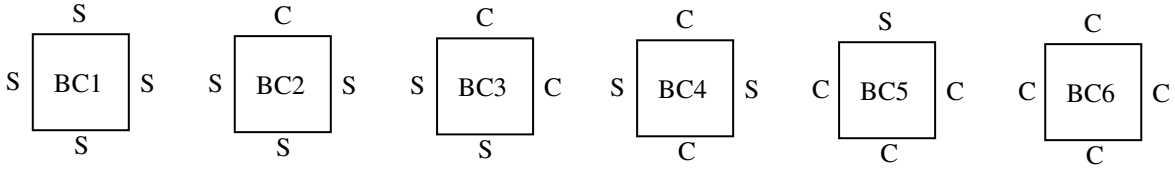

Four-ply	Boundary	Mode Sequence Number									
Ply angle	Condition	1	2	3	4	5	6	7	8	9	10
P1: (0^0, 0^0, 0^0, 0^0)	BC1	15.171	33.248	44.387	60.682	64.457	90.145	93.630	108.46	108.97	132.99
	BC2	17.354	38.989	45.511	64.670	73.628	94.356	97.646	111.76	120.97	142.36
	BC3	21.398	41.419	55.176	72.474	75.276	103.68	109.26	122.20	125.22	148.83
	BC4	20.402	45.638	46.998	69.434	83.677	95.247	106.06	115.06	134.34	148.94
	BC5	27.007	44.856	66.216	77.465	81.733	110.94	123.75	125.49	140.12	154.50
	BC6	29.087	50.792	67.279	85.629	87.112	118.50	126.18	136.87	142.84	165.84
P2: (15^0, -15^0, -15^0, 15^0)	BC1	15.490	34.235	43.904	61.333	66.520	91.446	92.217	109.11	111.03	133.86
	BC2	17.731	39.934	45.186	65.615	75.559	92.259	99.620	112.33	123.57	141.99
	BC3	21.506	42.315	54.281	72.645	77.427	105.48	106.51	124.40	125.19	149.82
	BC4	20.817	45.790	47.588	70.517	85.617	93.250	107.64	116.25	137.04	149.59
	BC5	26.772	45.525	64.795	78.272	82.550	112.22	122.04	126.40	138.81	156.34
	BC6	28.940	51.528	65.959	85.070	89.530	119.88	122.82	139.41	141.96	166.70
P3: (30^0, -30^0, -30^0, 30^0)	BC1	16.117	36.426	42.696	62.764	71.737	85.828	96.009	109.47	119.07	136.76
	BC2	18.568	41.621	45.017	67.500	81.072	86.958	102.96	114.14	132.16	144.38
	BC3	21.730	44.521	52.062	73.413	82.855	99.451	108.97	123.64	133.46	152.29
	BC4	21.874	44.957	50.539	72.771	88.109	91.747	109.71	120.32	146.19	148.09
	BC5	26.164	47.306	61.152	79.525	85.867	113.24	114.99	133.53	136.67	159.79
	BC6	28.648	53.597	62.720	85.093	95.088	114.26	122.85	139.08	148.93	168.72
P4: (45^0, -45^0, -45^0 , 45^0)	BC1	16.424	37.837	41.766	63.54	77.644	79.646	97.783	109.65	131.13	132.43
	BC2	19.316	40.909	47.419	68.692	80.174	89.503	103.80	117.00	132.94	145.76
	BC3	21.840	46.273	50.291	73.908	89.667	91.704	110.77	123.00	146.95	148.22
	BC4	23.190	43.540	55.058	74.218	82.562	101.30	109.67	125.91	134.51	153.18
	BC5	25.396	49.593	56.824	79.572	92.345	102.55	117.16	131.07	148.85	161.50
	BC6	28.503	55.534	60.197	85.254	102.52	105.18	124.59	137.64	163.64	165.32

Table 7.11 Natural frequency parameters of five-ply laminates $(\theta,-\theta,\theta,-\theta,\theta)$ with six different boundary conditions ($\beta=\omega a^2\sqrt{\rho h/D_0}$)

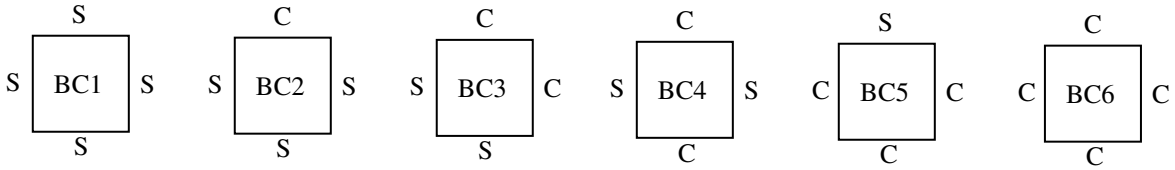

Five-ply Ply angle	Boundary Condition	Mode Sequence Number									
		1	2	3	4	5	6	7	8	9	10
P1: (0^0, 0^0, 0^0 , 0^0 ,0^0)	BC1	15.171	33.248	44.387	60.682	64.457	90.145	93.630	108.46	108.97	132.99
	BC2	17.354	38.989	45.511	64.670	73.628	94.356	97.646	111.76	120.97	142.36
	BC3	21.398	41.419	55.176	72.474	75.276	103.68	109.26	122.20	125.22	148.83
	BC4	20.402	45.638	46.998	69.434	83.677	95.247	106.06	115.06	134.34	148.94
	BC5	27.007	44.856	66.216	77.465	81.733	110.94	123.75	125.49	140.12	154.50
	BC6	29.087	50.792	67.279	85.629	87.112	118.50	126.18	136.87	142.84	165.84
P2: (15^0, -15^0, 15^0, -15^0, 15^0)	BC1	15.506	34.296	43.922	61.630	66.419	91.485	92.642	109.21	110.98	135.01
	BC2	17.749	40.026	45.180	65.861	75.526	92.295	100.12	112.33	123.56	143.21
	BC3	21.533	42.391	54.310	73.009	77.303	105.94	106.56	124.57	125.11	151.00
	BC4	20.837	46.036	47.436	70.757	85.610	93.280	108.29	116.11	137.04	150.69
	BC5	26.803	45.605	64.837	78.613	82.472	112.71	122.10	126.36	138.95	157.25
	BC6	28.972	51.620	65.995	85.527	89.350	120.40	122.87	139.48	142.00	167.91
P3: (30^0, -30^0, 30^0, -30^0, 30^0)	BC1	16.161	36.705	42.652	63.561	71.598	85.864	97.550	109.52	118.94	139.55
	BC2	18.622	42.109	44.792	68.264	81.065	86.946	104.75	113.93	132.12	147.17
	BC3	21.806	44.830	52.065	74.303	82.738	99.517	110.61	123.79	133.35	155.27
	BC4	21.939	45.330	50.459	73.569	88.172	91.688	111.68	120.00	146.26	148.10
	BC5	26.251	47.580	61.232	80.620	85.587	113.34	116.58	134.07	136.34	162.73
	BC6	28.740	53.951	62.741	86.097	94.968	114.35	124.61	139.33	148.80	171.89
P4: (45^0, -45^0, 45^0, -45^0, 45^0)	BC1	16.480	38.436	41.478	64.563	77.958	79.223	100.09	109.47	131.32	132.14
	BC2	19.391	41.354	47.333	69.808	80.102	89.468	106.09	116.98	132.85	146.63
	BC3	21.940	46.954	50.024	75.025	90.027	91.337	113.26	122.86	147.20	147.98
	BC4	23.286	43.905	55.110	75.506	82.324	101.37	111.85	126.28	134.24	156.97
	BC5	25.504	50.101	56.768	80.794	92.317	102.55	119.62	131.11	148.79	163.48
	BC6	28.624	56.308	59.917	86.486	102.95	104.81	127.27	137.56	163.95	165.06

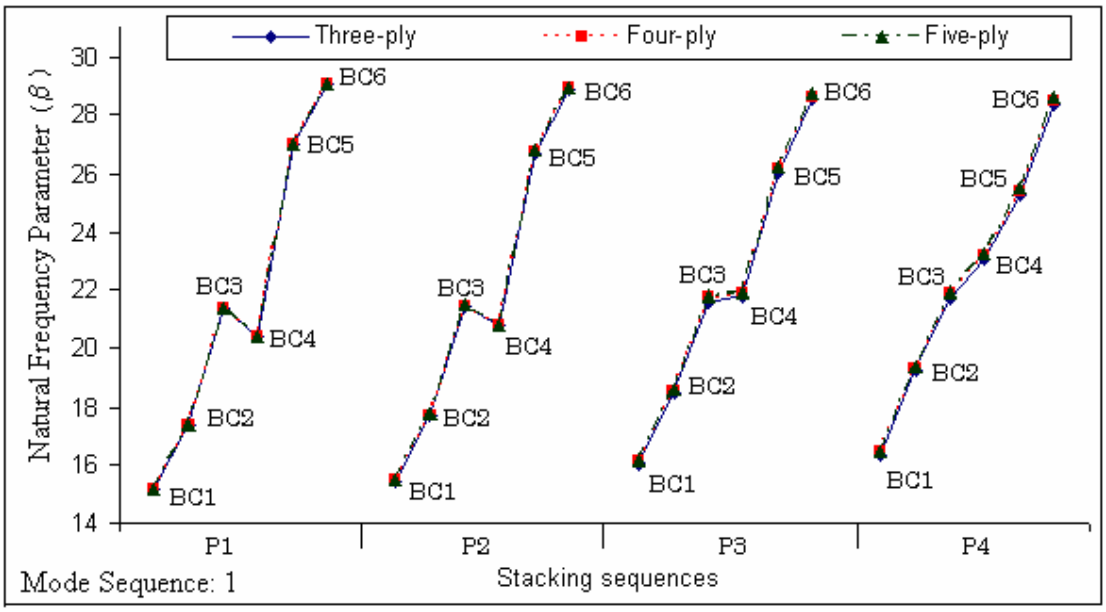

Figure 7.3 Natural frequency parameters of composite plates with respect to number of lamination, boundary condition and stacking sequence for Mode Sequence: 1.

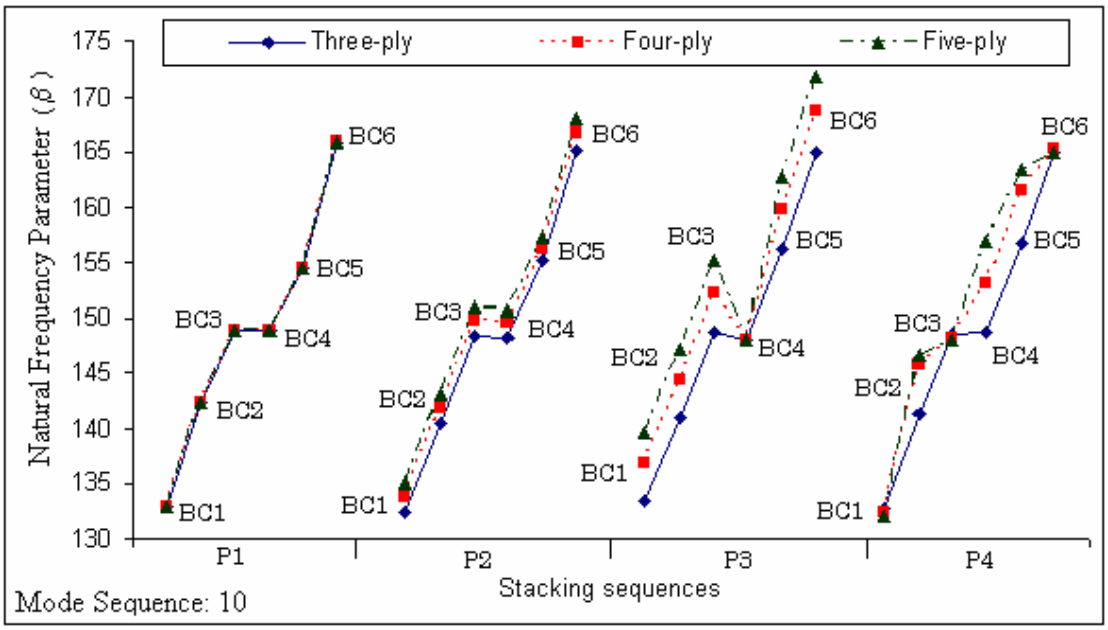

Figure 7.4 Natural frequency parameters of composite plates with respect to number of lamination, boundary condition and stacking sequence for Mode Sequence: 10.

7.4.2 The Effects of Material, Stacking Sequence and Boundary Conditions on Free Vibration Characteristics of Polymer Based Thin Composite Plates

In this application, three different polymer materials with six stacking sequences and two boundary conditions are considered. Modal behaviours of composite plates with various combinations of these three main variables are examined. Computed results are presented in Figures 7.5-7.10. The materials are E-glass/epoxy, Kevlar/epoxy and Carbon/epoxy. Physical properties of these materials are given in Table 7.12. The examined boundary conditions are fully simply supported and fully clamped. In the analysis, stacking sequences are labelled as S1, S2,…, S6. These are,

- Symmetric cross ply (S1): $[0/90]_{2S}$
- Quasi-isotropic (S2): $[0/90/45/-45]_{S}$
- Symmetric angle ply (S3-S6): $[\theta/-\theta]_{2S}$

where $\theta = 15^0, 30^0, 45^0$ and 60^0 corresponding to stacking sequences S3, S4, S5 and S6 respectively. It is assumed that plates are composed of eight layers. In this analysis, the natural frequency parameter is defined as $\Omega/\pi^2 = \omega a^2\sqrt{\rho h/D_{22}}$ for numerical facility.

Table 7.12 Physical properties of the polymer prepregs (Daniel & Ishai, 1994) and aluminium alloy (Harras, Benamar & White, 2002)

Properties	E-glass/epoxy	Kevlar/epoxy	Carbon/epoxy (AS4/3501-6)	Aluminium alloy
Fiber volume ratio (V_f)	0.55	0.60	0.63	-
Density (ρ. kg/m^3)	2100	1380	1580	-
Longitudinal modulus (E_1, GPa)	39	87	142	72.39
Transverse modulus (E_2, GPa)	8.6	5.5	10.3	72.39
In-plane shear modulus (G_{12}, GPa)	3.8	2.2	7.2	27.2
Major Poisson's ratio (υ_{12})	0.28	0.34	0.27	0.33

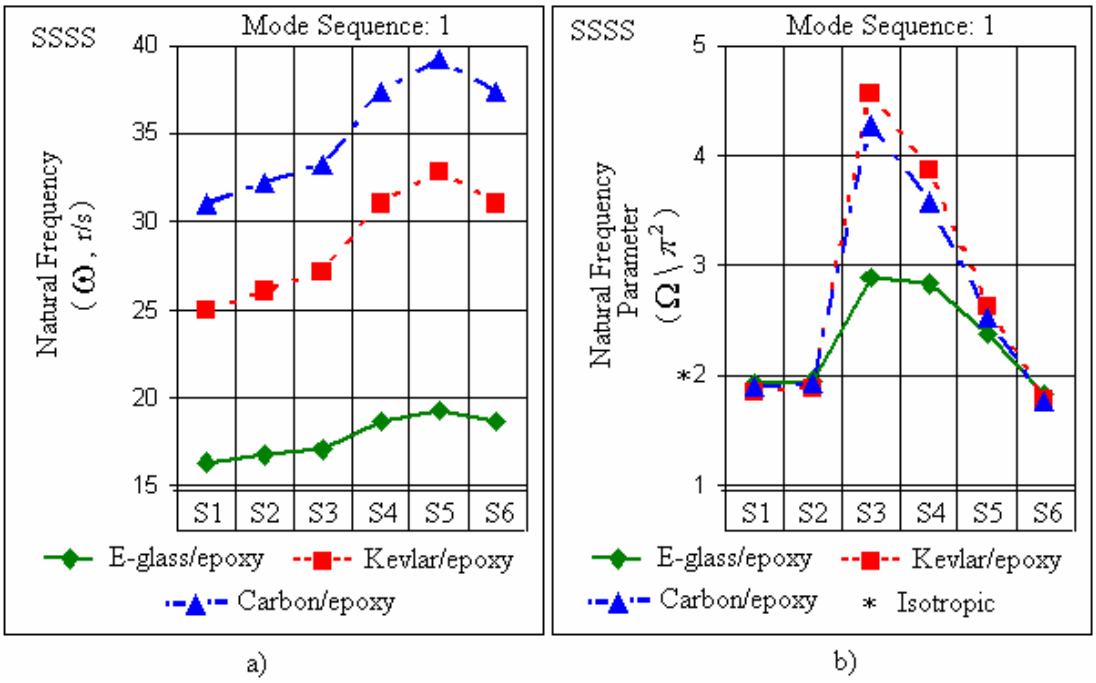

Figure 7.5 a) Natural frequencies b) Natural frequency parameters ($\Omega/\pi^2 = \omega a^2\sqrt{\rho h/D_{22}}$) of simply supported composite plates with several stacking sequences for Mode Sequence: 1.

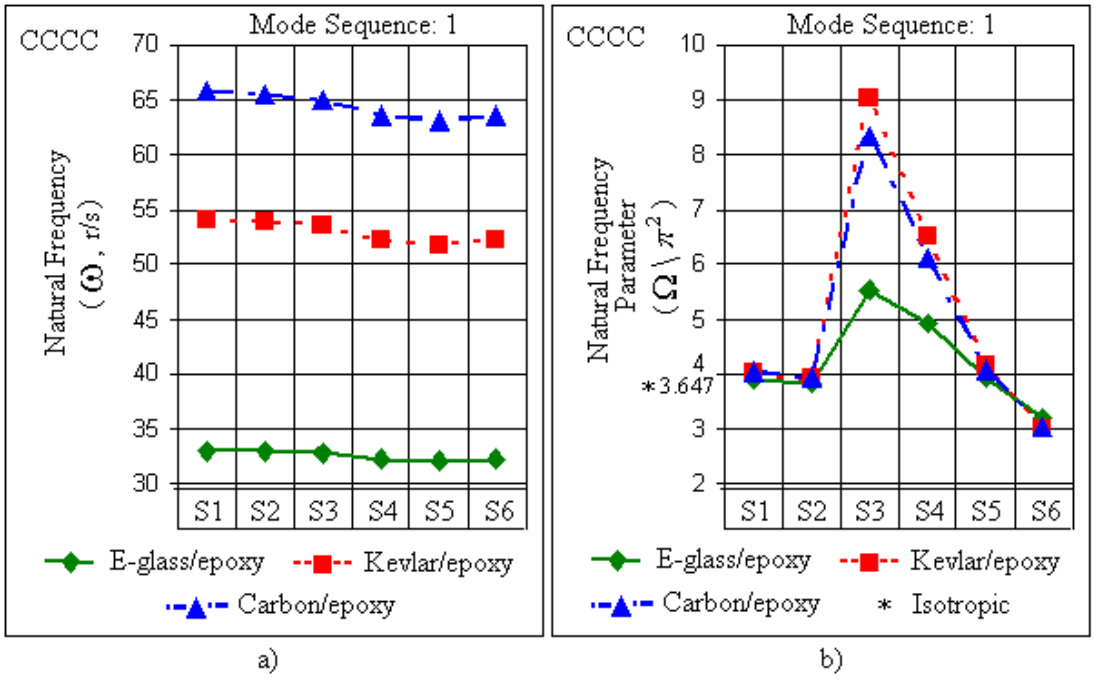

Figure 7.6 a) Natural frequencies b) Natural frequency parameters ($\Omega/\pi^2 = \omega a^2\sqrt{\rho h/D_{22}}$) of clamped composite plates with several stacking sequences for Mode Sequence: 1.

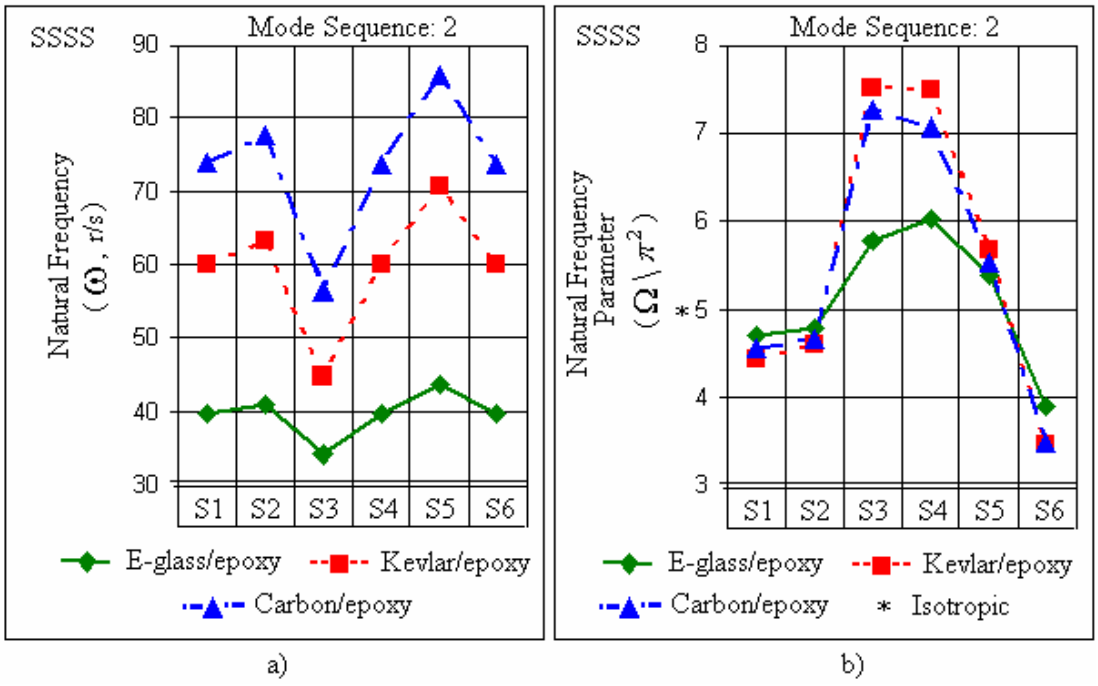

Figure 7.7 a) Natural frequencies b) Natural frequency parameters ($\Omega/\pi^2 = \omega a^2\sqrt{\rho h/D_{22}}$) of simply supported composite plates with several stacking sequences for Mode Sequence: 2.

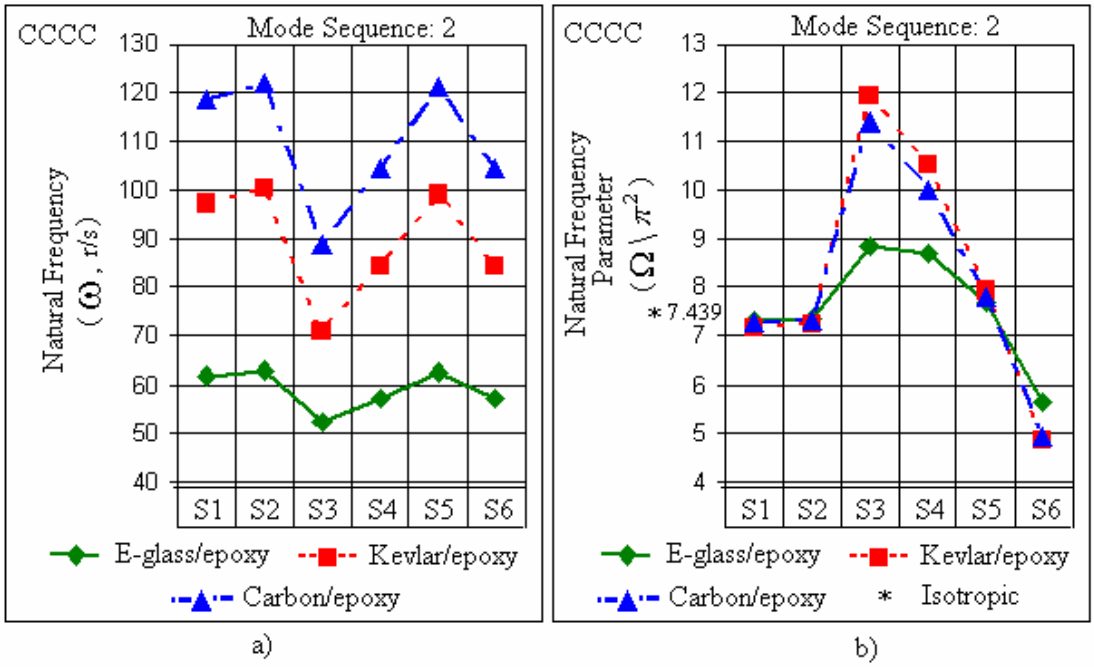

Figure 7.8 a) Natural frequencies b) Natural frequency parameters ($\Omega/\pi^2 = \omega a^2\sqrt{\rho h/D_{22}}$) of clamped composite plates with several stacking sequences for Mode Sequence: 2.

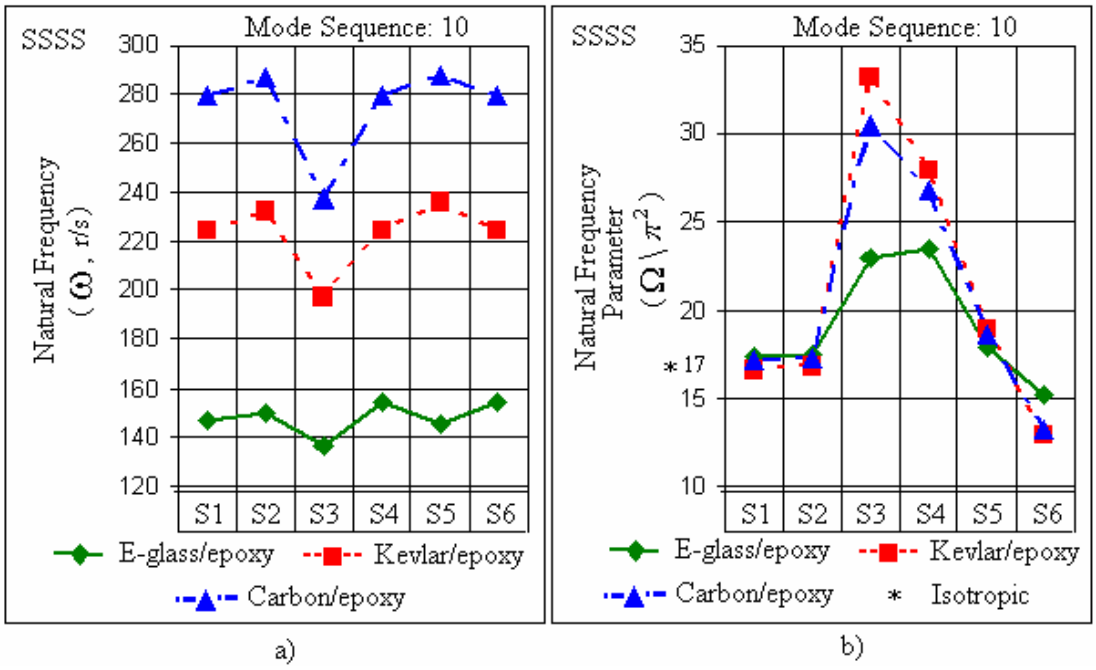

Figure 7.9 a) Natural frequencies b) Natural frequency parameters ($\Omega/\pi^2 = \omega a^2\sqrt{\rho h/D_{22}}$) of simply supported composite plates with several stacking sequences for Mode Sequence: 10.

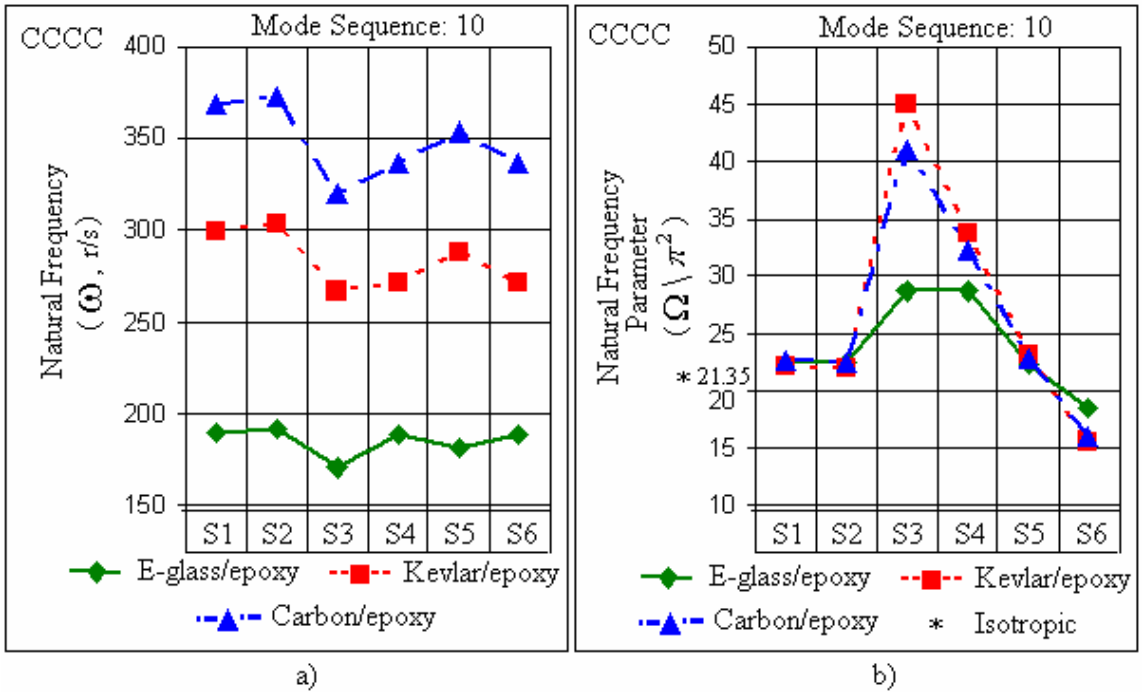

Figure 7.10 a) Natural frequencies b) Natural frequency parameters ($\Omega/\pi^2 = \omega a^2\sqrt{\rho h/D_{22}}$) of clamped composite plates with several stacking sequences for Mode Sequence: 10.

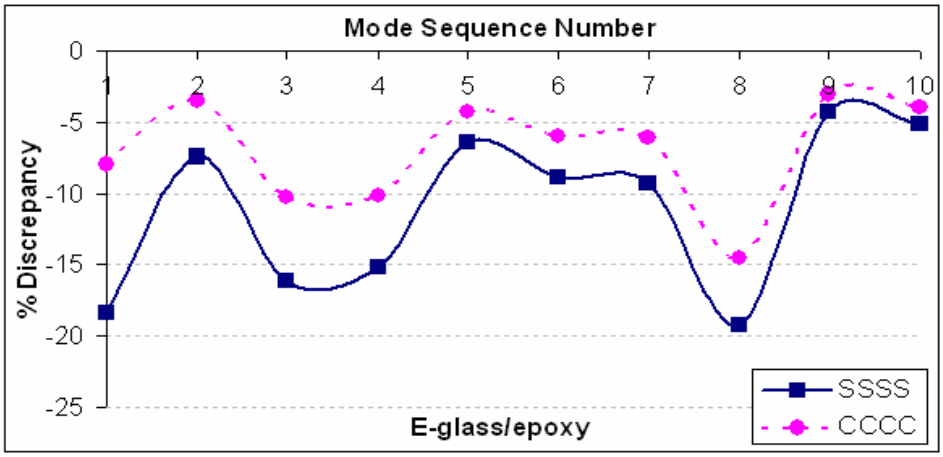

a)

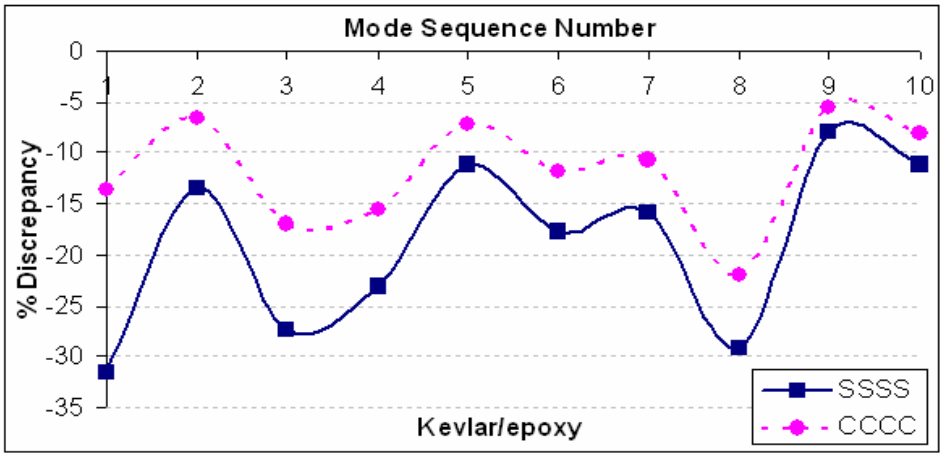

b)

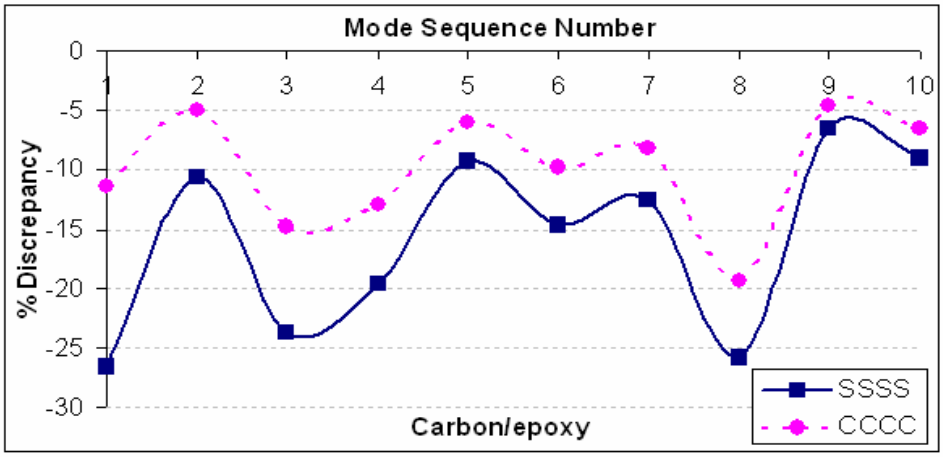

c)

Figure 7.11 Discrepancies of natural frequency parameters ($\Omega/\pi^2 = \omega a^2\sqrt{\rho h/D_{22}}$) of composite plates with S5 sequence made of a) E-glass/epoxy, b) Kevlar/epoxy and c) Carbon/epoxy materials, from an isotropic plate.

Tables 7.13-7.15 present the first ten natural frequency parameters of the considered plates. Figures 7.5.a-7.10.a display natural frequencies whereas Figures 7.5.b-7.10.b show frequency parameters of the plates for Mode Sequences 1, 2 and 10, respectively. Since similar variation trends for frequencies are observed in Figures 7.5-7.10, these modal features may be generalized to the other modes. Table 7.16 presents non-dimensional bending and bend-twist rigidity values which may give useful information for the examination of modal characteristics in detail. Table 7.17 displays the first twenty mode shapes of an isotropic plate and compares them with the first ten mode shapes of composite plates. When Figures 7.5-7.10 and Tables 7.16 and 7.17 are examined together; the following conclusions can be drawn:

- The variation of natural frequencies with respect to stacking sequences is very similar for the three composites for a specific boundary condition.

  - Natural frequencies of the plates made all of the examined three materials are not considerably affected by selecting S1 or S2 stacking sequences. This is due to the fact that materials with S1 and S2 have non-dimensional plate rigidities D_γ and D_ϕ in the same order of magnitude. On the contrary, symmetric angle ply sequences drastically influence natural frequencies depending on the orientation angle (Figures 7.5.a-7.10.a, Table 7.16).
  - The same natural frequencies are obtained for S4 and S6 due to the fact that their orientation angles are complementary angles of each others (Figures 7.5.a-7.10.a).
  - Apparently, the plate made of Carbon/epoxy has the highest natural frequencies and therefore is determined as the most rigid one. Kevlar/epoxy is less rigid and evidently the most elastic one is E-glass/epoxy (Figures 7.5.a-7.10.a). This property also may be inspected from Table 7.16 as E-glass/epoxy having generally the lowest non-dimensional rigidities.

- The change of boundary condition highly affects natural frequency-stacking sequence relation especially in the first mode, which is the most boundary condition-dependent mode (Figures 7.5.a and 7.10.a).

- The first natural frequencies of angle-plied plates (S3-S6) are higher than those of S1 and S2 plates for SSSS and vice versa for CCCC conditions. It may be stated that the change of boundary condition completely reverses the variation trend of the first natural frequency with respect to S1-S6 sequences.
- S5 plate made of Carbon/epoxy is the most rigid plate among simply supported plates (Figures 7.5.a, 7.7.a and 7.9.a) whereas S2 plate made of Carbon/epoxy is the most rigid one among the clamped plates (Figures 7.6.a, 7.8.a and 7.10.a). In particular, the plate with S2-Carbon/epoxy-clamped combination has the highest natural frequencies.

▪ Mode shapes clearly show that some modal replacements are encountered in composite plates, generally, after the first two modes.

- Considerable mode shape replacements with isotropic plates are observed in particular for angle ply sequences (except S5) compared to S1 and S2 sequences (Table 7.16). This is because S1 and S2 sequences have comparatively close rigidities to isotropic plates (Table 7.16).
- Stack S5 shows resembling modal characteristics to isotropic plates since it has equal rigidities in both directions ($D_\gamma = 1$) (Tables 7.16 and 7.17).
- Having close D_γ and D_ϕ values, stacks S1 and S2 have the same mode shapes and are shown together (Tables 7.16 and 7.17).
- Having complementary orientation angles, stacks S4 and S6 show inverse nodal lines with respect to each other except for diagonally symmetric mode shapes (Table 7.17).
- The same mode shapes are obtained for Carbon/epoxy and Kevlar/epoxy and they are shown together in Table 7.17. These two materials have similar rigidities as shown in Table 7.16. Natural frequencies are affected by small differences in variables but mode shapes are not.
- For these materials and orientations, boundary conditions do not considerably affect the mode shapes and thus, similar shapes are obtained for SSSS and CCCC conditions (Table 7.16).

- There is almost an explicit relation between mode shapes in Table 7.17 and non-dimensional rigidities in Table 7.16. For instance, $D_\gamma \neq 1$ implies that the rigidity of the plate in a direction is higher than the other one. The other non-dimensional rigidities D_ϕ, D_α and D_β reflect a coupling behaviour between the two directions. This coupling leads to small shape changes compared to isotropic plate; however, these small differences are not considerable in such a general analysis.

- Stacking sequences considerably change the deviation of a composite plate from an isotropic plate (Figures 7.5.b-7.10.b).

  - Plates with S1 and S2 sequences approximately have the same frequency parameters with an isotropic plate (Figures 7.5.b-7.10.b).
  - In the angle plies, S3 and S4 have higher positive deviations from isotropic plate. S5 is the least deviated angle ply, whereas S6 negatively deviates.
  - Frequency parameters of plates with 45° orientation angle (S5) are very close to those of an isotropic plate (Figures 7.5.b-7.10.b). The discrepancy for CCCC plates is less, as obviously seen from the modal spectra in Figure 7.11.

Table 7.13 Natural frequency parameters of composite plates made of E-glass/epoxy ($\Omega/\pi^2 = \omega a^2\sqrt{\rho h/D_{22}}$)

Mode Sequence Number	Isotropic		Symmetric cross ply (S1)		Quasi isotropic (S2)		Symmetric angle ply							
	SSSS	CCCC	SSSS	CCCC	SSSS	CCCC	SSSS				CCCC			
							Orientation Angle (Degree)				Orientation Angle (Degree)			
							15 (S3)	30 (S4)	45 (S5)	60 (S6)	15 (S3)	30 (S4)	45 (S5)	60 (S6)
1	2.000	3.647	1.929	3.897	1.948	3.830	2.885	2.823	2.366	1.828	5.522	4.907	3.936	3.177
2	5.000	7.439	4.690	7.326	4.769	7.350	5.776	6.022	5.371	3.900	8.840	8.700	7.702	5.634
3	5.000	7.439	5.607	8.660	5.451	8.348	8.817	7.596	5.808	4.919	13.344	11.090	8.203	7.182
4	8.000	10.971	7.716	11.232	7.780	11.145	10.688	10.810	9.217	7.001	14.482	14.375	12.085	9.309
5	10.000	13.340	9.615	13.108	9.722	13.185	11.560	11.546	10.647	7.477	16.262	15.257	13.912	9.880
6	10.000	13.403	11.952	16.218	11.452	15.495	16.195	15.347	10.884	9.939	21.262	20.369	14.215	13.191
7	13.000	16.733	12.098	16.257	12.306	16.343	17.754	16.469	14.206	10.665	22.439	20.778	17.764	13.456
8	13.000	16.733	13.685	18.276	13.517	17.885	18.752	18.303	15.503	11.853	25.255	22.767	19.161	14.744
9	17.000	21.350	16.586	21.018	16.699	21.111	21.378	19.411	17.728	12.570	27.983	24.533	21.998	15.887
10	17.000	21.350	17.361	22.451	17.462	22.325	22.975	23.490	17.877	15.212	28.674	28.577	22.186	18.506

Table 7.14 Natural frequency parameters of composite plates made of Kevlar/epoxy ($\Omega/\pi^2 = \omega a^2\sqrt{\rho h/D_{22}}$)

Mode Sequence Number	Isotropic		Symmetric cross ply (S1)		Quasi isotropic (S2)		Symmetric angle ply							
	SSSS	CCCC	SSSS	CCCC	SSSS	CCCC	SSSS				CCCC			
							Orientation Angle (Degree)				Orientation Angle (Degree)			
							15 (S3)	30 (S4)	45 (S5)	60 (S6)	15 (S3)	30 (S4)	45 (S5)	60 (S6)
1	2.000	3.647	1.841	3.997	1.884	3.899	4.558	3.862	2.630	1.772	9.003	6.508	4.143	2.986
2	5.000	7.439	4.427	7.184	4.581	7.242	7.511	7.490	5.672	3.437	11.946	10.515	7.933	4.825
3	5.000	7.439	5.865	9.224	5.637	8.764	12.458	10.669	6.371	4.896	17.229	15.410	8.703	7.072
4	8.000	10.971	7.365	11.199	7.513	11.092	15.286	12.684	9.846	5.821	23.275	16.445	12.678	7.547
5	10.000	13.340	9.307	12.861	9.508	13.020	18.181	15.435	11.117	7.083	24.789	20.162	14.307	9.252
6	10.000	13.403	11.282	15.704	11.703	15.907	19.380	19.536	11.769	8.965	26.065	24.172	14.981	11.092
7	13.000	16.733	12.867	17.565	12.128	16.496	23.087	21.629	15.059	9.926	30.944	27.110	18.529	12.441
8	13.000	16.733	13.836	18.874	13.620	18.318	28.143	22.012	16.787	10.101	34.416	28.570	20.427	13.110
9	17.000	21.350	16.261	20.725	16.468	20.910	30.126	27.003	18.358	12.392	38.073	33.469	22.531	15.359
10	17.000	21.350	16.570	22.116	16.792	21.916	33.219	27.927	18.907	12.815	44.833	33.773	23.074	15.498

Table 7.15 Natural frequency parameters of composite plates made of Carbon/epoxy ($\Omega/\pi^2 = \omega a^2\sqrt{\rho h/D_{22}}$)

Mode Sequence Number	Isotropic		Symmetric cross ply (S1)		Quasi isotropic (S2)		Symmetric angle ply							
	SSSS	CCCC	SSSS	CCCC	SSSS	CCCC	SSSS				CCCC			
							Orientation Angle (Degree)				Orientation Angle (Degree)			
							15 (S3)	30 (S4)	45 (S5)	60 (S6)	15 (S3)	30 (S4)	45 (S5)	60 (S6)
1	2.000	3.647	1.904	4.030	1.929	3.922	4.271	3.582	2.533	1.764	8.343	6.098	4.061	3.003
2	5.000	7.439	4.541	7.278	4.663	7.311	7.255	7.059	5.530	3.476	11.389	9.999	7.807	4.924
3	5.000	7.439	5.917	9.247	5.673	8.774	12.213	9.904	6.184	4.877	16.762	14.357	8.537	7.070
4	8.000	10.971	7.615	11.401	7.694	11.240	14.077	12.134	9.569	5.976	21.384	15.841	12.401	7.801
5	10.000	13.340	9.431	12.979	9.598	13.104	17.052	14.366	10.928	7.075	24.282	18.859	14.139	9.288
6	10.000	13.403	11.674	16.052	11.987	16.164	19.113	18.795	11.469	9.256	24.357	23.396	14.721	11.522
7	13.000	16.733	12.874	17.538	12.123	16.460	22.058	20.107	14.632	9.902	29.317	25.651	18.112	12.632
8	13.000	16.733	14.096	19.084	13.807	18.463	27.705	20.755	16.355	10.221	33.950	26.604	19.985	13.101
9	17.000	21.350	16.389	20.853	16.562	21.001	29.296	25.062	18.113	12.342	36.650	31.451	22.316	15.489
10	17.000	21.350	17.134	22.611	17.207	22.291	30.478	26.786	18.530	13.191	41.068	32.259	22.754	15.887

Table 7.16 Non-dimensional bending rigidities (D_γ, D_ϕ) and bend-twist coupling rigidities $\left(D_\alpha, D_\beta\right)$ of composite plates consisting of eight layers with different material properties and stacking sequences

Stacking Sequences	E-glass/epoxy				Kevlar/epoxy				Carbon/epoxy			
	D_γ	D_ϕ	D_α	D_β	D_γ	D_ϕ	D_α	D_β	D_γ	D_ϕ	D_α	D_β
Symmetric cross ply (S1)	1.6298	0.5457	0	0	1.9869	0.2014	0	0	1.9598	0.3324	0	0
Quasi isotropic (S2)	1.4583	0.6694	0.0382	0.0382	1.7099	0.4255	0.0592	0.0592	1.6867	0.5224	0.0572	0.0572
Symmetric angle ply												
15^o (S3)	3.9594	1.6972	0.2873	0.0331	12.8470	3.5654	1.1865	0.0960	10.7140	3.3425	0.9341	0.1175
30^o (S4)	2.3845	2.3264	0.3278	0.1219	4.7487	4.7148	0.9076	0.3099	4.1234	3.9620	0.7346	0.2798
45^o (S5)	1.0000	1.8269	0.1693	0.1693	1.0000	2.5246	0.2911	0.2911	1.0000	2.2663	0.2648	0.2648
60^o (S6)	0.4194	0.9756	0.0511	0.1375	0.2106	0.9929	0.0653	0.1911	0.2425	0.9609	0.0679	0.1781
Isotropic	1.0000	1.0000	0	0								

Table 7.17 Isotropic plate bending mode shapes (1-20) and corresponding laminated composite plate bending mode sequences (1-10)

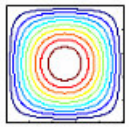 m,n (Md.Sq.) 1,1 (1)	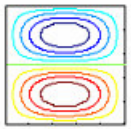 1,2 (2)	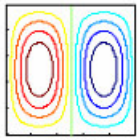 2,1 (3)	 2,2 (4)	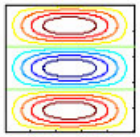 1,3 (5)	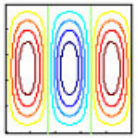 3,1 (6)	 2,3 (7)	 3,2 (8)	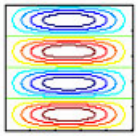 1,4 (9)	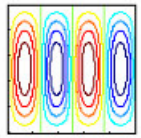 4,1 (10)
St. Sq.	**Material:** *E-glass/epoxy composite (Mode Sequence: 1-10)*								
S1-S2	1	2	3	4	5	6	7	8	9	-
S3	1	2	3	5	4	8	6	9	7	-
S4	1	2	3	5	4	6	7	9	8	-
S5	1	2	3	4	5	6	7	8	9	10
S6	1	3	2	5	6	4	8	7	-	8
St. Sq.	**Material:** *Kevlar/epoxy and Carbon/epoxy composites (Mode Sequence: 1-10)*								
S1-S2	1	2	3	4	5	7	6	8	9	-
S3	1	2	4	5	3	10	7	-	6	-
S4	1	2	3	5	4	7	8	9	6	-
S5	1	2	3	4	5	6	7	8	9	10
S6	1	3	2	5	7	4	9	8	-	6

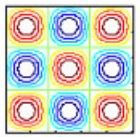 3,3 (11)	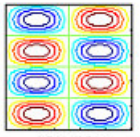 2,4 (12)	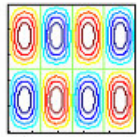 4,2 (13)	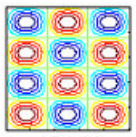 3,4 (14)	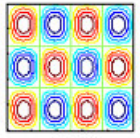 4,3 (15)	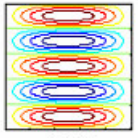 1,5 (16)	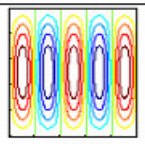 5,1 (17)	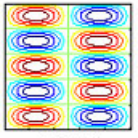 2,5 (18)	 5,2 (19)	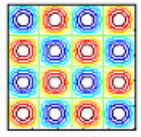 4,4 (20)
St. Sq.	**Material:** *E-glass/epoxy composite (Mode Sequence: 1-10)*								
S1-S2	10	-	-	-	-	-	-	-	-	-
S3	-	10	-	-	-	-	-	-	-	-
S4	-	10	-	-	-	-	-	-	-	-
S5	-	-	-	-	-	-	-	-	-	-
S6	-	-	10	-	-	-	-	-	-	-
St. Sq.	**Material:** *Kevlar/epoxy and Carbon/epoxy composites (Mode Sequence: 1-10)*								
S1-S2	10	-	-	-	-	-	-	-	-	-
S3	-	9	-	-	-	8	-	-	-	-
S4	-	-	-	-	-	10	-	-	-	-
S5	-	-	-	-	-	-	-	-	-	-
S6	-	-	-	-	-	-	10	-	-	-

7.4.3 The Effects of Material, Orientation Angle and Boundary Conditions on Natural Frequency Parameters of Thin FML Plates

Natural frequency parameters of aluminium/E-glass-epoxy, aluminium/Kevlar-epoxy and aluminium/Carbon-epoxy plates with five stacking sequences orientated by various fiber angles shown in Figure 7.12 were obtained in this application. Tables 7.18-7.20 show frequency parameters (Ω/π^2) for fully simply supported and fully clamped FML plates. Figures 7.13-7.16 display the summary of all results given in Tables 7.18-7.20 and hence exhibit the effects of material, boundary condition and fiber orientation on natural frequency parameters. Figures 7.13 and 7.14 for Mode 1 generally reflect the characteristics of the first few modes whereas Figures 7.15 and 7.16 for Mode 10 reflect the feature of higher modes. The following observations may be made from Figures 7.13-7.16:

- For the first few modes of all polymer prepregs, S3 plates with simply supported and S1 plates with clamped boundary conditions have higher frequency parameters. However, for higher modes, stacks having small orientation angles (S1, S2) provide higher frequency parameters independent of the boundary conditions.

- Frequency parameters of S4 plates seem to be very close to those of monolithic aluminium alloy plates, except for the first few modes of simply supported plates shown in Figure 7.13. This similarity is mostly encountered at higher modes where boundary conditions lose their effect.

- In general, aluminium/polymer prepregs have higher frequency parameters compared to monolithic aluminium alloys.

- In general aluminium/Carbon-epoxy plates have higher frequency parameters than the other FMLs.

- The exception to the previous two observations is the variation of S5. This stack triggers different modal tendencies from the others. Therefore, S5 should be exclusively taken into consideration in engineering design.

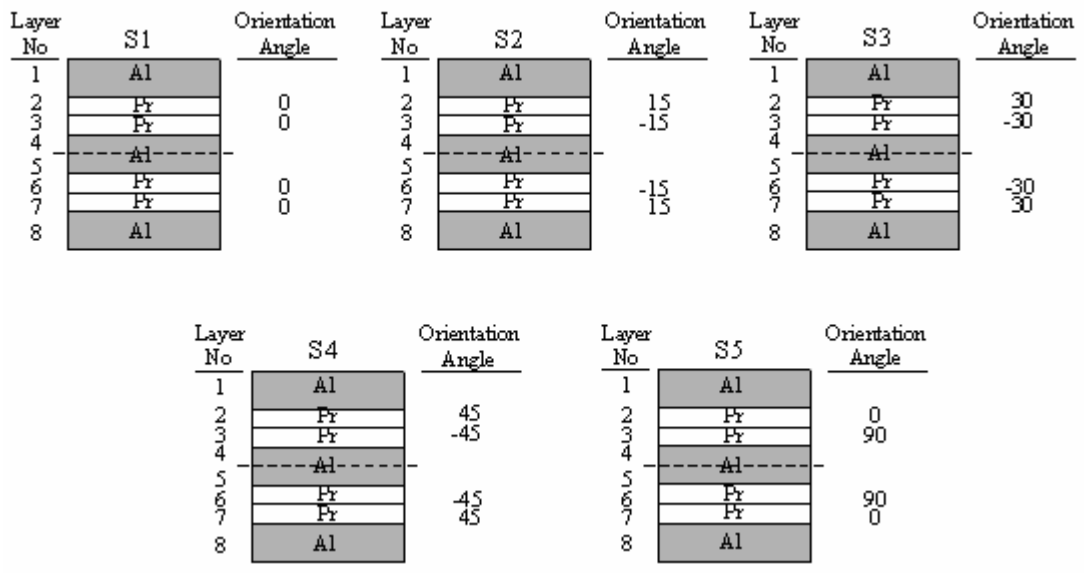

Figure 7.12 Schematic representation of five different stacking sequences of FML composite plates (Al.: aluminium, Pr.: prepregs).

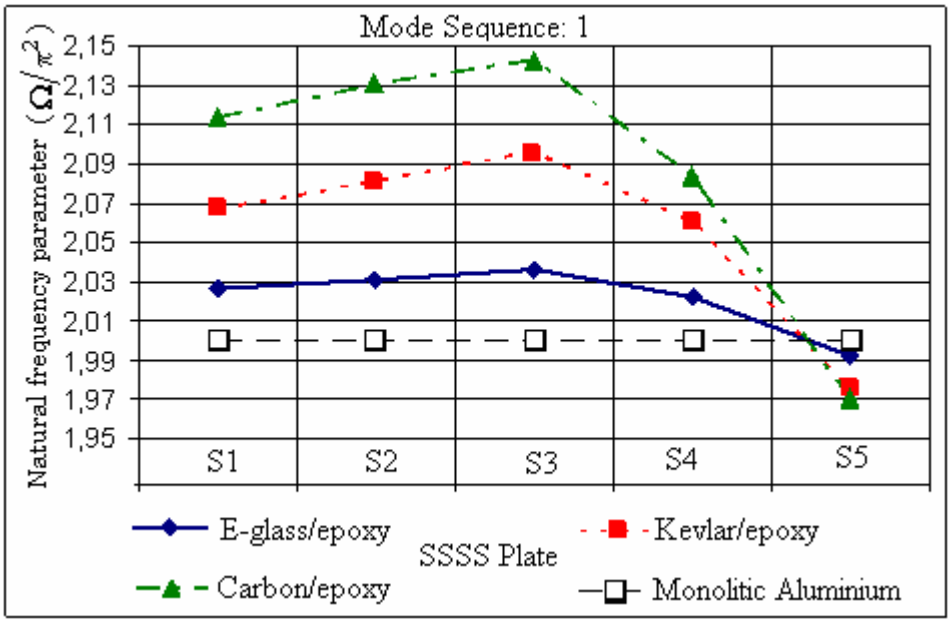

Figure 7.13 Natural frequency parameters ($\Omega/\pi^2 = \omega a^2\sqrt{\rho h/D_{22}}$) of simply supported FML composite plates with several stacking sequences for Mode Sequence: 1.

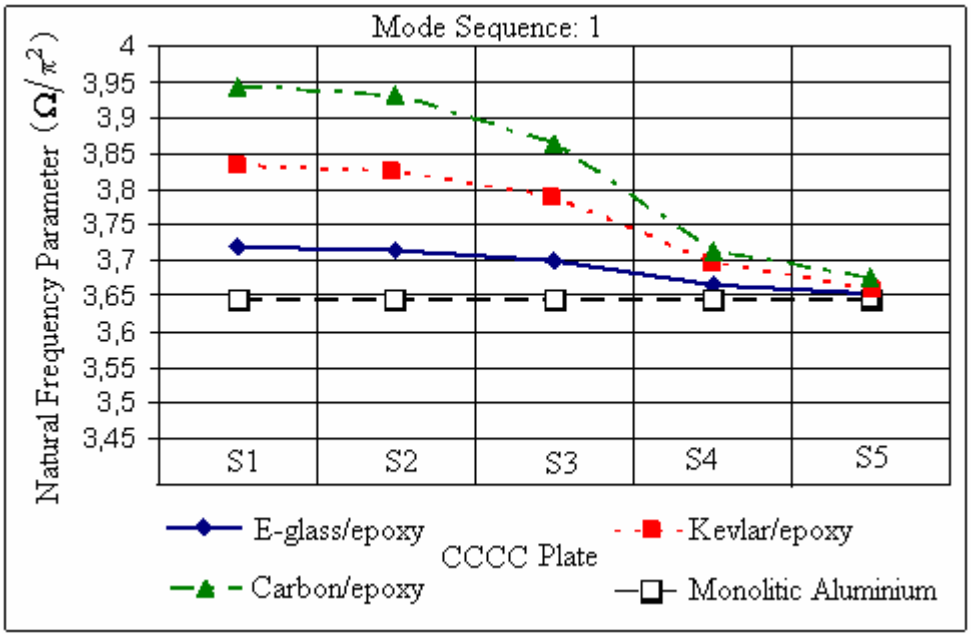

Figure 7.14 Natural frequency parameters ($\Omega/\pi^2 = \omega a^2\sqrt{\rho h/D_{22}}$) of clamped FML composite plates with several stacking sequences for Mode Sequence: 1.

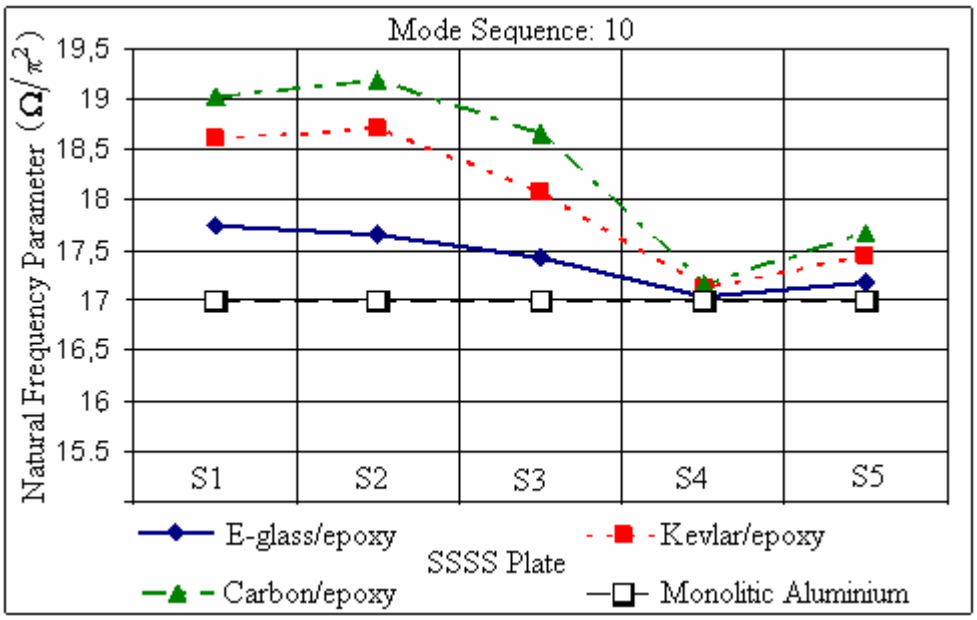

Figure 7.15 Natural frequency parameters ($\Omega/\pi^2 = \omega a^2\sqrt{\rho h/D_{22}}$) of simply supported FML composite plates with several stacking sequences for Mode Sequence: 10.

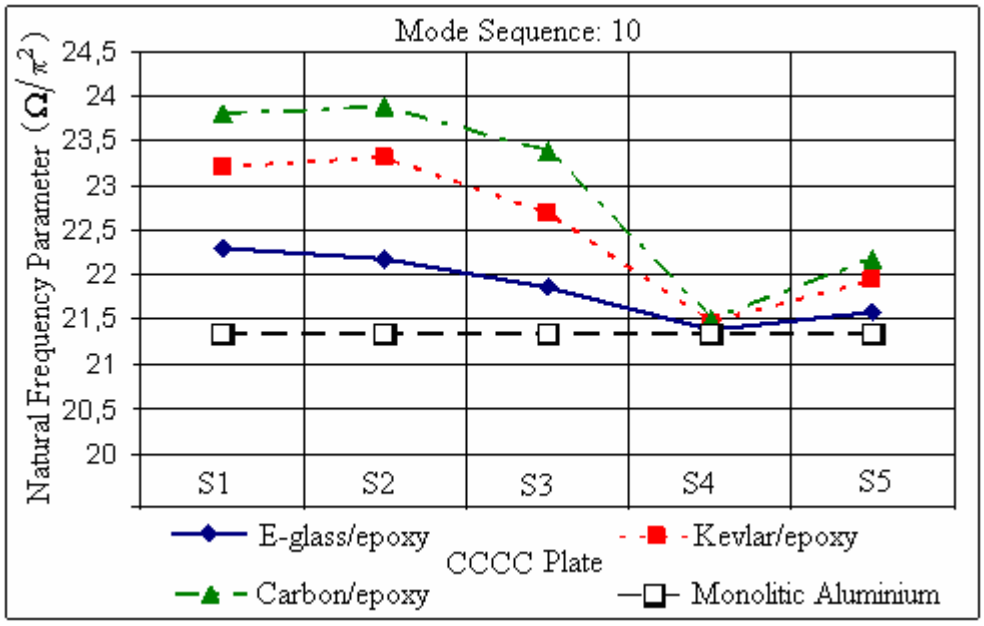

Figure 7.16 Natural frequency parameters ($\Omega/\pi^2 = \omega a^2\sqrt{\rho h/D_{22}}$) of clamped FML composite plates with several stacking sequences for Mode Sequence: 10.

Table 7.18 Natural frequency parameters ($\Omega/\pi^2 = \omega a^2\sqrt{\rho h/D_{22}}$) of FML composite plates made of aluminium/E-glass/epoxy

Mode Sequence Number	S1		S2		S3		S4		S5	
	SSSS	CCCC	SSSS	CCCC	SSSS	CCCC	SSSS	CCCC	SSSS	CCCC
1	2.027	3.718	2.031	3.715	2.036	3.700	2.022	3.665	1.992	3.6537
2	5.013	7.478	5.025	7.485	5.042	7.491	5.035	7.471	4.978	7.4267
3	5.160	7.699	5.152	7.677	5.115	7.601	5.035	7.471	5.019	7.4886
4	8.107	11.157	8.125	11.163	8.142	11.147	8.088	11.054	7.966	10.963
5	10.008	13.395	10.022	13.405	10.045	13.418	10.040	13.377	9.974	13.345
6	10.399	13.925	10.361	13.866	10.240	13.689	10.040	13.441	10.083	13.505
7	13.072	16.864	13.108	16.890	13.160	16.916	13.122	16.849	12.932	16.685
8	13.317	17.185	13.320	17.168	13.281	17.076	13.122	16.849	13.000	16.774
9	17.007	21.369	17.021	21.381	17.046	21.400	17.041	21.390	16.972	21.326
10	17.738	22.292	17.656	22.181	17.412	21.862	17.041	21.390	17.176	21.584

Table 7.19 Natural frequency parameters ($\Omega/\pi^2 = \omega a^2\sqrt{\rho h/D_{22}}$) of FML composite plates made of aluminium/Kevlar/epoxy

Mode Sequence Number	S1		S2		S3		S4		S5	
	SSSS	CCCC	SSSS	CCCC	SSSS	CCCC	SSSS	CCCC	SSSS	CCCC
1	2.067	3.832	2.081	3.826	2.096	3.790	2.060	3.696	1.975	3.661
2	5.028	7.537	5.063	7.558	5.116	7.580	5.097	7.527	4.938	7.402
3	5.412	8.113	5.394	8.057	5.305	7.866	5.097	7.527	5.043	7.559
4	8.267	11.446	8.324	11.470	8.382	11.441	8.242	11.200	7.898	10.936
5	10.015	13.431	10.056	13.463	10.123	13.508	10.110	13.442	9.926	13.312
6	11.032	14.800	10.937	14.652	10.629	14.195	10.110	13.507	10.202	13.688
7	13.169	17.059	13.277	17.140	13.433	17.229	13.335	17.053	12.805	16.590
8	13.813	17.900	13.831	17.866	13.747	17.642	13.335	17.053	12.980	16.818
9	17.010	21.392	17.054	21.430	17.126	21.487	17.115	21.460	16.921	21.283
10	18.601	23.220	18.702	23.302	18.077	22.688	17.115	21.460	17.437	21.933

Table 7.20 Natural frequency parameters ($\Omega/\pi^2 = \omega a^2\sqrt{\rho h/D_{22}}$) of FML composite plates made of aluminium/Carbon/epoxy

Mode Sequence Number	S1		S2		S3		S4		S5	
	SSSS	CCCC	SSSS	CCCC	SSSS	CCCC	SSSS	CCCC	SSSS	CCCC
1	2.114	3.944	2.131	3.931	2.143	3.864	2.083	3.715	1.969	3.675
2	5.059	7.606	5.106	7.633	5.173	7.652	5.134	7.561	4.919	7.395
3	5.654	8.496	5.618	8.402	5.462	8.090	5.134	7.561	5.077	7.630
4	8.455	11.748	8.525	11.766	8.573	11.682	8.333	11.285	7.878	10.947
5	10.041	13.481	10.097	13.525	10.183	13.579	10.152	13.481	9.903	13.297
6	11.609	15.591	11.455	15.355	10.960	14.629	10.152	13.547	10.318	13.858
7	13.317	17.294	13.460	17.396	13.648	17.480	13.463	17.176	12.749	16.559
8	14.316	18.595	14.317	18.516	14.128	18.112	13.463	17.176	13.013	16.903
9	17.033	21.433	17.093	21.485	17.188	21.556	17.159	21.502	16.896	21.263
10	19.023	23.806	19.180	23.892	18.647	23.399	17.159	21.502	17.670	22.183

CHAPTER EIGHT
NUMERICAL STUDIES 3:
FREE VIBRATION ANALYSES OF
THICK BEAMS AND PLATES BY THE DSC

8.1 Introduction

It is known that thin structure theories yield inaccurate results when the thickness of structure is not negligible compared to one of the size length of that structure. In this case, thick structure theories, Timoshenko for beams and Mindlin for plates, considering the effects of rotary inertia and transverse shear must be of interest for reliable dynamic analyses.

Several studies have been performed for free vibration analysis of thick structural elements. Discretization techniques such as finite element and finite difference methods are the most widely used methods in this field of engineering. However, various alternative techniques such as Rayleigh-Ritz, differential quadrature, pseudospectral and radial basis function methods were also commonly used in several studies for thick structural elements as stated in Chapter 1. In this chapter, a collocation scheme for the DSC is introduced for thick structures. The accuracy of the given approach is discussed by comparing DSC results with those of the some published studies.

8.2 DSC for Timoshenko Beams

The equations of motion of a homogeneous rectangular thick beam in $x \in [0, a]$ are given based on Timoshenko theory as (Lee & Schultz, 2004),

$$EI\frac{d^2\theta(x)}{dx^2} + \alpha hG\left(\frac{dw(x)}{dx} - \theta(x)\right) = -\omega^2 \rho I\theta(x) \quad , \tag{8.1.a}$$

$$-\alpha hG\frac{d\theta(x)}{dx} + \alpha hG\frac{d^2w(x)}{dx^2} = -\omega^2 \rho hw(x) \tag{8.1.b}$$

where α is the shear coefficient. The boundary conditions are given as:

Simply supported (S) : $\dfrac{\partial \theta}{\partial x} = 0, \;\; w = 0$. (8.2.a)

Clamped (C) : $\theta = 0, \;\; w = 0$. (8.2.b)

Applying appropriate boundary conditions with the definitions of $\boldsymbol{\Theta} = \{\theta_0, \theta_1, \cdots, \theta_{N-1}\}^T$, $\mathbf{X} = \{w_0, w_1, \cdots, w_{N-1}\}^T$ and $\boldsymbol{\Omega} = diag\{\omega_0, \omega_1, \cdots, \omega_{N-1}\}$, one can obtain following DSC system of equations:

$$a^2 \boldsymbol{\Gamma}_x^{(2)} \boldsymbol{\Theta} + b^2 \boldsymbol{\Gamma}_x^{(1)} \mathbf{X} - b^2 \mathbf{I} \boldsymbol{\Theta} = -\boldsymbol{\Omega}^2 \boldsymbol{\Theta} \;, \tag{8.3.a}$$

$$-c^2 \boldsymbol{\Gamma}_x^{(1)} \boldsymbol{\Theta} + c^2 \boldsymbol{\Gamma}_x^{(2)} \mathbf{X} = -\boldsymbol{\Omega}^2 \mathbf{X} \tag{8.3.b}$$

where $a = \sqrt{E/\rho}$, $b = \sqrt{\alpha h G/\rho I}$ and $c = \sqrt{\alpha G/\rho}$. The matrix $\boldsymbol{\Gamma}_p^{(n)}$ ($n = 1, 2$, p is the direction of differentiation) is obtained by boundary condition implementation of $\boldsymbol{\Psi}_p^{(n)}$ given in Equation (4.11). Equations (8.3.a) and (8.3.b) can be represented by following eigenvalue equation:

$$\mathbf{T}\mathbf{Y} = \boldsymbol{\Omega}^2 \mathbf{Y} \;. \tag{8.4}$$

Here elements of the matrix $\mathbf{T}$ can be evaluated as

$$\mathbf{T}_{11} = -a^2 \boldsymbol{\Gamma}_x^{(2)} + b^2 \mathbf{I}, \qquad \mathbf{T}_{12} = -b^2 \boldsymbol{\Gamma}_x^{(1)}, \tag{8.5)(a, b}$$

$$\mathbf{T}_{21} = c^2 \boldsymbol{\Gamma}_x^{(1)}, \qquad \mathbf{T}_{22} = -c^2 \boldsymbol{\Gamma}_x^{(2)} \;. \tag{8.5)(c, d}$$

The vector $\mathbf{Y}$ is in the form $\mathbf{Y} = \left\{\boldsymbol{\Theta}^T, \mathbf{X}^T\right\}^T$, where $\boldsymbol{\Theta}$ and $\mathbf{X}$ are column vectors.

Solving Equation (8.4) yields natural frequencies and mode shapes of Timoshenko beams. DSC solutions of thin and thick beam theories for beams with various thickness to length (*h*/*a*) ratios, simply supported and clamped at both ends are presented in Tables 8.1 and 8.2, respectively. As it is expected, thin beam solutions diverge from those of the thick beams as the beams get thicker and mode number gets higher. Tables 8.1 and 8.2 also compare the thick beam natural frequency parameters with the results in the literature.

The results of Ferreira & Fasshauer (2006) for simply supported beams show considerable differences with the other two solutions when the thickness increases. It is clearly seen that thick beam DSC solutions are the same as Lee & Schultz's pseudospectral method results at least up to the one thousandths digit. Therefore, natural frequency parameters for relatively thick beams calculated by the DSC and tabulated in Table 8.3 may be reliably used for different applications.

The accuracy of the DSC algorithm is mostly dependent on the optimum selection of DSC parameters such as number of structure nodes, number of fictitious nodes and discretization parameter for regularization *r*. Therefore for a more accurate analysis, the convergence of results may be examined with regard to the variation of discretization parameter. In all analyses performed in this study, DSC parameters were selected utilizing convergence curves.

Table 8.1 Natural frequency parameters ($\Omega = \left(\omega^2 a^4 \rho_0 A / EI\right)^{1/2}$) of Timoshenko beams simply supported at both ends ($\upsilon = 0.3$, $\alpha = 5/6$)

		h/a=0.01			*h/a* =0.02			*h/a* =0.1			*h/a* =0.2		
Mode Number	Thin Beam Theory DSC	Thick Beam Theory DSC	Lee & Schultz (2004)	Ferreira & Fasshauer (2006)	Thick Beam Theory DSC	Lee & Schultz (2004)	Ferreira & Fasshauer (2006)	Thick Beam Theory DSC	Lee & Schultz (2004)	Ferreira & Fasshauer (2006)	Thick Beam Theory DSC	Lee & Schultz (2004)	Ferreira & Fasshauer (2006)
1	3.141592	3.141331	3.14133	3.1413	3.140532	3.14053	3.1405	3.11568	3.11568	3.1112	3.04533	3.04533	2.3124
2	6.283195	6.281061	6.28106	6.2811	6.274711	6.27471	6.2747	6.09066	6.09066	5.9102	5.67155	5.67155	4.2672
3	9.424781	9.417612	9.41761	9.4176	9.396322	9.39632	9.3963	8.84052	8.84052	7.9769	7.83952	7.83952	6.4193
4	12.56637	12.54941	12.5494	12.5494	12.49941	12.4994	12.4994	11.34310	11.3431	10.0102	9.65709	9.65709	8.2855
5	15.70796	15.67492	15.6749	15.6749	15.57841	15.5784	15.5784	13.61317	13.6132	12.1817	11.22204	11.222	9.9037
6	18.84956	18.79263	18.7926	18.7926	18.62823	18.6282	18.6282	15.67904	15.679	14.2427	12.60221	12.6022	11.3487
7	21.99115	21.90107	21.9011	21.9011	21.64431	21.6443	21.6443	17.57050	17.5705	16.1520	13.03233	13.0323	12.6402
8	25.13274	24.99881	24.9988	24.9988	24.62267	24.6227	24.6226	19.31418	19.3142	17.9226	13.44427	13.4443	13.4567
9	28.27433	28.08450	28.0845	28.0845	27.55993	27.5599	27.5597	20.93255	20.9325	19.5727	13.84329	13.8433	13.8101
10	31.41593	31.15682	31.1568	31.1568	30.45331	30.4533	30.4529	22.44408	22.4441	21.1187	14.43776	14.4378	14.4806

Table 8.2 Natural frequency parameters ($\Omega = \left(\omega^2 a^4 \rho_0 A / EI\right)^{1/2}$) of Timoshenko beams clamped at both ends ($\upsilon = 0.3$, $\alpha = 5/6$)

		h/a =0.01			*h/a* =0.02			*h/a* =0.1			*h/a* =0.2		
Mode Number	Thin Beam Theory DSC	Thick Beam Theory DSC	Lee & Schultz (2004)	Ferreira & Fasshauer (2006)	Thick Beam Theory DSC	Lee & Schultz (2004)	Ferreira & Fasshauer (2006)	Thick Beam Theory DSC	Lee & Schultz (2004)	Ferreira & Fasshauer (2006)	Thick Beam Theory DSC	Lee & Schultz (2004)	Ferreira & Fasshauer (2006)
1	4.730041	4.728451	4.7284	4.7284	4.723509	4.72350	4.7235	4.579547	4.57955	4.5795	4.242014	4.24201	4.2420
2	7.853212	7.846992	7.8469	7.8469	7.828194	7.82817	7.8282	7.331219	7.33122	7.3312	6.417938	6.41794	6.4179
3	10.99563	10.98007	10.9800	10.9800	10.93415	10.9341	10.9341	9.856114	9.85611	9.8561	8.285317	8.28532	8.2853
4	14.13720	14.10631	14.1062	14.1061	14.01546	14.0154	14.0154	12.14535	12.1454	12.1454	9.903723	9.90372	9.9037
5	17.27883	17.22478	17.2246	17.2246	17.06792	17.0679	17.0679	14.23243	14.2324	14.2324	11.34874	11.3487	11.3487
6	20.42047	20.33407	20.3338	20.3338	20.08685	20.0868	20.0868	16.14875	16.1487	16.1487	12.64025	12.6402	12.6402
7	23.56213	23.43277	23.4325	23.4325	23.06824	23.0682	23.0682	17.92148	17.9215	17.9215	13.45674	13.4567	13.4567
8	26.70380	26.51948	26.5192	26.5192	26.00866	26.0086	26.0086	19.57235	19.5723	19.5723	13.81014	13.8101	13.8101
9	29.84550	29.59291	29.5926	29.5926	28.90529	28.9052	28.9052	21.11852	21.1185	21.1185	14.48056	14.4806	14.4806
10	32.98722	32.65180	32.6514	32.6513	31.75589	31.7558	31.7557	22.57351	22.5735	22.5735	14.93829	14.9383	14.9383

Table 8.3 Natural frequency parameters ($\Omega = \left(\omega^2 a^4 \rho_0 A / EI\right)^{1/2}$) of simply supported-simply supported, clamped-clamped and clamped-simply supported Timoshenko beams ($\upsilon = 0.3$, $\alpha = 5/6$)

Mode Number	Simply supported-Simply supported					Clamped-Clamped					Clamped-Simply supported				
	h/*a*					*h*/*a*					*h*/*a*				
	0.1	0.2	0.4	0.6	0.8	0.1	0.2	0.4	0.6	0.8	0.1	0.2	0.4	0.6	0.8
1	3.11568	3.04533	2.83578	2.61317	2.41427	4.57955	4.24201	3.55151	3.04901	2.69507	3.85176	3.66561	3.20897	2.81892	2.52012
2	6.09066	5.67155	4.82855	4.20074	3.25808	7.33122	6.41794	5.04024	4.21888	3.68421	6.73057	6.07268	4.95186	4.21626	3.56608
3	8.84052	7.83952	6.30111	4.34411	3.74414	9.85612	8.28532	6.36636	5.23248	4.28774	9.36591	8.07437	6.32012	4.64066	3.79202
4	11.34310	9.65709	6.51616	5.22255	4.23961	12.14536	9.90372	7.13217	5.33500	4.67985	11.75841	9.78617	6.72837	5.33488	4.67090
5	13.61317	11.22204	7.21888	5.34138	4.69820	14.23243	11.34875	7.58405	6.27304	5.46804	13.93309	11.28676	7.46915	5.86404	4.89480
6	15.67904	12.60221	7.48829	6.26426	5.46751	16.14875	12.64025	8.30773	6.48016	5.47672	15.92091	12.62393	7.84982	6.27382	5.47672
7	17.57050	13.03233	8.47921	6.49763	5.47693	17.92149	13.45674	8.66554	7.07881	6.15871	17.75055	13.14153	8.49994	7.01456	6.00890
8	19.31418	13.44427	8.50096	7.05843	6.15187	19.57235	13.81014	9.34180	7.60538	6.51763	19.44613	13.78451	9.10718	7.13886	6.16335
9	20.93255	13.84329	9.39639	7.66511	6.53585	21.11853	14.48056	9.78960	7.82242	6.77357	21.02729	13.95633	9.41323	7.76445	6.75363
10	22.44408	14.43776	9.74645	7.76638	6.75651	22.57352	14.93829	10.19255	8.39419	7.29470	22.50985	14.90650	10.18335	8.19845	7.01992
11	23.86391	14.97658	10.20727	8.41164	7.30944	23.94787	15.69964	10.93608	8.72700	7.48778	23.90648	15.10788	10.37213	8.41779	7.31100
12	25.20442	15.66764	10.93501	8.71447	7.47540	25.24786	16.00404	10.95343	9.00522	7.81975	25.22661	15.99984	10.95343	9.00409	7.81724
13	26.06465	16.02413	10.95386	9.00868	7.82225	26.28307	16.96209	11.65781	9.56802	8.30278	26.11891	16.33126	11.48567	9.20450	7.91199
14	26.28141	16.95842	11.64957	9.56712	8.30270	26.45954	16.99988	12.01780	9.66497	8.31882	26.45166	16.99988	11.66253	9.56805	8.30278
15	26.47583	17.00192	12.04048	9.66746	8.31906	26.92368	17.93568	12.32670	10.09804	8.75800	26.57075	17.59154	12.29869	10.07804	8.70736
16	26.88855	17.92180	12.30375	10.09375	8.75633	27.56903	18.21437	12.89353	10.51971	9.08233	27.29895	17.93807	12.56680	10.12943	8.76130
17	27.68657	18.24190	12.92319	10.54346	9.08952	27.91266	18.82647	13.09855	10.61671	9.19426	27.69326	18.74656	12.92527	10.59323	9.18688
18	27.78724	18.79278	13.07170	10.59353	9.18723	28.67525	19.40266	13.50725	11.06621	9.59597	28.31082	18.91640	13.49703	10.95489	9.45177
19	28.84371	19.49290	13.51301	11.07027	9.59855	29.04726	19.71075	14.03985	11.35975	9.80418	28.84570	19.61756	13.57798	11.07298	9.59940
20	28.87553	19.62186	14.03881	11.35712	9.80225	29.81301	20.36670	14.07683	11.52616	9.99226	29.46095	20.09759	14.07683	11.52605	9.99212

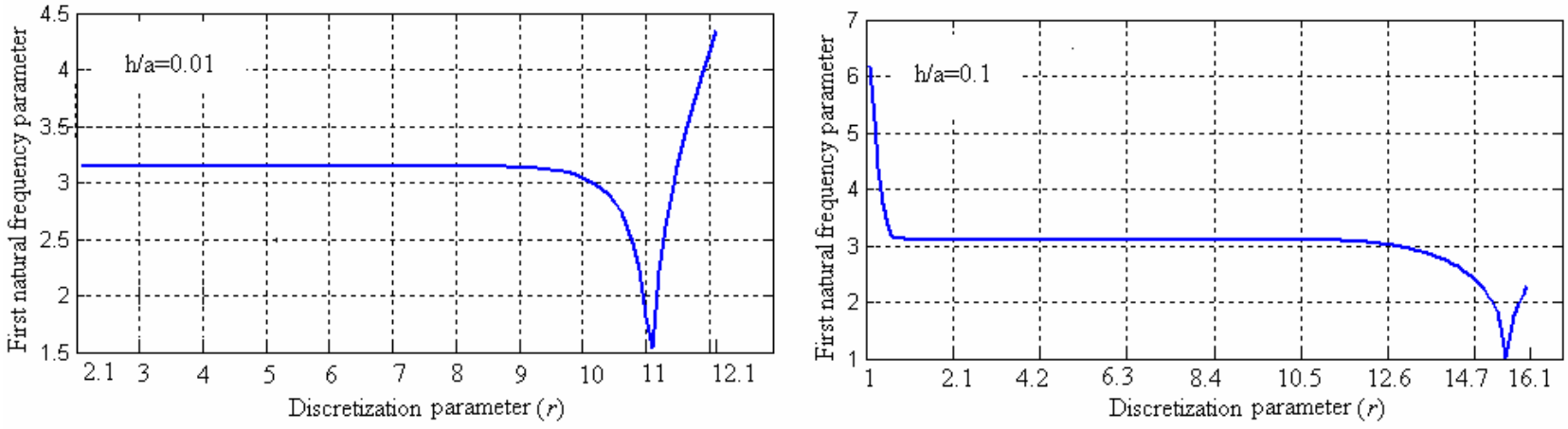

Figure 8.1 Convergence curves for the first natural frequency parameter of beams simply supported at both ends (h/a=0.01 and 0.1).

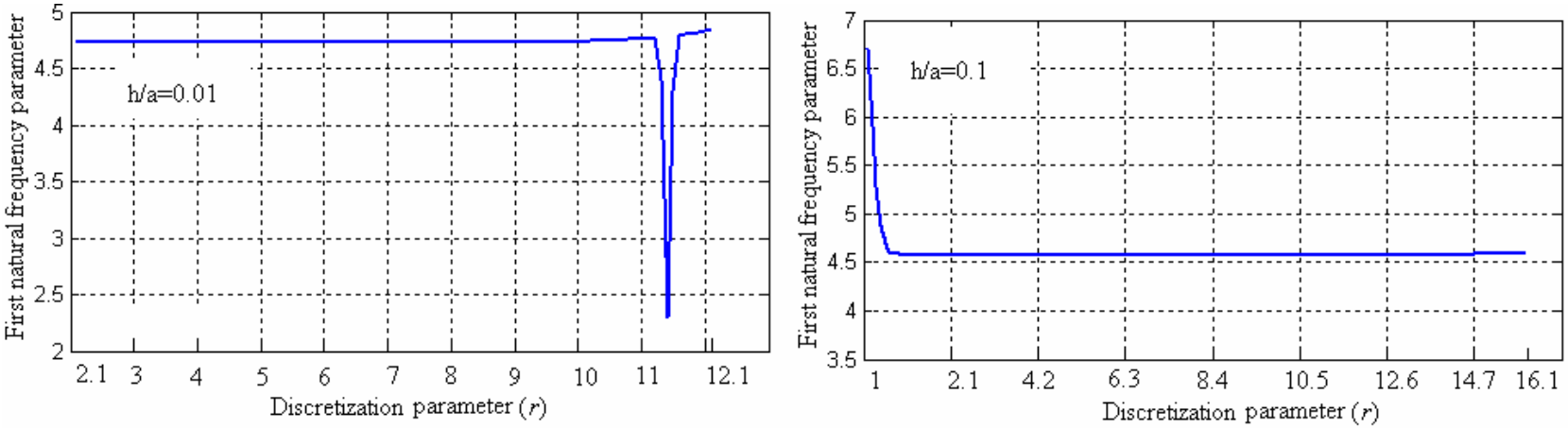

Figure 8.2 Convergence curves for the first natural frequency parameter of beams clamped at both ends (h/a=0.01 and 0.1).

As an example, some convergence curves for the fundamental modes of simply supported-simply supported and clamped-clamped beams are presented in Figures 8.1 and 8.2, respectively. These curves represent the variation of fundamental frequency parameter with respect to discretization parameter when the number of structure and fictitious nodes are held constant. For an accurate analysis, discretization parameter should be selected as one of the values in the range where frequency results are not sensitive.

8.3 DSC for Mindlin Plates

Based on Mindlin plate theory, the governing equations for free vibration of isotropic rectangular thick plates are given as follows (Liew et al., 2003; Ferreira & Fasshauer, 2006):

$$D\frac{\partial^2\theta_x(x,y)}{\partial x^2}+(\upsilon D+Gh^3/12)\frac{\partial^2\theta_y(x,y)}{\partial x\partial y}+\left(Gh^3/12\right)\frac{\partial^2\theta_x(x,y)}{\partial y^2}$$
$$-\kappa^2 Gh\left(\theta_x(x,y)+\frac{\partial w(x,y)}{\partial x}\right)=-I_2\omega^2\theta_x(x,y), \qquad (8.6.a)$$

$$\left(Gh^3/12\right)\frac{\partial^2\theta_y(x,y)}{\partial x^2}+(\upsilon D+Gh^3/12)\frac{\partial^2\theta_x(x,y)}{\partial x\partial y}+D\frac{\partial^2\theta_y(x,y)}{\partial y^2}$$
$$-\kappa^2 Gh\left(\theta_y(x,y)+\frac{\partial w(x,y)}{\partial y}\right)=-I_2\omega^2\theta_y(x,y)\ , \qquad (8.6.b)$$

$$\kappa^2 Gh\left[\frac{\partial^2 w(x,y)}{\partial x^2}+\frac{\partial^2 w(x,y)}{\partial y^2}+\frac{\partial\theta_x(x,y)}{\partial x}+\frac{\partial\theta_y(x,y)}{\partial y}\right]=-I_0\omega^2 w(x,y). \qquad (8.6.c)$$

The mass inertias I_i are defined as (Liew et al., 2003)

$$I_0=\int_{-h/2}^{h/2}\rho\,dz\,,\quad I_2=\int_{-h/2}^{h/2}\rho\,z^2dz\quad . \qquad (8.7)(a, b)$$

The boundary conditions for plates are given as (Han & Liew, 1997):

$$\text{Simply supported (S)} \quad : \quad w = 0,\ \upsilon\frac{\partial \theta_x}{\partial x} + \frac{\partial \theta_y}{\partial y} = 0,\ \theta_x = 0, \tag{8.8.a}$$

$$\text{Clamped (C)} \quad : \quad w = 0,\ \theta_x = 0,\ \theta_y = 0\,. \tag{8.8.b}$$

Equations (8.6.a)-(8.6.c) can be expressed by DSC matrices with similar matrix demonstrations given in Section (8.2) as follows:

$$d^2\boldsymbol{\Gamma}_x^{(2)}\boldsymbol{\Theta}_x + f^2\boldsymbol{\Gamma}_x^{(1)}\boldsymbol{\Gamma}_y^{(1)}\boldsymbol{\Theta}_y + g^2\boldsymbol{\Gamma}_y^{(2)}\boldsymbol{\Theta}_x - {s_2}^2\mathbf{I}\boldsymbol{\Theta}_x - {s_2}^2\boldsymbol{\Gamma}_x^{(1)}\mathbf{X} = -\boldsymbol{\Omega}^2\boldsymbol{\Theta}_x\ , \tag{8.9.a}$$

$$g^2\boldsymbol{\Gamma}_x^{(2)}\boldsymbol{\Theta}_y + f^2\boldsymbol{\Gamma}_x^{(1)}\boldsymbol{\Gamma}_y^{(1)}\boldsymbol{\Theta}_x + d^2\boldsymbol{\Gamma}_y^{(2)}\boldsymbol{\Theta}_y - {s_2}^2\mathbf{I}\boldsymbol{\Theta}_y - {s_2}^2\boldsymbol{\Gamma}_y^{(1)}\mathbf{X} = -\boldsymbol{\Omega}^2\boldsymbol{\Theta}_y\ , \tag{8.9.b}$$

$${s_0}^2\boldsymbol{\Gamma}_x^{(2)}\mathbf{X} + {s_0}^2\boldsymbol{\Gamma}_y^{(2)}\mathbf{X} + {s_0}^2\boldsymbol{\Gamma}_x^{(1)}\boldsymbol{\Theta}_x + {s_0}^2\boldsymbol{\Gamma}_y^{(1)}\boldsymbol{\Theta}_y = -\boldsymbol{\Omega}^2\mathbf{X} \tag{8.9.c}$$

where $d = \sqrt{D/I_2}$, $f = \sqrt{\upsilon D/I_2 + Gh^3/12I_2}$, $g = \sqrt{Gh^3/12I_2}$, $s_i = \sqrt{\kappa^2 Gh/I_i}$ ($i = 0, 2$). Equations (8.9.a)-(8.9.c) can be rewritten in the following form:

$$\mathbf{TY} = \boldsymbol{\Omega}^2\mathbf{Y} \tag{8.10}$$

where $\mathbf{Y} = \left\{\boldsymbol{\Theta}_x{}^T, \boldsymbol{\Theta}_y{}^T, \mathbf{X}^T\right\}^T$. $\boldsymbol{\Theta}_x, \boldsymbol{\Theta}_y$ and $\mathbf{X}$ are column vectors. Here the elements of matrix $\mathbf{T}$ can be determined as

$$\mathbf{T}_{11} = -d^2\left(\boldsymbol{\Gamma}_x^{(2)} \otimes \mathbf{I}_y\right) - g^2\left(\mathbf{I}_x \otimes \boldsymbol{\Gamma}_y^{(2)}\right) + s_2^2\left(\mathbf{I}_x \otimes \mathbf{I}_y\right), \tag{a}$$

$$\mathbf{T}_{12} = -f^2\left(\boldsymbol{\Gamma}_x^{(1)} \otimes \boldsymbol{\Gamma}_y^{(1)}\right), \tag{b}$$

$$\mathbf{T}_{13} = {s_2}^2\left(\boldsymbol{\Gamma}_x^{(1)} \otimes \mathbf{I}_y\right), \tag{c}$$

(8.11)

$$\mathbf{T}_{21} = -f^2\left(\boldsymbol{\Gamma}_x^{(1)} \otimes \boldsymbol{\Gamma}_y^{(1)}\right), \quad \text{(d)}$$

$$\mathbf{T}_{22} = -d^2\left(\mathbf{I}_x \otimes \boldsymbol{\Gamma}_y^{(2)}\right) - g^2\left(\boldsymbol{\Gamma}_x^{(2)} \otimes \mathbf{I}_y\right) + s_2^2\left(\mathbf{I}_x \otimes \mathbf{I}_y\right), \quad \text{(e)}$$

$$\mathbf{T}_{23} = s_2{}^2\left(\mathbf{I}_x \otimes \boldsymbol{\Gamma}_y^{(1)}\right), \quad \text{(f)}$$

$$\mathbf{T}_{31} = -s_0{}^2\left(\boldsymbol{\Gamma}_x^{(1)} \otimes \mathbf{I}_y\right), \quad \text{(g)} \quad (8.11)$$

$$\mathbf{T}_{32} = -s_0{}^2\left(\mathbf{I}_x \otimes \boldsymbol{\Gamma}_y^{(1)}\right), \quad \text{(h)}$$

$$\mathbf{T}_{33} = -s_0{}^2\left(\boldsymbol{\Gamma}_x^{(2)} \otimes \mathbf{I}_y\right) - s_0{}^2\left(\mathbf{I}_x \otimes \boldsymbol{\Gamma}_y^{(2)}\right). \quad \text{(i)}$$

Finally, natural frequencies and mode shapes of Mindlin plates can be obtained by solving Equation (8.10).

In this analysis, fully simply-supported and fully clamped square Mindlin plates are considered. Table 8.4 compares frequency parameters predicted by the present DSC and DSC-Ritz approaches. The DSC-Ritz results presented by Hou et al. have been obtained by using Gauss kernel. The results of both approaches are relatively close to each other.

Tables 8.5 and 8.6 present some other calculated natural frequency parameters together with those of some published studies in the open literature. In these studies, Ferreira & Fasshauer (2006) use RBF-pseudospectral approach; Liew et al. (2004) utilize a mesh free method based on the first order shear deformation theory whereas Dave & Roufaeil (1980) perform Rayleigh-Ritz approach. Additionally, Mindlin closed form solutions for fully simply supported plates presented in Ferreira & Fasshauer (2006) are also tabulated.

Table 8.4 Comparison of frequency parameters ($\Omega = \omega a^2 (\rho_0 h / D)^{1/2}$) of the present DSC and DSC-Ritz approaches for square Mindlin plates ($\upsilon = 0.3$, $\kappa = 5/6$)

	SSSS h/a =0.1		CCCC h/a =0.1		CCCC h/a =0.2	
Mode Sequence Number	Present DSC $N = (9 \times 9)$ Shannon	DSC-Ritz (Hou et al., 2005) $N = (9 \times 9)$ Gauss	Present DSC $N = (9 \times 9)$ Shannon	DSC-Ritz (Hou et al., 2005) $N = (9 \times 9)$ Gauss	Present DSC $N = (9 \times 9)$ Shannon	DSC-Ritz (Hou et al., 2005) $N = (9 \times 9)$ Gauss
1	1.9290	1.9317	3.2812	3.2956	2.6549	2.6875
2	4.5658	4.6084	6.2690	6.2867	4.6587	4.6908
3	4.5658	4.6084	6.2690	6.2867	4.6587	4.6908
4	6.9590	7.0716	8.7900	8.8122	6.2577	6.2988
5	8.4713	8.6162	10.4233	10.3794	7.2103	7.1767
6	8.4713	8.6162	10.5085	10.4783	7.2886	7.2760

Computed DSC results present good agreement with those of the compared studies and show less than 4% deviation from the Mindlin solutions (Table 8.5). The discrepancy values exhibit an unstable behaviour with respect to the sequence of modes.

Table 8.5 Natural frequency parameters ($\Omega = \omega a(\rho_0 / G)^{1/2}$) of SSSS square Mindlin plates ($\upsilon = 0.3$, $\kappa = 5/6$)

Mode Sequence Number	*h/a* =0.01					*h/a* =0.1					
	DSC $N = (13\times13)$	Ferreira & Fasshauer (2006) $N = (13\times13)$	Liew et al. (2004)	Mindlin[1]	% Discrepancy[2]	DSC $N = (13\times13)$	Hou et al. (2005)[3]	Ferreira & Fasshauer (2006) $N = (13\times13)$	Liew et al. (2004)	Mindlin[1]	% Discrepancy[2]
1	0.0960	0.0963	0.0961	0.0963	0.3115	0.929	0.930	0.930	0.922	0.930	0.10753
2	0.2405	0.2406	0.2419	0.2406	0.0416	2.203	2.219	2.219	2.205	2.226	1.03324
3	0.2405	0.2406	0.2419	0.2406	0.0416	2.203	2.219	2.219	2.205	2.226	1.03324
4	0.3835	0.3847	0.3860	0.3848	0.3378	3.353	3.406	3.406	3.337	3.406	1.55608
5	0.4847	0.4807	0.4898	0.4809	-0.7902	4.104	4.149	4.149	4.139	4.149	1.08460
6	0.4847	0.4807	0.4898	0.4809	-0.7902	4.104	4.149	4.149	4.139	4.149	1.08460
7	0.6256	0.6246	0.6315	0.6249	-0.1120	5.106	-	5.204	5.170	5.206	1.92086
8	0.6256	0.6246	0.6315	0.6249	-0.1120	5.106	-	5.204	5.170	5.206	1.92086
9	0.8480	0.8156	0.8447	0.8167	-3.8325	6.458	-	6.530	6.524	6.520	0.95092
10	0.8480	0.8156	0.8447	0.8167	-3.8325	6.458	-	6.530	6.524	6.520	0.95092

[1]: Closed form solution (Ferreira & Fasshauer, 2006), [2]: % Discrepancy of the DSC and Mindlin solutions

[3]: The original work presents frequency parameters as $\Omega = \omega a^2 (\rho_0 h / D)^{1/2}$

Table 8.6 Natural frequency parameters ($\Omega = \omega a(\rho_0 / G)^{1/2}$) of CCCC square Mindlin plates ($\upsilon = 0.3$, $\kappa = 0.8601$)

Mode Sequence Number	*h/a* =0.01				*h/a* =0.1			
	DSC $N = (13\times13)$	Ferreira & Fasshauer (2006) $N = (13\times13)$	Liew et al. (2004)	Dave & Roufaeil (1980)	DSC $N = (13\times13)$	Ferreira & Fasshauer (2006) $N = (13\times13)$	Liew et al. (2004)	Dave & Roufaeil (1980)
1	0.1759	0.1754	0.1743	0.1754	1.5896	1.5910	1.5582	1.5940
2	0.3530	0.3574	0.3576	0.3576	3.0430	3.0389	3.0182	3.0390
3	0.3530	0.3574	0.3576	0.3576	3.0430	3.0389	3.0182	3.0390
4	0.5214	0.5265	0.5240	0.5274	4.2695	4.2625	4.1711	4.2650
5	0.6443	0.6399	0.6465	0.6402	5.0675	5.0247	5.1218	5.0350
6	0.6472	0.6430	0.6505	0.6432	5.1096	5.0723	5.1594	5.0780
7	0.8054	0.8018	0.8015	-	6.1149	6.0798	6.0178	-
8	0.8054	0.8018	0.8015	-	6.1149	6.0798	6.0178	-
9	1.0309	1.0227	1.0426	-	7.5681	7.4123	7.5169	-
10	1.0309	1.0227	1.0426	-	7.5681	7.4123	7.5169	-

CHAPTER NINE
CONCLUSIONS

9.1 Introduction

In vibro-acoustics, the resonance phenomenon may cause unwanted structural deformations and failure of many vital machine parts or structures. Besides, due to the further improvements in industrial applications and increasing consumer demands on comfort, vibro-acoustic specifications of products have become one of the most important design criteria. Nowadays, vibration analysis is generally performed by either experimental methods or numerical algorithms simulating the real-life system. However, especially for the systems subjected to high frequency excitation, performing experimental tests and using available numerical techniques give no efficient vibration data for a realistic design.

Conventional high frequency approaches are generally based on energy equilibrium between substructures or structural elements. These methods consider average prediction of energy as a system variable to describe the response level. Therefore, they disregard modal information and thus, loose discrete response behaviour. This generally characterized high frequency data is not sufficient for developing comprehensive, detailed, reliable, high-technology, high-frequency engineering products. In spite of the great effort in the past few decades, the prediction of high-frequency vibrations is still a challenging task. There is a consensus in the literature on the lack of a sufficient approach which can reliably predict high frequency vibrations. This thesis mainly purposes to develop such an efficient tool for predicting discrete high frequency response without any restriction for the frequency range of the operation.

9.2 Review of the Thesis

Present doctorate study firstly considered a recent technique, the DSC, due to its capabilities for predicting very higher order vibration modes.

Secondly, the thesis introduced a novel scheme “DSC-MS approach” for the prediction of spatially distributed and discrete frequency response of structures subjected to time-harmonic point forces. The comparisons with the analytical solutions of thin beams and plates showed that the present approach can be reliably used for discrete high frequency vibration analysis.

By this powerful approach, for the first time in literature, it became possible to disregard the energetic parameters and to consider primary response variables for high frequencies. The scheme DSC-MS coming on the scene in the present doctorate study showed a perfect resolution for frequency response spectra and spatial distribution. The scheme also proved its accuracy to precisely sweep the entire audible frequencies without any pre-conditioning of modal density and damping. DSC-MS approach promises new horizons on recovering uncertainties at high frequencies by providing basic system characteristics such as discrete bending displacements, velocities, accelerations and modal contents of damped systems.

Due to their high quality mechanical properties, composite materials have substituted for plastic and metal alloys. Therefore, on the last decade, researchers have been increasingly dealing with dynamic analysis of structural elements made of various polymer and/or polymer-metal materials. In this regard, thirdly, as a contribution to studies on the DSC and composite plate vibrations, DSC implementation for free vibration analysis of composite plates was introduced. Here the DSC scheme is adapted to solve differential equation of symmetrically laminated composite plates. Then verification of the DSC was clearly presented by performing comprehensive comparisons with several distinguished studies in the open literature. Very accurate predictions have been obtained for composite plates by using small grid numbers leading to very small computation time and memory. Moreover, very good agreement between the DSC and other approaches used in the selected references has been obtained for symmetrically laminated composite plates. The perfect match between the DSC and exact solutions promises that DSC approach can be reliably used in vibration analysis of composite plates having no analytical solution. Besides, in order to show the practical applicability of the DSC for

vibration analysis of thin composites, various composite plates were considered on the basis of three free vibration applications. Effects of material type and orientation angle along with boundary conditions on the modal characteristics of various symmetrically laminated composite plates were examined in detail.

Finally, as a new contribution, the classical DSC technique is introduced for free vibration analysis of thick beams and plates. The results showed that the DSC is also capable of solving more than one differential equation in a single domain simultaneously. This ability promises that the DSC can also be improved for the coupled problems such as structure-structure and fluid-structure interactions. However, the DSC still has challenging issues for implementing complex boundaries. Therefore, it needs further studies to cure drawbacks of the DSC.

9.3 Contributions of the Thesis

It is congruous to remark the following three main contributions of this Doctorate study to the literature:

- A novel scheme named as DSC-MS was introduced for the discrete high frequency vibration response analysis for the first time in literature and the scheme has been accurately verified.
- The classical DSC method was extended by implementing the approach to free vibration analysis of thin composite plates. The superiority of the DSC for composites over several numerical techniques has been clearly demonstrated. Besides, practical applicability of the DSC was displayed by performing several case studies for composite plates.
- The classical DSC method was improved for free vibrations of thick structures based on Timoshenko and Mindlin theories. This is the first implementation of the classical DSC for thick structures.

9.4 Suggestions for the Future Work

For future works, in order to spread the use of DSC and DSC-MS methods in vibro-acoustic engineering, the following improvement and development studies can be performed:

- Boundary condition implementation procedure of DSC method can be generalized to treat complex boundaries such as stiffened and damped ends and impedance boundaries.

- Then, structure-structure and fluid-structure interaction models can be constructed by the DSC. Therefore, high frequency structural-acoustic coupling problems can be treated by the DSC and DSC-MS.

- As a global method, a unified approach can be developed to treat build-up structures by implementing transform and assembly algorithms.

- DSC-MS approach can be applied to high frequency vibration analyses of thick beams and plates by using better computational configurations.

- The DSC-MS can be implemented to high frequency analyses of composite structures based on CLPT or higher-order plate theories. In this regard, the effects of composite plate parameters on their vibration response may be examined.

- As an alternative to energy based high frequency techniques, DSC method can be applied to energy flow differential equations; and therefore, averaged energetic parameters also can be predicted.

REFERENCES

Bellman, R., Kashef, B. G., & Casti, J. (1972). Differential quadrature: A technique for the rapid solution of nonlinear partial differential equations. *Journal of Computational Physics*, 10(1), 40-52.

Bert, C. W., & Malik, M. (1996). The differential quadrature method for irregular domains and application to plate vibration. *International Journal of Mechanical Sciences*, 38(6), 589–606.

Bitsie, F. (1996). The structural-acoustic energy finite element method and energy boundary element method. PhD Thesis, Purdue University Graduate School, USA.

Carcaterra, A., & Sestieri, A. (1997). Complex envelope displacement analysis: A quasi-static approach to vibrations. *Journal of Sound and Vibration*, 201(2), 205-233.

Chae, K. S., & Ih, J. G. (2001). Prediction of vibrational energy distribution in the thin plate at high-frequency bands by using the ray tracing method. *Journal of Sound and Vibration*, 240(2), 263-292.

Chen, Z. S., Hofstetter, G., & Mang, H. A. (1998). A Galerkin-type BE-FE formulation for elasto-acoustic coupling. *Computational Methods of Applied Mechanical Engineering*, 152, 147-155.

Cho, P. E. H. (1993). Energy flow analysis of coupled structures. Ph.D Thesis, Purdue University Graduate School, USA.

Cho, J. R., Lee, H. W., & Kim, K. W. (2002). Free vibration analysis of baffled liquid-storage tanks by the structural-acoustic finite element formulation. *Journal of Sound and Vibration*, 258(5), 847-866.

Chow, S. T., Liew, K. M., & Lam, K. Y. (1992). Transverse vibration of symmetrically laminated rectangular composite plates. *Composite Structures*, 20(4), 213-226.

Civalek, Ö. (2007a). Numerical analysis of free vibrations of laminated composite conical and cylindrical shells: Discrete singular convolution (DSC) approach. *Journal of Computational and Applied Mathematics*, 205, 251-271.

Civalek, Ö. (2007b). Three-dimensional vibration, buckling and bending analyses of thick rectangular plates based on discrete singular convolution method. *International Journal of Mechanical Sciences*, 49(6), 752-765.

Civalek, Ö. (2007c). Free vibration and buckling analyses of composite plates with straight-sided quadrilateral domain based on DSC approach. *Finite Elements in Analysis and Design*, 43(13), 1013-1022.

Civalek, Ö. (2007d). A parametric study of the free vibration analysis of rotating laminated cylindrical shells using the method of discrete singular convolution. *Thin Walled Structures*, 45(7-8), 692-698.

Coyette, J. P. (1999). The use of finite-element and boundary-element models for predicting the vibro-acoustic behaviour of layered structures. *Advances in Engineering Software*, 30, 133-139.

Cremer, L., Heckl, M., & Ungar, E. E. (1998). *Structure-borne sound*. Berlin: Springer.

Cummings, P. (2001). Analysis of finite element based numerical methods for acoustic waves, and fluid-solid interactions in the frequency domain. Ph.D Thesis, The University of Tennessee, USA.

Dai, K.Y., Liu, G. R., Lim, K. M., & Chen, X. L. (2004). A mesh-free method for static and free vibration analysis of shear deformable laminated composite plates. *Journal of Sound and Vibration*, 269, 633–652.

Daniel, I. M., & Ishai, O. (1994). *Engineering mechanics of composite materials*. New York: Oxford University Press.

Dawe, D. J., & Roufaeil, O. L. (1980). Rayleigh–Ritz vibration analysis of Mindlin plates. *Journal of Sound and Vibration*, 69 (3), 345–359.

Desmet, W. (2002). Mid-frequency vibro-acoustic modeling: Challenges and potential solutions. Proceedings of ISMA-Volume II.

Dong, J. (2004). Design sensitivity analysis and optimization of high frequency structural-acoustic problems using energy finite element and energy boundary element method. Ph.D Thesis, The Graduate College of the University of Iowa, USA.

Everstine, G. C. (1997). Finite element formulations of structural acoustics problems. *Computers & Structures*, 65(3), 307-321.

Fahy, F. J., & Mohammed, A. D. (1992). A study of uncertainty in applications of SEA to coupled beam and plate systems, part I: Computational experiments. *Journal of Sound and Vibration*, 158(1), 45-67.

Ferreira, A. J. M., & Fasshauer, G. E. (2006). Computation of natural frequencies of shear deformable beams and plates by an RBF-pseudospectral method. *Computer Methods in Applied Mechanics and Engineering*, 196, 134-146.

Fredö, C. R. (1997). A SEA-like approach for the derivation of energy flow coefficients with a finite element model. *Journal of Sound and Vibration*, 199(4), 645-666.

Fritze, D., Marburg, S., & Hardtke H. J. (2005). FEM-BEM-coupling and structural-acoustic sensitivity analysis for shell geometries. *Computers and Structures*, 83, 143-154.

Gaul, L., & Wenzel, W. (2002). A coupled symmetric BE-FE method for acoustic fluid-structure interaction. *Engineering Analysis with Boundary Elements*, 26, 629-636.

Graff, K. F. (1973). *Wave motion in elastic solids*. Ohio: Ohio State University Press.

Hal, B. V., Desmet, W., & Vandepitte, D. (2005). Hybrid-finite element method-wave based method for steady-state interior structural acoustic problems. *Computers and Structures*, 83, 167-180.

Han, F., Bernhard, R. J., & Mongeau, L. G. (1997). Energy flow analysis of vibrating beams and plates for discrete random excitations. *Journal of Sound and Vibration*, 208(5), 841-859.

Han, J. B., & Liew, K. M. (1997). Numerical differential quadrature method for Reissner/Mindlin plates on two-parameter foundations. *International Journal of Mechanical Sciences*, 39(9), 977-989.

Han, F. (1999). Prediction of flow induced sound and vibration using the energy flow analysis method. Ph.D Thesis, Purdue University Graduate School, USA.

Han, F., Bernhard, R. J., & Mongeau, L. G. (1999). Prediction of flow-induced structural vibration and sound radiation using energy flow analysis. *Journal of Sound and Vibration*, 227(4), 685-709.

Harras, B., Benamar, R., & White, R. G. (2002). Experimental and theoretical investigation of the linear and non-linear dynamic behaviour of a Glare 3 hybrid composite panel. *Journal of Sound and Vibration*, 252(2), 281–315.

Harris, C. M., & Piersoll, A. (Eds.). (2002a). *Shock and Vibration Handbook*. Newyork: McGraw-Hill.

Hearmon, R. (1959). The frequency of flexural vibrations of rectangular orthotropic plates with clamped or simply supported edges. *Journal of Applied Mechanics*, 26, 537–542.

Hou, Y., Wei, G. W., & Xiang, Y. (2005). DSC-Ritz method for the free vibration analysis of Mindlin plates. *International Journal for Numerical Methods in Engineering*, 62, 262-288.

Hung, K. C., Liew, K. M., Lim, K. M., & Leong, L. M. (1993). Boundary beam characteristics orthonormal polynomials in energy approach for vibration of symmetric laminates-I: Classical boundary conditions. *Composite Structures*, 26, 167-184.

Kaiser, G. (1999). *A friendly guide to wavelet*. Boston: Birkhaeuser.

Kopuz, Ş. (1995). An integrated FEM\BEM approach to the prediction of interior noise levels of vehicle body structures. Ph.D Thesis, The Graduate School of Natural and Applied Sciences of The Middle East Technical University, TURKEY.

Kim, S. H., Lee, J. M., & Sung, M. H. (1999). Structural-acoustic modal coupling analysis and application to noise neduction in a vehicle passenger compartment. *Journal of Sound and Vibration*, 225(5), 899-999.

Langley, R. S. (1992). A wave intensity technique for the analysis of high frequency vibrations. *Journal of Sound and Vibration*, 159(3), 483-502.

Langley, R. S. (1995). On the vibrational conductivity approach to high frequency dynamics for two-dimensional structural components. *Journal of Sound and Vibration*, 182(4), 637-657.

Lanhe, W., Hua, L., & Daobin, W. (2005). Vibration analysis of generally laminated composite plates by the moving least squares differential quadrature method. *Composite Structures*, 68, 319-330.

LeBot, A. (1998). A vibro-acoustic model for high frequency analysis. *Journal of Sound and Vibration*, 211(4), 537-554.

Lee, J., & Schultz, W. W. (2004). Eigenvalue analysis of Timoshenko beams and axisymmetric Mindlin plates by the pseudospectral method. *Journal of Sound and Vibration*, 269, 609–621.

Leissa, A. W., & Narita, Y. (1989). Vibration studies for simply supported symmetrically laminated rectangular plates. *Composite Structures*, 12, 113–132.

Leissa, A. W. (1969). *Vibration of plates*. Washington D.C: NASA.

Lim, T. C. (2000). Automotive panel noise contribution modeling based on finite element and measured structural-acoustic spectra. *Applied Acoustics*, 60, 505-519.

Liew, K. M., Lam, K. Y., & Chow, S. T. (1989). Study on flexural vibration of triangular composite plates influenced by fibre orientation. *Composite Structures*, 13(2), 123-132.

Liew, K. M., & Lim, C. W. (1995). Vibratory characteristics of general laminates, I: Symmetric trapezoids. *Journal of Sound and Vibration*, 183(4), 615–642.

Liew, K. M. (1996). Solving the vibration of thick symmetric laminates by Reissner/Mindlin plate theory and the p-Ritz method. *Journal of Sound and Vibration*, 198(3), 343–360.

Liew, K. M., Huang, Y. Q., & Reddy, J. N. (2003). Vibration analysis of symmetrically laminated plates based on FSDT using the moving least squares differential quadrature method. *Computer Methods in Applied Mechanics and Engineering*, 192(19), 2203-2222.

Liew, K. M., Wang, J., Ng, T. Y., & Tan, M. J. (2004). Free vibration and buckling analyses of shear-deformable plates based on FSDT mesh-free method. *Journal of Sound and Vibration*, 276, 997–1017.

Lim, C. W., Li, Z. R., & Wei, G. W. (2005). DSC-Ritz method for high-mode frequency analysis of thick shallow shells. *International Journal for Numerical Methods in Engineering*, 62, 205-232.

Liu, L., Chua, L. P., & Ghista, D. N. (2007). Mesh-free radial basis function method for static, free vibration and buckling analysis of shear deformable composite laminates. *Composite Structures*, 78, 58-69.

Lyon, R. H., & DeJong, R. G. (1995). *Theory and application of statistical energy analysis*. Butterworth-Heinemann.

Mariem, J. B., & Hamdi, M. A. (1987). A new boundary finite element method for fluid-structure interaction problems. *International Journal for Numerical Methods in Engineering*, 24, 1251-1267.

Misiti, M., Misiti, Y., Oppenheim, G., & Poggie, J. M. (2005). *Wavelet toolbox*. Mathworks.

Moens, I., Vandepitte, D., & Sas, P. (2002). A wavelength criterion for the validity of the energy finite element method for plates. Proceedings of ISMA-Volume II.

Ng, C. H. W., Zhao, Y. B., & Wei, G. W. (2004). Comparison of discrete singular convolution and generalized differential quadrature for the vibration analysis of rectangular plates. *Computer Methods in Applied Mechanics and Engineering*, 193, 2483-2506.

Qian, L. W., & Wei, G. W. (2000). A note on regularized Shannon's sampling formulae, Preprint, *arXiv:math*., SC/0005003.

Rabbiolo, G., Bernhard, R. J., & Milner, F. A. (2004). Definition of a high-frequency threshold for plates and acoustical spaces. *Journal of Sound and Vibration*, 277, 647-667.

Rao, M. R., & Bopardikar, A. S. (1998). *Wavelet transforms: Introduction to theory and application*s. Addison-Wesley.

Schroeder, M. S. (1969). Digital simulation of sound transmission in reverberant spaces. *Journal of Acoustical Society of America*, 47, 424-431.

Seçgin, A., Atas, C., & Sarıgül, A. S. (2007). Investigation of the effects of material and fiber orientation angles on the modal characteristics of thin FML composite plates by using discrete singular convolution (DSC) approach. 4th Ankara International Aerospace Conference, Article No: AIAC-2007-045, TURKEY.

Seçgin, A., & Sarıgül, A. S. (2008). Free vibration analysis of symmetrically laminated thin composite plates by using discrete singular convolution (DSC) approach: Algorithm and verification. *Journal of Sound and Vibration*, 315(1-2), 197-211.

Sestieri, A., & Carcaterra, A. (2001). On the spurious solutions in complex envelope displacement analysis. *Journal of Sound and Vibration*, 240(2), 293-302.

Smith, M. J. (1997). A hybrid energy method for predicting high frequency vibrational response of point-loaded plates. *Journal of Sound and Vibration*, 202(3), 375-394.

Song, C. K., Hwang, J. K., Lee, J. M., & Hedrick, J. K. (2003). Active vibration control for structural-acoustic coupling system of a 3-D vehicle cabin model. *Journal of Sound and Vibration*, 267, 851-865.

Timoshenko, S., Young, D., & Weaver, W. (1971). *Vibration problems in engineering*. New York: John Wiley.

Venini, P., & Mariani, C. (1997). Free vibrations of uncertain composite plates via stochastic Rayleigh-Ritz approach. *Computers and Structures*, 64(1), 407-423.

Vlahopoulos, N., Raveandra, S. T., Vallance, C., & Messer, S. (1999). Numerical implementation and applications of a coupling algorithm for structural-acoustic models with unequal discretization and partially interfacing surfaces. *Finite Elements in Analysis and Design*, 32, 257-277.

Vorlaender, M. (1989). Simulation of the transient and steady-state sound propagation in rooms using a new combined ray-tracing/image-source algorithm. *Journal of Acoustical Society of America*, 86(1), 172-178.

Wachulec, M., Kirkegaard, P. H., & Nielsen, S. R. K. (2000). Methods of estimation of structure borne noise in structures – review, *Structural Dynamics*, Aalborg University, Paper No. 20.

Wang, S. (2000). High frequency energy flow analysis methods: Numerical implementation, applications and verification. Ph.D Thesis, Purdue University Graduate School, USA.

Wang, J., Liew, K. M., Tan, M. J., & Rajendran, S. (2002). Analysis of rectangular laminated composite plates via FSDT meshless method. *International Journal of Mechanical Sciences*, 44(7), 1275-1293.

Wei, G. W. (1999). Discrete singular convolution for the solution of Fokker-Plank equation. *Journal of Chemical Physics*, 110(18), 8930-8942.

Wei, G. W. (2000a). Discrete singular convolution for the sine-Gordon equation. *Physica D*, 137, 247-259.

Wei, G. W. (2000b). Wavelets generated by using discrete singular convolution. *Journal of Physics A*, 33, 8577-8596.

Wei, G. W. (2000c). Solving quantum eigenvalue problems by discrete singular convolution. *Journal of Physics B*, 33, 343-352.

Wei, G. W. (2001a). Discrete singular convolution for beam analysis. *Engineering Structures*, 23, 1045-1053.

Wei, G. W. (2001b). Vibration analysis by using discrete singular convolution. *Journal of Sound and Vibration*, 244(3), 535-553.

Wei, G. W. (2001c). A new algorithm for solving some mechanical problems. *Computational Methods in Applied Mechanics and Engineering*, 190, 2017–2030.

Wei, G. W., Zhao, Y. B., & Xiang, Y. (2001). The determination of natural frequencies of rectangular plates with mixed boundary conditions by discrete

singular convolution. *International Journal of Mechanical Sciences*, 43, 1731–1746.

Wei, G. W., Zhao, Y. B., & Xiang, Y. (2002a). Discrete singular convolution and its application to the analysis of plates with internal supports. Part 1: Theory and algorithm. *International Journal for Numerical Methods in Engineering*, 55, 913–946.

Wei, G. W., Zhao, Y. B., & Xiang, Y. (2002b). A novel approach for the analysis of high-frequency vibrations. *Journal of Sound and Vibration*, 257(2), 207–246.

Whitney, J. M. (1987). *Structural analysis of laminated anisotropic plates*. Pennsylvania: Technomic Publishing Company Inc.

Xiang, Y., Zhao, Y. B., & Wei, G. W. (2002). Discrete singular convolution and its application to the analysis of plates with internal supports. Part 2: Applications. *International Journal for Numerical Methods in Engineering*, 55, 947–971.

Zeng, H., & Bert, C. W. (2001). A differential quadrature analysis of vibration for rectangular stiffened plates. *Journal of Sound and Vibration*, 241(2), 247–252.

Zhang, J. C., Ng, T. Y., & Liew, K. M. (2003). Three-dimensional theory of elasticity for free vibration analysis of composite laminates via layerwise differential quadrature modelling. *International Journal for Numerical Methods in Engineering*, 57, 1819-1844.

Zhao, Y. B., & Wei, G. W. (2002). DSC analysis of rectangular plates with non-uniform boundary conditions. *Journal of Sound and Vibration*, 255(2), 203–228.

Zhao, Y. B., Wei, G. W., & Xiang, Y. (2002a). Plate vibrations under irregular internal supports. *International Journal of Solids and Structures*, 39, 1361-1383.

Zhao, Y. B., Wei, G. W., & Xiang, Y. (2002b). Discrete singular convolution for the prediction of high frequency vibration of plates. *International Journal of Solids and Structures*, 39, 65–88.

Zhao, S., Wei, G. W., & Xiang, Y. (2005). DSC analysis of free-edged beams by an iteratively matched boundary method. *Journal of Sound and Vibration*, 284, 487–493.

APPENDICES

APPENDIX A
WAVELET TRANSFORMS

A.1 Wavelet, Wavelet Analysis

A wavelet is a waveform of effectively limited duration that has an average value of zero. Comparing the wavelets with sine waves, which are the basis of Fourier analysis, sinusoids are smooth and do not have limited duration, they extend from minus to plus infinity. However, wavelets tend to be irregular and asymmetric as shown in Figure A.1.

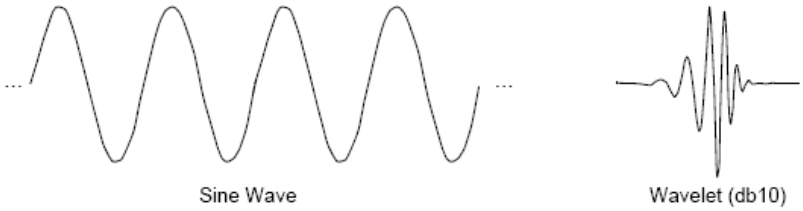

Figure A.1 Comparison of a sine wave and a wavelet (db10 type wavelet) (Misiti, Misiti, Oppenheim, & Poggie , 2005).

Wavelet analysis is a mathematical technique which can be used to split a signal into different frequency bands or components so that each one can be studied with a resolution, matching its scale. Thus it provides higher frequency and spatial resolution.

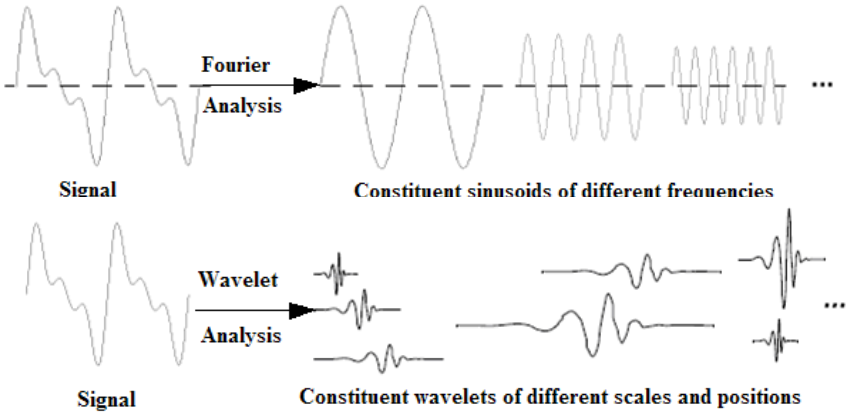

Figure A.2 Graphical representation of the comparison of Fourier Analysis and Wavelet Analysis (Misiti, Misiti, Oppenheim, & Poggie , 2005).

Fourier analysis consists of breaking up a periodic signal into sine waves of various frequencies. Similarly, wavelet analysis is the breaking up of any signal into shifted and scaled versions of the original wavelet (Figure A.2). Since the wavelets have local extensions, local features of a signal such as sharp peaks, irregularities or non-smoothness can be described well with wavelets.

A.2 Continuous Wavelet Transform (CWT)

Mathematically, the process of continuous Fourier analysis is the Fourier transforms (Rao & Bopardikar, 1998).

$$F(\omega) = \int_{-\infty}^{\infty} f(t)\, e^{-i\omega t}\, dt \tag{A.1}$$

which is the integration over all time of the signal $f(t)$ multiplied by a complex exponential $e^{-i\omega t}$. Similarly the process of continuous wavelet analysis is the Continuous Wavelet Transform (CWT) and defined as;

$$W(a,b) \equiv \int_{-\infty}^{\infty} f(t)\, \psi^{*}_{a,b}(t)\, dt \tag{A.2}$$

where $\psi_{a,b}(t)$ is a wavelet (also called *mother* wavelet), * denotes complex conjugation and $W(a,b)$ is the wavelet transform which is a function of two variables; a and b are scale and position parameters respectively. A wavelet can be determined in the following form by scaling with a and translated with b;

$$\psi_{a,b}(t) \equiv \frac{1}{\sqrt{|a|}} \psi\left(\frac{t-b}{a}\right) \tag{A.3}$$

This real or complex valued continuous-time function $\psi(t)$ has the following properties;

1. The function integrates to zero: $\int_{-\infty}^{\infty} \psi(t)\,dt = 0$ (A.4)

2. It has a finite energy: $\int_{-\infty}^{\infty} |\psi(t)|^2 dt < \infty$. (A.5)

A wavelet also satisfies the following condition known as the *admissibility condition*,

$$C \equiv \int_{-\infty}^{\infty} \frac{|\varphi(\omega)|^2}{|\omega|} d\omega < +\infty \ . \tag{A.6}$$

Here $\varphi(\omega)$ is the Fourier transform of $\psi(t)$. The *admissibility condition* implies that the Fourier transform of $\psi(t)$ vanishes at the zero frequency, i.e.

$$|\varphi(\omega)|^2 \Big|_{\omega=0} = 0 \tag{A.7}$$

This condition means that wavelets must have a band-pass like spectrum. A zero at the zero frequency also means that the average value of the wavelet in the time domain must be zero as presented in Equation (A.4), and therefore it must be oscillatory. In other words, $\psi(t)$ must be a *wave*. The inverse wavelet transform can be constructed as

$$f(t) = \frac{1}{C} \int_{a=-\infty}^{\infty} \int_{b=-\infty}^{\infty} \frac{1}{|a|^2} W(a,b)\, \psi_{a,b}(t)\, da\, db \tag{A.8}$$

Another condition for a wavelet is the *regularity condition*. It states that the wavelets should have some smoothness and concentration in both time and frequency domains. Regularity is a quite complex concept, however, a simple explanation can be found in (Kaiser, 1999). Scaling a wavelet is directly related with the frequency. A low scale (lower *a*) wavelet reflects higher frequency behaviour whereas the higher scales (higher *a*) imply low frequencies (Figure A.3).

Figure A.3 Scale and frequency relation in wavelets (Misiti, Misiti, Oppenheim, & Poggie , 2005).

There is a lot of *mother* wavelets determined and used in the signal analysis. A few wavelet, which are called by their shapes or names of their creators, is demonstrated in Figure A.4.

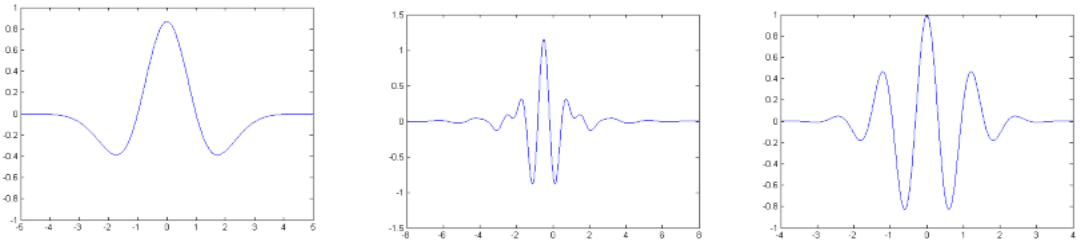

(a) (b) (c)

Figure A.4 (a) Mexican hat wavelet, (b) Meyer wavelet, (c) Morlet wavelet.

A.3 Discrete Wavelet Transform (DWT)

A.3.1 Discrete Wavelets

The wavelet transform has three difficulties in the direct application of Equation (A.2). The first is redundancy of CWT. In Equation (A.2), the wavelet transform is calculated by continuously shifting (continuous b) continuously scalable function (continuous a) over a signal and continuously calculating the wavelet coefficients (a kind of correlation coefficients between original signal and wavelets). A non-redundant wavelet representation, which demonstrates a discrete wavelet by making *dyadic* sampling both for time and frequency axes, can be introduced as

$$\psi_{j,k}(t) \equiv \frac{1}{\sqrt{2^j}}\psi\left(\frac{t-2^j k}{2^j}\right) \quad . \tag{A.9}$$

Here j and k are integers. The *dyadic* samplings state that the scale parameter a and translational parameter b in Equation (A.3) are discretized as $a = 2^j$ and $b = 2^j k$, respectively. Equation (A.9) is the non-redundant version of Equation (A.3). In order to complete the removal of the redundancy, the discrete wavelets should satisfy the orthogonality,

$$\int \psi_{j,k}(t)\, \psi_{m,n}(t)\, dt = \begin{cases} 1 & \text{if} \quad j = m \quad \text{and} \quad k = n \\ 0 & \text{otherwise} \end{cases} . \tag{A.10}$$

An arbitrary signal can be reconstructed by summing the orthogonal wavelet basis functions, weighted by the wavelet transform coefficients $W(j,k)$:

$$f(t) = \sum_{j=-\infty}^{\infty} \sum_{k=-\infty}^{\infty} W(j,k)\, \psi_{j,k}(t) \quad . \tag{A.11}$$

Equation (A.11) shows the Inverse Wavelet Transform (IWT) for discrete wavelets.

A.3.2 Scaling Function (Father Wavelet)

Although the removal of the redundancy of CWT is completed by using discrete wavelets, there are still an infinite number of wavelets in the wavelet transforms. This is the second difficulty in CWT and it can be solved by reducing the number of wavelets to a sufficient count by introducing scaling functions. Wavelets are also defined by a scaling function $\phi(t)$ (also called *father* wavelet). The *mother* wavelet is in effect a band-pass filter and scaling it for each level in *dyadic* sampling (stretching it with a factor of 2) in the time domain halves its bandwidth in frequency domain. This creates a problem that entire spectrum must be covered by an infinite number of levels. The scaling function filters the lowest level of the transform and ensures the entire spectrum is covered. The scaling function can be decomposed with wavelet components, as being just a signal in Equation (A.11);

$$\phi(t) = \sum_{j=-\infty}^{\infty} \sum_{k=-\infty}^{\infty} W(j,k)\, \psi_{j,k}(t) \quad . \tag{A.12}$$

A scaling function has the following properties;

1. The function integrates to unity: $\int_{-\infty}^{\infty} \phi(t)\, dt = 1.$ (A.13)

2. It has unit energy: $\int_{-\infty}^{\infty} |\phi(t)|^2\, dt = 1.$ (A.14)

If one analyzes a signal using the combination of scaling function and *mother* wavelets, the scaling function covers the wavelets up to any scale *j*, while the rest is done by the *mother* wavelets. In this way, the number of wavelets is limited from an infinite number to a finite number (Figure A.5).

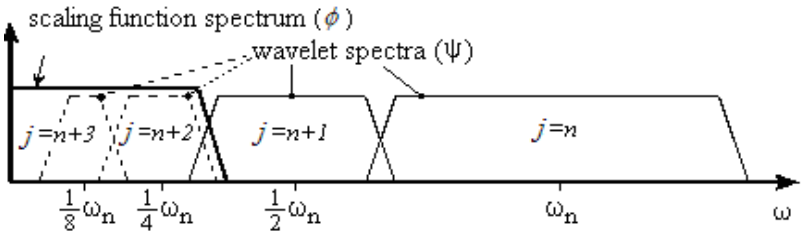

Figure A.5 How an infinite set of wavelets is replaced by one scaling function (Kaiser, 1999) (*n*: the number of wavelets, *j*: scale, ω: frequency).

As an example, the Shannon scaling function $\phi(x) = \dfrac{\sin n\pi x}{n\pi x}$ and *mother* wavelet $\psi(x) = \dfrac{\sin 2n\pi x - \sin n\pi x}{n\pi x}$ for $n = 1$ are presented in Figure A.6.

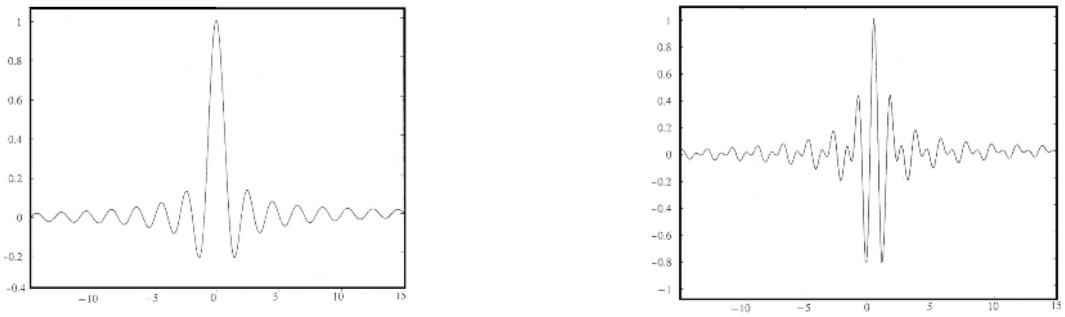

(a) (b)

Figure A.6. (a) Shannon scaling function (*father* wavelet), (b) Shannon wavelet (*mother* wavelet).

APPENDIX B
DSC MATRIX REPRESENTATION

B.1 DSC Matrix

The DSC matrix representation for an eigenvalue equation can be written by the following form:

$$\mathbf{D}\,\overline{W} = \mathbf{\Omega}^2 W \tag{B.1}$$

where

$$\mathbf{D} = \begin{bmatrix} C_{-M}^{(n)} & . & . & C_0^{(n)} & . & . & C_M^{(n)} & 0 & . & . & 0 \\ 0 & C_{-M}^{(n)} & . & . & C_0^{(n)} & . & . & C_M^{(n)} & 0 & . & 0 \\ . & 0 & . & . & . & . & . & . & . & . & 0 \\ . & . & . & . & . & . & . & . & . & . & . \\ 0 & . & . & 0 & C_{-M}^{(n)} & . & . & C_0^{(n)} & . & . & C_M^{(n)} \end{bmatrix}_{N\times(N+2M)}, \tag{B.2}$$

$$\mathbf{\Omega}^2 = \begin{bmatrix} \Omega_0^2 & 0 & . & 0 \\ 0 & . & . & . \\ . & . & . & 0 \\ 0 & . & 0 & \Omega_{N-1}^2 \end{bmatrix}, \tag{B.3}$$

$$\overline{W} = \begin{Bmatrix} W_{-M} \\ . \\ . \\ . \\ W_{N-1+M} \end{Bmatrix}_{(N+2M)\times 1} \quad \text{and} \quad W = \begin{Bmatrix} W_0 \\ . \\ . \\ . \\ W_{N-1} \end{Bmatrix}_{N\times 1} \tag{B.4), (B.5}$$

Applying boundary conditions by using Equations (3.34)-(3.37), the DSC matrix **D** becomes

$$\mathbf{D}' = \begin{bmatrix} \left(C_0^{(n)} + \sum_{k=-M}^{-1}(1-A)C_k^{(n)}\right) & \left(C_1^{(n)} + C_{-1}^{(n)}A\right) & . & . & \left(C_1^{(n)} + C_{-1}^{(n)}A\right) & 0 & . & . & . & 0 \\ \left(C_{-1}^{(n)} + \sum_{k=-M}^{-2}(1-A)C_k^{(n)}\right) & \left(C_0^{(n)} + C_{-2}^{(n)}A\right) & . & . & C_{M-1}^{(n)} & C_M^{(n)} & 0 & . & . & 0 \\ . & . & . & . & . & . & . & . & . & . \\ . & . & . & . & . & . & . & . & . & . \\ 0 & . & . & . & . & . & . & . & . & . \\ . & . & . & . & . & . & \left(C_{-M+2}^{(n)} + C_M^{(n)}A\right) & . & \left(C_0^{(n)} + C_2^{(n)}A\right) & \left(C_1^{(n)} + \sum_{k=2}^{M}(1-A)C_k^{(n)}\right) \\ 0 & . & 0. & 0 & \left(C_{-M}^{(n)} + C_M^{(n)}A\right) & . & . & . & \left(C_{-1}^{(n)} + C_1^{(n)}A\right) & \left(C_0^{(n)} + \sum_{k=1}^{M}(1-A)C_k^{(n)}\right) \end{bmatrix} \quad \text{(B.6)}$$

Finally, eigenvalue equations in a matrix representation reduce to the following equality:

$$\mathbf{D}'W = \mathbf{\Omega}^2 W \quad \text{(B.7)}$$

APPENDIX C
COMPARISION OF THE DSC AND FEM

C.1 The DSC and Finite Element Method (FEM) at Higher Frequencies

Figure C.1 shows high frequency accuracies of the exact solutions given in Equation (4.22) by comparing them with DSC and FEM. The first 999 natural frequencies of a simply supported beam are presented in Figure C.1. In this demonstration, beam's physical properties are chosen as a=1m, A=10^{-6} m^2, $\rho_0 = 7930\ kg/m^3$, $E = 2.1\times10^{11}\ N/m^2$, $\mathrm{I} = 0.0833\times10^{12}\ m^4$.

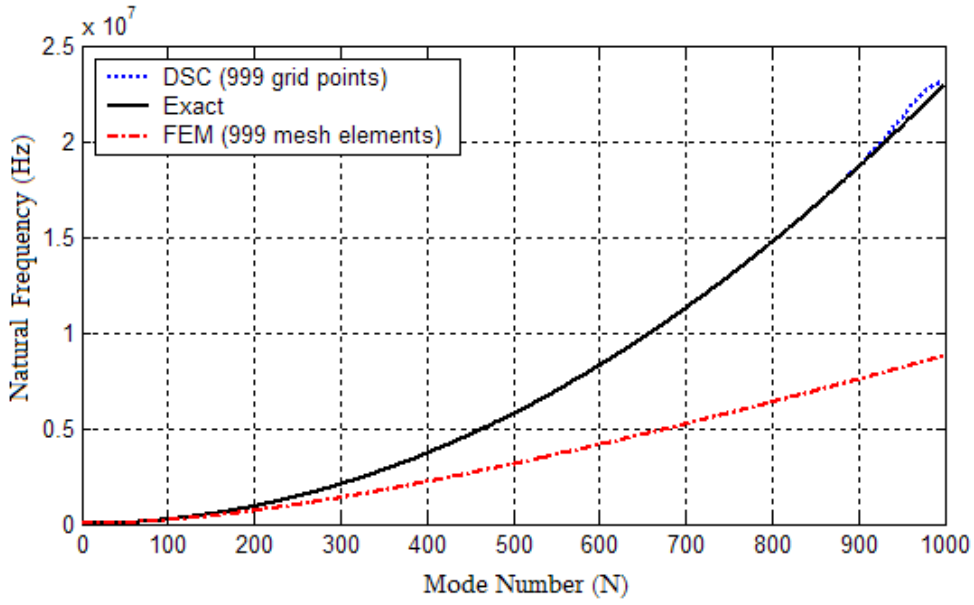

Figure C.1 Comparison of the DSC and FEM results for the first 999 natural frequencies of simply supported beam.

It is obviously seen from Figure C.1 that, FEM results hugely diverge from the exact results after the Mode 200. However, even at higher modes, DSC results show almost exact values. This indicates that the FEM can not be reliably used in high frequency analysis. In order to demonstrate the low and mid-frequency behaviour of the methods, the comparison for the first 50 modes and 51 to 101 modes are presented in Figure C.2 and Figure C.3, respectively.

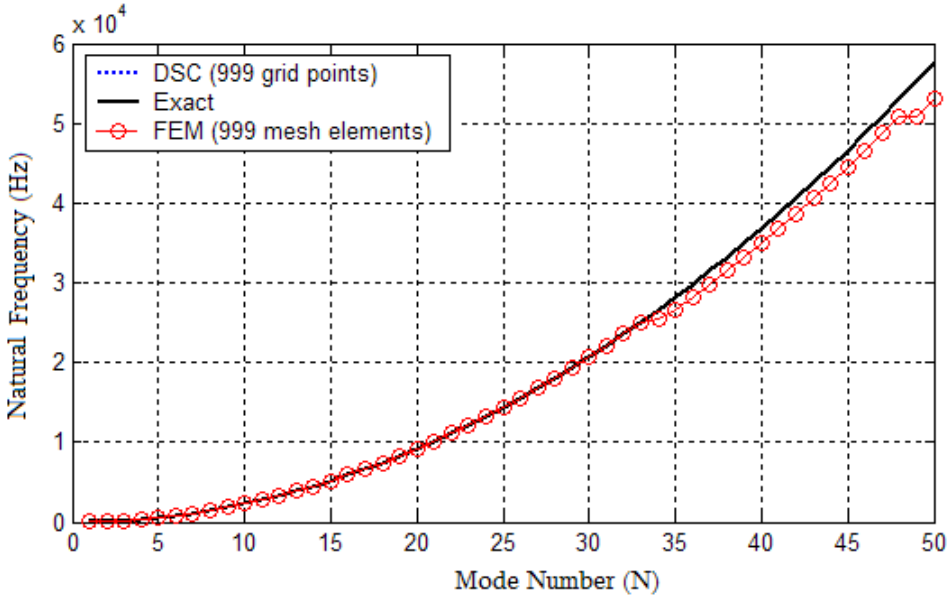

Figure C.2 The comparison of the DSC and FEM results for the first 50 natural frequencies of simply supported beam.

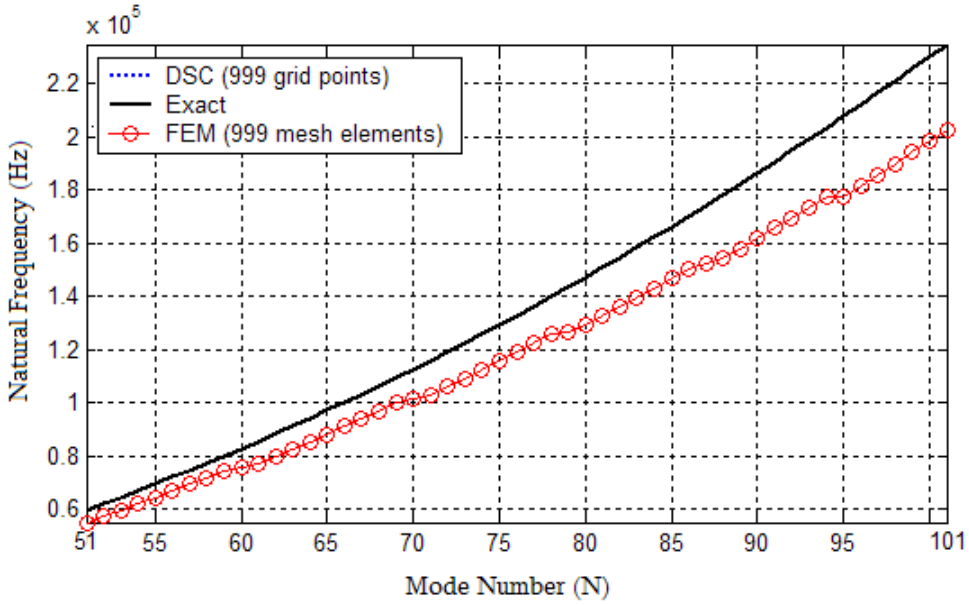

Figure C.3 The comparison of the DSC and FEM results for 51 to 101 natural frequencies of simply supported beam.

According to Figure C.2, FEM predicts reliable results until Mode 35. After that mode, a discrepancy is observed; however, the first 50 modes can be acceptable for low frequency analysis. Figure C.3 displays a considerable discrepancy of the FEM from the exact results all through the spectrum. However, DSC exhibits totally exact

behaviour. Figure C.4 indicates the relative error of FEM and DSC in comparison with the exact results by calculating from the expression $\%\ Error = 100 \cdot \left| \frac{f_n - f_{FEM,DSC}}{f_n} \right|$ where f_n represents the exact result. These figures clearly imply that the FEM can only be reliably used in low frequencies.

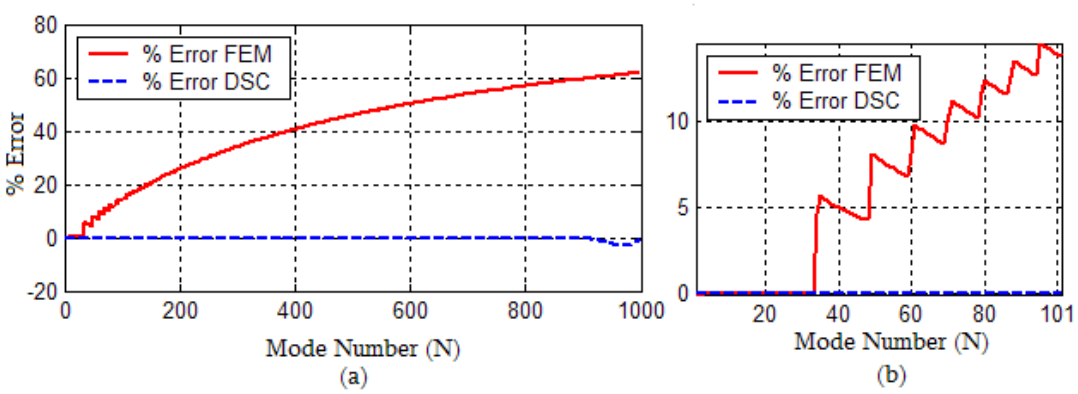

Figure C.4 Relative errors of FEM and DSC results.

APPENDIX D
COMPUTER CODES FOR THE DSC

D.1 Introduction

In the present study, DSC codes for free and forced vibration analyses are developed by using MatLAB® for isotropic beams and plates, and composite plates separately. In this chapter, only the codes for thin isotropic beams and plates are presented with utilized functions.

D.2 The DSC Code for Isotropic Beams and Plates

D.2.1 main_beam.m

```
% main_beam.m by Abdullah Seçgin @2006
% Definitions -------------------------------------------------------
% N      :Number of Discretization points
% M      :Number of Auxilary points
% lb     :Beam length
% r      :Discretization parameter r=sigma/delta
% bc     :Boundary condition parameter
%         bc=-1 for pinned end, bc=1 for fixed end
% v      :Eigenvectors
% A      :Eigenvalues
% om     :Natural frequency parameter
% wn     :Natural frequeency
% E      :Modulus of Elasticity
% h      :Beam thickness
% As     :Area of cross section
% rho    :Mass density
% I      :Moment of Inertia
% Utilized functions ------------------------------------------------
% shn_d4(N,M,lb,r)         :Fourth order Shannon's kernel function
% app_bc_beam(bc,N,M,Dx4):Apply boundary condition
%--------------------------------------------------------------------
clc;clear;
% Beam mechanical properties
  E=2.1e11; h=1e-3; As=h^2; I=h^4/12; rho=7900;
% Discretization parameters
  N=3001; lb=1; M=N-1; r=12.1;
```

```
%-------------------------------------------------------------------
[Dx4]=shn_d4(N,M,lb,r);
[D]=app_bcbeam(-1,N,M,Dx4);
[v,A]=eig(D);

for i=1:length(A)
 om(i)=abs(A(i,i))^0.25;
end
wn=om*((E*I)/(rho*As))^0.5;
```

D.2.2 main_plate.m

```
% main_plate.m by Abdullah Seçgin @2006 revised in @2008
% Definitions -------------------------------------------------------
% N      :Number of Discretization points
% M      :Number of Auxilary points
% a,b    :Plate lengths
% lp     :Plate aspect ratio
% r      :Discretization parameter r=sigma/delta
% bcl    :Left(Top) boundary condition parameter
% bcr    :Right (Bottom) boundary condition parameter
%         bc=-1 for simply-supported, bc=1 for clamped edges
% v      :Eigenvectors
% A      :Eigenvalues
% om     :Natural frequency parameter
% wn     :Natural frequeency
% E      :Modulus of Elasticity
% De     :Plate rigidity
% h      :Plate thickness
% rho    :Mass density
% I      :Moment of Inertia
% Utilized functions ------------------------------------------------
% shn_d2(N,M,lb,r)              :Second order Shannon's kernel function
% shn_d4(N,M,lb,r)              :Fourth order Shannon's kernel function
% app_bc_sec(bcl,bcr,N,M,Dx4)   :Apply secondary boundary conditions
% app_bc_prim(DA,N)             :Apply primary boundary conditions
%-------------------------------------------------------------------
clc;clear;
% Plate mechanical properties
  h=1e-3; E=2.1e11;  rho=7900; De=(E*h^3)/(12*(1-0.3^2));
% Discretization parameters
  a=1; b=a; lp=a/b; N=71; M=N-1; r=12.1;
```

```
%-------------------------------------------------------------------
[Dx4]=shn_d4(N,M,a);[DX4]=app_bc_sec(1,-1,N,M,Dx4);
[Dx2]=shn_d2(N,M,a);[DX2]=app_bc_sec(1,-1,N,M,Dx2);

[Dy4]=shn_d4(N,M,b);[DY4]=app_bc_sec(1,1,N,M,Dy4);
[Dy2]=shn_d2(N,M,b);[DY2]=app_bc_sec(1,1,N,M,Dy2);

clear('Dx4');clear('Dx2');clear('Dy4');clear('Dy2');
IX=eye(N); IY=eye(N);

DA=kron(DX4,IY)+2*(lp^2)*kron(DX2,DY2)+(lp^4)*kron(IX,DY4);
clear('DX4');clear('DX2');clear('DY4');clear('DY2');

%-------------------------------------------------------------------
[DA]=app_bc_prim(DA,N);
[v,A]=eig(DA);
%-------------------------------------------------------------------
 for i=1:length(A)
   wn(i)=(A(i,i)/(ro*h)).^0.5;
   om(i)=wn(i)*(a^2/pi^2)*((ro*h)/De)^(0.5);
 end
```

D.2.3 DSC Functions

D.2.3.1 shn_d2.m

```
 % shn_d2.m by Abdullah Seçgin @2006
 % Definitions -------------------------------------------------
 % sig    :Regularization parameter
 % del    :Grid size
 % -------------------------------------------------------------------
 function [Da]=shn_d2(N,M,a,r)
 %--------------------------------
 del=a/(N-1); sig=r*del; pd=pi/del;
 di=[0:N-1]; dgj=[-M:N-1+M]; sd=M+1;
 %--------------------------------
 xxk=-M*del:del:M*del;
 C2=-sin(pd*xxk)*pd./xxk.*exp(-1/2*xxk.^2/sig^2)-2*cos(pd*xxk) ...
 ./xxk.^2.*exp(-1/2*xxk.^2/sig^2)-2*cos(pd*xxk)./sig^2. ...
 *exp(-1/2*xxk.^2/sig^2)+2*sin(pd*xxk)./pd./xxk.^3. ...
 *exp(-1/2*xxk.^2/sig^2)+sin(pd*xxk)./pd./xxk./sig^2. ...
 *exp(-1/2*xxk.^2/sig^2)+sin(pd*xxk)./pd./sig^4.*xxk. ...
 *exp(-1/2*xxk.^2/sig^2);
 c21=C2(1:sd-1); c22=C2(sd+1:length(xxk));
 C2(sd)=-sum(c21')-sum(c22');
```

```
%------------------------------
for i=1:N
    for j=1:2*M+N
      if (dgj(j)-di(i))>-M-1 & (dgj(j)-di(i))<M+1;
         D2(i,j)=C2((dgj(j)-di(i))+M+1);
      else  D2(i,j)=0;
      end
    end
end
Da=D2;
end
```

D.2.3.2 shn_d4.m

```
% shn_d4.m by Abdullah Seçgin @2006
% Definitions ----------------------------------------------------
% sig   :Regularization parameter
% del   :Grid size
% ----------------------------------------------------------------
function [Da]=shn_d4(N,M,a,r)
%---------------------------------
del=a/(N-1); sig=r*del; pd=pi/del;
di=[0:N-1]; dgj=[-M:N-1+M]; sd=M+1;
%---------------------------------
xxk=-M*del:del:M*del;
C4=-24*cos(pd*xxk)./xxk.^4.*exp(-1/2*xxk.^2/sig^2) ...
    -12*cos(pd*xxk)./xxk.^2/sig^2.*exp(-1/2*xxk.^2/sig^2) ...
    -4*cos(pd*xxk)./sig^6.*xxk.^2.*exp(-1/2*xxk.^2/sig^2) ...
    +sin(pd*xxk)*pd^3./xxk.*exp(-1/2*xxk.^2/sig^2) ...
    +4*cos(pd*xxk)*pd^2/sig^2.*exp(-1/2*xxk.^2/sig^2) ...
    -12*sin(pd*xxk)*pd./xxk.^3.*exp(-1/2*xxk.^2/sig^2)...
    +4*cos(pd*xxk)*pd^2./xxk.^2.*exp(-1/2*xxk.^2/sig^2) ...
    -6*sin(pd*xxk)*pd./xxk./sig^2.*exp(-1/2*xxk.^2/sig^2)...
    -6*sin(pd*xxk)*pd/sig^4.*xxk.*exp(-1/2*xxk.^2/sig^2) ...
    +24*sin(pd*xxk)./pd./xxk.^5.*exp(-1/2*xxk.^2/sig^2) ...
    +12*sin(pd*xxk)./pd./xxk.^3/sig^2.*exp(-1/2*xxk.^2/sig^2)...
    +3*sin(pd*xxk)./pd./xxk./sig^4.*exp(-1/2*xxk.^2/sig^2) ...
    -2*sin(pd*xxk)./pd./sig^6.*xxk.*exp(-1/2*xxk.^2/sig^2) ...
    +sin(pd*xxk)./pd./sig^8.*xxk.^3.*exp(-1/2*xxk.^2/sig^2);
c41=C4(1:sd-1); c42=C4(sd+1:length(xxk));
C4(sd)=-sum(c41')-sum(c42');
```

```
%-------------------------------
for i=1:N
    for j=1:2*M+N
      if (dgj(j)-di(i))>-M-1 & (dgj(j)-di(i))<M+1;
         D4(i,j)=C4((dgj(j)-di(i))+M+1);
      else  D4(i,j)=0;
      end
    end
end; Da=D4;
end
```

D.2.3.3 app_bc_beam.m

```
% app_bc_beam.m by Abdullah Seçgin @2006
%-------------------------------------------------------------------
function [Dbc]=app_bcbeam(bc,N,M,DX)
Dleft=zeros(N); Dright=zeros(N);
Dleft(1:N,N-M+1:N)=DX(1:N,1:M);
Dright(1:N,1:M)=DX(1:N,M+N+1:2*M+N);
DN=DX(1:N,M+1:M+N);

for j=1:N
     DNN(j,1)=DN(j,1)+(1-bc)*sum(Dleft(j,1:N));
     DNN(j,N)=DN(j,N)+(1-bc)*sum(Dright(j,1:N));
   end

for i=1:N
    for j=2:N-1
      DNN(i,j)=DN(i,j)+bc*Dleft(i,N+2-j)+bc*Dright(i,N-j);
    end
end
Dbc=DNN(2:N-1,2:N-1);
end
```

D.2.3.4 app_bc_sec.m

```
% app_bc_sec.m by Abdullah Seçgin @2006
%-------------------------------------------------------------------
function [DN]=app_bc_sec(bcl,bcr,N,M,DX);
Dleft=zeros(N); Dright=zeros(N);
Dleft(1:N,N-M+1:N)=DX(1:N,1:M);
Dright(1:N,1:M)=DX(1:N,M+N+1:2*M+N);
DN=DX(1:N,M+1:M+N);
```

```
for j=1:N
     DN(j,1)=DN(j,1)+(1-bcl)*sum(Dleft(j,1:N));
     DN(j,N)=DN(j,N)+(1-bcr)*sum(Dright(j,1:N));
end

for i=1:N
    for j=2:N-1
      DN(i,j)=DN(i,j)+bcl*Dleft(i,N+2-j)+bcr*Dright(i,N-j);
    end
end
end
```

D.2.3.5 app_bc_prim.m

```
% app_bc_prim.m by Abdullah Seçgin @2006
%-------------------------------------------------------------------
function [Dbc]=app_bc_prim(DA,N)
%Apply left and right boundaries W=0
DA=DA(N+1:N^2-N,N+1:N^2-N);
%-------------------------------------------------------------------
%Apply top and bottom boundaries W=0
NN=length(DA); cc=length(DA);
for p=1:N-1:NN
 if(p>cc); break; end
  DA(:,p) = [];
  DA(p,:) = [];
  cc=length(DA);
end

 cp=length(DA);
 for p=N-1:N-2:NN
  if(p>cp); break; end
   DA(:,p) = [];
   DA(p,:) = [];
   cp=length(DA);
 end
Dbc=DA;
end
```

APPENDIX E
LIST OF SYMBOLS

a	length of beam or a side length of plate
A	area of beam cross-section
A_s	surface area of plate
b	the other side length of plate
c_g	group velocity
D_0	flexural rigidity
D_{ij}	flexural rigidity of composite plate in i, j principle material directions
E	elasticity modulus
f_c	center frequency
f_h	higher frequency
f_l	lower frequency
f_n	natural frequency
G	shear modulus
h	total thickness
I	moment of inertia
k	complex wavenumber
k_0	wavenumber in the absence of damping
M	number of fictitious nodes
MO	modal overlap count
M_x	bending moment per unit length about y axis
M_y	bending moment per unit length about x axis
M_{xy}	twisting moment per unit length in x axis
M_{yx}	twisting moment per unit length in y axis
$n(f)$	modal density in a frequency bandwidth
N	number of structure nodes
P	number of modes in a frequency bandwidth

q	load
Q_x	transverse shear force per unit length in x axis
Q_y	transverse shear force per unit length in y axis
r	discretization parameter for regularization
V_x	in-plane force per unit length in x axis
V_y	in-plane force per unit length in y axis
V_{xy}	in-plane shear force per unit length
w	flexural displacement
(x, y)	cartesian coordinates
α	sampling parameter
δf	average modal spacing between two adjacent modes in a frequency bandwidth
$\delta^{(n)}$	nth degree delta kernel
Δ	grid spacing
Δf_n	modal bandwidth
ϕ_p	pth mode shape
γ	damping coefficient
κ	shear correction factor
λ	aspect ratio
ν	Poisson's ratio
θ_x	rotation of normal x axis
θ_y	rotation of normal y axis
ρ	average mass density of a composite plate
ρ_0	mass density
σ	standard deviation
ω	circular frequency
Ω	frequency parameter
ζ	internal loss factor
$\otimes$	tensorial product